MODELING AND SIMULATION OF COEFFICIENT OF
FRICTION ON GEAR TEETH CONTACTS

A THESIS SUBMITTED TO
THE GRADUATE SCHOOL OF NATURAL AND APPLIED SCIENCES
OF
MIDDLE EAST TECHNICAL UNIVERSITY

BY

YELİZ OKŞAYAN

IN PARTIAL FULFILLMENT OF THE REQUIREMENTS
FOR
THE DEGREE OF MASTER OF SCIENCE
IN
MECHANICAL ENGINEERING

SEPTEMBER 2014

Approval of the thesis:

MODELING AND SIMULATION OF COEFFICIENT OF FRICTION ON GEAR TEETH CONTACTS

submitted by **YELİZ OKŞAYAN** in partial fulfillment of the requirements for the degree of **Master of Science in Mechanical Engineering Department, Middle East Technical University** by,

Prof. Dr. Canan Özgen ───────────────
Dean, Graduate School of **Natural and Applied Sciences**

Prof. Dr. Suha Oral ───────────────
Head of Department, **Mechanical Engineering**

Prof. Dr. Metin Akkök ───────────────
Supervisor, **Mechanical Engineering Dept., METU**

Examining Committee Members

Prof. Dr. R. Orhan Yıldırım ───────────────
Mechanical Engineering Dept., METU

Prof. Dr. Metin Akkök ───────────────
Mechanical Engineering Dept., METU

Prof. Dr. F. Suat Kadıoğlu ───────────────
Mechanical Engineering Dept., METU

Assoc. Prof. Ender Ciğeroğlu ───────────────
Mechanical Engineering Dept., METU

Hakan İşçi, M.Sc ───────────────
Manager, Rotary Wing Technology Center, TAI

Date: ───────────────

I hereby declare that all information in this document has been obtained and presented in accordance with academic rules and ethical conduct. I also declare that, as required by these rules and conduct, I have fully cited and referenced all material and results that are not original to this work.

Name, Last name: Yeliz OKŞAYAN

Signature:

ABSTRACT

MODELING AND SIMULATION OF COEFFICIENT OF FRICTION ON GEAR TEETH CONTACTS

Okşayan, Yeliz

M.S., Department of Mechanical Engineering

Supervisor: Prof. Dr. Metin Akkök

September 2014, 98 Pages

Friction is defined as the resistance to motion between two dry or lubricated contacted surfaces. The contact load, contact geometry, surface speeds, surface roughness parameters and oil properties affect the lubrication condition or regime. The purpose of this thesis is to develop a mixed EHL (Elastohydrodynamic Lubrication) model that is capable of calculating the variation of friction coefficient between gear teeth contacts. Gear systems operate commonly in mixed EHL regime where the elastic deformations of the surfaces are in the order of the film thickness. In this regime, metal to metal asperity contact and hydrodynamic film thickness occurs together. In the model, the effects of deformation of surface asperities, oil viscosity change with pressure, slide to roll ratio, surface roughness parameters are taken into account. The model is capable of plotting the Stribeck curve that specifies the regimes with friction coefficient and Lubrication number. For higher loads, due to the shift on the Stribeck curve, lower coefficient of friction is observed for the same Lubrication number.

 In the present study, the model is adopted to non-Gaussian asperity height distributions since the surfaces do not always have Gaussian distributions in practice.

Applying the Weibull distribution, the mixed EHL model is modified with the contact pressure calculation that is load carried by asperities. The effect of load and surface roughness parameters on the Stribeck curve is analyzed. The effect of Skewness and Kurtosis parameters on the mixed EHL regime is investigated and for comparison, the Stribeck curves are plotted for both Gaussian and non-Gaussian asperity height distributions. Eventually, the mixed EHL model for non-Gaussian surfaces is applied to a spur gear pair to determine the frictional power loss. For smaller Sk values and for higher Ku values than the Gaussian values, the friction coefficient values are lower giving low power loss than the Gaussian asperity summit distribution. Therefore, the gear tooth surfaces are to be machined giving smaller Sk than zero and Ku value that is higher than 2.72.

ÖZ

DİŞLİ TEMAS NOKTALARINDA SÜRTÜNME KATSAYISININ BELİRLENMESİ VE MODELLENMESİ

Okşayan, Yeliz

Yüksek Lisans, Makine Mühendisliği Bölümü

Tez Yöneticisi: Prof. Dr. Metin Akkök

Eylül 2014, 98 sayfa

Sürtünme, kuru veya yağlanmış kontak halindeki iki yüzeyin arasındaki harekete karşı direnç olarak tanımlanır. Kontak yükü, kontak geometrisi, yüzey hızları, yüzey pürüzlülüğü parametreleri ve yağ özellikleri yağlama durumunu ya da rejimini etkilemektedir. Bu tezin amacı, dişli temas noktaları arasındaki sürtünme katsayısının dağılımını hesaplayabilen bir karışık EHD (Elastohidrodinamik Yağlama) modeli geliştirmektir. Dişli sistemleri genellikle elastik deformasyonların film kalınlığı ile aynı seviyede olduğu karışık EHD rejimlerinde çalışırlar. Bu rejimde, metal- metal pürüzlü yüzey kontağı ve hidrodinamik film kalınlığı birlikte görülür. Modelde, yüzey pürüzlerinin deformasyon etkileri, yağ viskozitesinin basınç ile değişimi, kayma yuvarlanma hızı oranı, yüzey pürüzlülüğü etkileri hesaplamalara katılır. Model, yağlama rejimlerini sürtünme katsayısı ve yağlama sayısı ile belirleyen Stribeck eğrisi grafiğini çizebilmektedir. Yüksek yüklerde Stribeck eğrisinin kaymasından dolayı aynı yağlama sayısı için daha küçük sürtünme katsayısı gözlemlenir.

Bu çalışmada, model, pratikte yüzeyler her zaman Gauss dağılım göstermediği için, Gauss olmayan pürüzlü yüzey yüksekliği dağılımlarına adapte edilmiştir. Weibull

dağılımı uygulanarak, karışık EHD modeli, pürüzlü yüzeyler tarafından taşınan yükler olan kontak basınç hesaplamaları ile değiştirilmiştir. Yük ve yüzey pürüzlüğü parametrelerinin Stribeck eğrisi üzerine etkileri analiz edilmiştir. Skewness ve Kurtosis parametrelerinin karışık EHD rejimi üzerine etkileri incelenmiş ve karşılaştırma yapmak için Stribeck eğrisi, hem Gauss hem Gauss olmayan pürüzlü yüzey yüksekliği dağılımları için çizdirilmiştir. Son olarak, Gauss olmayan yüzeyler için karışık EHD modeli, sürtünmesel güç kayıplarını hesaplamak için bir düz dişli çiftine uygulanmıştır. Gauss değerinden daha küçük Sk değerleri ve daha yüksek Ku değerleri için, Gauss pürüzlü yüzey yüksekliği dağılımından daha küçük sürtünmesel güç kaybı veren sürtünme katsayısı daha küçüktür. Bu yüzden, dişli diş yüzeyleri sıfırdan küçük Sk değerleri ve 2.72 değerinden küçük Ku değerlerini verecek şekilde işlenmelidir.

Anahtar Kelimeler: Dişli Yağlaması, Karışık EHD Modeli, Sürtünme Katsayısı, Yüzey Pürüzlülüğü, Gauss Dağılımı, Pürüzlü Yüzey Kontağı, Yağ Film Kalınlığı, Stribeck Eğrisi, Weibull Dağılımı, Sürtünme Güç Kaybı.

ACKNOWLEDGMENTS

I would like to express my appreciation to my supervisor Prof. Dr. Metin Akkök for his guidance and support to my thesis studies.

I would also like to thank to Hakan İşçi and TAI, for advice and supports to this research and to have opportunity of this thesis to expand a supported project (SAYP Project) between TAI and METU.

I am thankful to my parents and to my sisters for their endless support.

Finally, thanks to my husband Feyyaz Okşayan for full of love in my whole life.

Ankara, 01 September 2014

Yeliz Okşayan

TABLE OF CONTENTS

LIST OF TABLES

TABLES

LIST OF FIGURES

FIGURES

NOMENCLATURE

A_{C_i}	Area of contact of a single asperity, $[m^2]$
A_H	Contact area of the hydrodynamic component, $[m^2]$
A_{ie}	Elastic contact area for asperity deformations, $[m^2]$
A_{iep}	Elastic plastic contact area, $[m^2]$
A_{ip}	Plastic contact area for asperity deformations, $[m^2]$
A_{nom}	Nominal area, $[m^2]$
A_r	Total real contact area, $[m^2]$
a_i	Gelinck et al. fitting parameters, [-]
B	Length of cylinder or face width, [m]
B_n	Gamma function, [-]
b	Half Hertzian width of the contact, [m]
C_T	Constant for EHL line contact, [-]
CR	Gear pair contact ratio, [-]
D x	Elastic deformation, [m]
d_d	Distance between the mean plane through the summits and the heights, [m]
E	Reduced elastic modulus, [Pa]
F	Applied load, [N]
F_C	Load carried by the interacting asperities, [N]
F_f	Friction Force, [N]
F_{f_C}	Asperity friction force, [N]
F_{f_H}	Hydrodynamic friction force, [N]
F_H	Load carried by the hydrodynamic component, [N]
F_{ie}	Load carried by an elastically deformed asperity, [N]
F_{iep}	Load carried by an elasto-plastically deformed asperity, [N]

F_{ie}	Load carried by a plastic deformed asperity, [N]
F_T	Total normal load, [N]
f_C	Constant, coefficient of friction of an asperity part, [-]
f	Coefficient of Friction, [-]
fr	Frequency, [Hz]
G	Dimensionless lubricant number, [-]
H	Dimensionless the film thickness, [-]
H_C	Dimensionless central film thickness
H_{EI}	Dimensionless film thickness asymptote for elastic-isoviscous situation, [-]
H_{EP}	Dimensionless film thickness asymptote for elastic-piezoviscous situation, [-]
H_{RI}	Dimensionless film thickness asymptote for rigid-isoviscous situation, [-]
H_{RP}	Dimensionless film thickness asymptote for rigid-piezoviscous situation, [-]
H_m	Hardness of the material, [GPa]
h	Film Thickness, [m]
h	Dimensionless film thickness number, [-]
h_c	Central Film Thickness, [m]
h_0	Initial film thickness, [m]
h_s	Film thickness between the mean plane through the summits and the heights, [m]
$h_{starved}$	Starved oil film thickness, [m]
$h_{thermal}$	Thermal oil film thickness, [m]
k	Thermal conductivity, $[W \; m.K]$
Ku	Kurtosis parameter of Weibull distribution, [-]
L	Lubricant number, [-]
M	Load number, [-]
m	Module, [mm/tooth]

N	Number of asperities in contact, [-]
N_1	Number of tooth for pinion, [teeth]
N_2	Number of tooth for gear, [teeth]
n	Density of asperities, $[m^{-2}]$
n_1	Pinion speed, [rpm]
n_2	Gear speed, [rpm]
n'	Dimensionless density of asperities, [-]
$P_{Sliding}$	Sliding power loss, [W]
p	Distributed pressure, [Pa]
p_{av}	Average pressure in the contact, [Pa]
p_b	Base pitch, [m]
p_C	Central asperity pressure, [Pa]
$p_{Contact}$	Nominal contact pressure, [Pa]
p_H	Hydrodynamic pressure, [Pa]
p_T	Total pressure, [Pa]
p_{Hertz}	Hertz Pressure, [Pa]
p	Dimensionless pressure parameter, [-]
p_C	Dimensionless average central asperity pressure, [Pa]
Q	Thermal loading parameter, [-]
R	Reduced radius of curvature, [m]
R_a	Combined surface roughness values, [m]
R_{A1}	Radius to point A, gear, [mm]
R_{A2}	Radius to point A, pinion, [mm]
R_{sa}	Radius of hemispherical asperity, [m]
R_1	Radius of curvature of contacting surface 1, [m]
R_2	Radius of curvature of contacting surface 2, [m]
$r_{b,1}$	Base radius for pinion, [mm]
$r_{b,2}$	Base radius for gear, [mm]
$r_{o,1}$	Outer radius for pinion, [mm]
$r_{o,2}$	Outer radius for gear, [mm]

$r_{p,1}$	Pitch radius for pinion, [mm]
$r_{p,2}$	Pitch radius for gear, [mm]
s	Dimensionless form of argument of the height distribution $\emptyset$ s , m
Sk	Skewness parameter of Weibull distribution, [-]
SR	Slip ratio, [-]
S_y	Yield strength, [Pa]
s_p	Distance along the line of action to point chosen from the pitch point, [m]
s_0	Temperature Constant, [-]
T	Temperature of lubricant, [$°C$]
T_0	Ambient temperature, [$°C$]
U_Σ	Dimensionless velocity number, [-]
u	Velocity component in x direction,[m/s]
u_{dif}	Sliding velocity, [m/s]
u_R	Rolling velocity, [m/s]
u_s	Sum Velocity, [m/s]
v	Velocity component in y direction,[m/s]
v_{RA1}	Rolling velocity at point A, pinion, [m/s]
v_{RA2}	Rolling velocity at point A, gear, [m/s]
v_{TA1}	Tangential velocity at point A, pinion, [m/s]
v_{TA2}	Tangential velocity at point A, gear, [m/s]
W	Dimensionless load number, [-]
w	Velocity component in y direction,[m/s]
ω_c	Indentation for plastic deformation, [m]
w_e	Critical indentation of an asperity for elastic deformations, [m]
w_i	Indentation of an asperity for deformations, [m]
w_p	Critical indentation of an asperity for plastic deformations, [m]
X	Dimensionless half width parameter, [-]
x	Direction of the fluid, [m]
y	Direction axis perpendicular to x direction,[m]
Z	Contact Length, [m]

z	Direction of the thickness height, [m]
z	Argument of the height distribution $\emptyset_s$, m
z_i	Individual summit height, [m]
Δ_c	Amplitude of the sinusoidal surface, [m]
α	Pressure viscosity index, $[Pa^{-1}]$
β	Asperity radius, [m/s]
β_W	Correction factor of numerical solution of Wolveridge, [-]
$\beta_{Weibull}$	Shape parameter of Weibull distribution, [-]
γ	Temperature coefficient of viscosity, $[K^{-1}]$
γ_1	Load share factor for hydrodynamic component in mixed lubrication regime, [-]
γ_2	Load share factor for asperity contact component in mixed lubrication regime, [-]
γ	Shear rate, $[s^{-1}]$
μ	Dynamic viscosity, [Pas]
η	Fluid viscosity, [Pas]
η_0	Viscosity at ambient pressure, [Pas]
η_w	Scale parameter of Weibull distribution, [-]
η_∞	Viscosity Constant, [-]
λ_s	Separation, [-]
$\lambda_{starved}$	Starved Separation, [-]
ρ	Fluid density, $[kg/m^3]$
ρ_0	Density at ambient pressure, $[kg/m^3]$
σ_s	Standard deviation of asperities, [m]
σ_s'	Dimensionless standard deviation of asperities, [-]
τ	Shear stress, [Pa]
τ_{C_i}	Shear stress at the asperity contact, [Pa]
τ_0	Eyring shear stress, [Pa]
τ_H	Hydrodynamic shear stress, [Pa]
φ	Pressure angle, [degree]

ϕ_A	Pressure angle at point A, [degree]	
$\emptyset\ s$	Standardized height distribution of the summits, [-]	
$\int$	Lubrication number, [-]	
ω_1	Angular velocity of pinion, [rad/sec]	
ω_2	Angular velocity of gear, [rad/sec]	
ϑ	Poisson's modulus, [-]	
ψ	Plasticity index, [-]	
ψ_i	Dimensionless lubricant inlet length, [-]	

CHAPTER 1

INTRODUCTION

1.1.   Introduction

The gearbox function is to transform a revolving moment to either a slower rotating and reduce the engine speed in order to generate a large torque.

Reduction in friction is a wide effect on getting low power loss of gears. Besides this, selection of oil that produces less friction between gears and modifying the tooth geometry produces less sliding. In order to keep the losses at a minimum, the gears are lubricated with oil or other lubricants. The surfaces are separated from each other by the lubricant.

Gear systems operate in elastohydrodynamic lubrication (EHL) regime or in boundary lubrication regime or mostly in mixed lubrication and therefore it is important to know that these systems operate in which lubrication regimes. Boundary lubrication is the lubrication regime where the elastic deformations of the asperities are mostly in contact with even though a fluid is present. Mixed lubrication is the lubrication regime where the average film thickness is in the order of the roughness of the surfaces and the contact load is carried by both asperity contact and oil film. Elastohydrodynamic lubrication is the lubrication regime where the elastic deformations of the surfaces are in the order of the film thickness. Hydrodynamic lubrication is the lubrication regime where the average film thickness is much larger than the roughness of the surfaces.

There are many factors i.e. load, surface roughness parameters, oil type, viscosity change, surface velocities that define in which regime the system operates. To obtain

the regimes, friction of coefficient and surface difference known also as sliding velocity must be known. Load, surface roughness, oil viscosity, oil temperature, surface velocities and any other inputs contributes to friction coefficient calculations. The film thickness also an important effects on the system. Surface roughness and surface velocities directly effects the film thickness formation. Any variation on film thickness changes the lubrication regimes and friction coefficient. The Stribeck curve helps the specify regimes with known friction coefficient and velocities. Moreover, determining friction coefficient is achieved to be capable of obtaining power loss of the system. The value of the friction coefficient helps to improve the system and optimization studies. There are many lubrication models or studies present for friction of coefficient calculations.

1.2. Motivation of the Study

The work presented in this thesis aims to obtain a mixed EHL lubrication model and calculating the coefficient of friction on gear teeth contacts. Some input parameters are taken into account and the variation of friction coefficient is obtained. In the present study, for any gear pear and operating conditions, a mathematical program is developed in order to calculate friction coefficient taken into account viscosity change with pressure, surface roughness parameters, rough surface contact, and film thickness formation with using available models. This situation can allow the factors that effect the model or system.

In this thesis, Gelinck and Schipper's mixed lubrication model is used as a reference. Gelinck and Schipper proposed a mixed elastohydrodynamic lubrication model by taking the Moes central film thickness equation and Greenwood's asperity contact pressure expression, including Johnson's load share concept that applies load share factors. This model is presented in order to predict the Stribeck curve for line contacts. It can be said that this model is based on the combination of the Greenwood and Williamson contact model and the full film theory using the mixed lubrication model of Johnson. With this model, this is able to predict friction and determine the transitions between the different lubrication regimes: elastohydrodynamic

lubrication, mixed lubrication, and boundary lubrication. A program is developed by Matlab. With this program, it is able to calculate and plot variation of pressure, film thickness for isothermal and thermal conditions, separation, coefficient of friction and the Stribeck Curve for line contact conditions. In the calculations, the effects of contact load and deformation of surface asperities on the oil film thickness and friction coefficient, oil viscosity change with pressure and temperature, gear type and gear geometry, slide to roll ratio, surface roughness effects are taken into account. The program also gives a calculation method for point contact conditions.

Moreover, mixed EHL model is adopted and applicable to rough surface contacts including non-Gaussian distribution surface heights. Weibull distributions method is used to simulate non-Gaussian distribution surface heights instead of the method of Greenwood and Williamson.

There is a solution method of friction power loss and kinematics of velocities of gear pair after the coefficient of friction calculations.

1.3. Scope

This thesis consists of seven chapters. The explanation of the chapters is written as follows respectively.

Chapter 1 includes the introduction and motivation of the study.

Chapter 2 gives the literature survey of lubrication theory, oil film thickness calculations and formulations, surface roughness effects, asperity contacts, EHL lubrication and isothermal mixed EHL lubrication models. Studies include analytical formulations, numerical formulations and experimental data.

Chapter 3 focuses on mixed EHL models that used as a reference for this study and obtains an isothermal, steady state mixed EHL model.

Chapter 4 details about the Stribeck curve and the parameters how they effect the Stribeck curve and friction coefficient.

Chapter 5 focuses on applying Weibull distribution on mixed EHL model for non-Gaussian asperity summit distributions conditions.

Chapter 6 gives information about power losses of the gear systems and a case study for spur gear pair to calculate frictional power loss.

Chapter 7 comprises a conclusion for the whole study. This chapter also gives a summary on the contribution of the thesis.

CHAPTER 2

LITERATURE SURVEY ON MIXED ELASTOHYDRODYNAMIC LUBRICATION

2.1. Introduction

Friction studied by many scientists and the studies start with first friction laws obtained by Leonardo Da Vinci; then roughness theory of friction by Leonard Euler, contacts of deformable solids by Heinrich Hertz, real contact areas and adhesion theory by Holm, Ernst and Merchant, Bowden and Tabor [1]. The Deformation of solid materials was investigated by Robert Hooke. Later, the lubrication theories have been added to friction. Osborne Reynolds derived the Reynolds equation for fluid film lubrication. In this literature survey, Elastohydrodynamic lubrication theories will be explained including the following subjects: EHL film thickness, EHL surface contact, rheological models and mixed EHL.

2.2. Rough Surface Contact

Contact problems between rough surfaces have been studied by many researchers. It is known that in the real life, the surfaces that are in contact are always rough. The first attempt is done in 1966 by Greenwood and Williamson [2] for elastic rough surface contacts and assumed that rough surface asperities deforms elastically. Actually, in reality, if material's yield strength is exceeded, elastic-plastic deformations occur. This situation is investigated at later times. Greenwood and Williamson [2] model assumes a Gaussian distribution for asperity summits and the contacting two rough surfaces are assumed like a rough surface that deforms elastically and a flat surface that is rigid. In the model, asperities have the same

radius for simplicity and summits have Gauss height distribution. By Greenwood and Tripp [3] the contact model is applied for two rough surfaces.

In 1972, Johnson et al. [4] proposed the load sharing concept for mixed lubrications or for an asperity contact in EHL. They used the Greenwood Williamson [2] asperity contact model for rough surfaces.

After, asperity contact studies of Greenwood and Williamson and Johnson et al., in 1999, Gelinck D. and J. Schipper [5] studied the elastic deformation of rough surfaces for EHL line contact conditions. They used Greenwood and Tripp [3] model for line contacts. The model calculates the real contact area, number of contacts and half-width of the contact region. In their solution, the central pressure is expressed as a function of fit parameters using numerical techniques.

In 2000, Zhao et al. [6] proposed a model which includes a formula that express the transition of elastic, elastic-plastic- plastic behaviors or regions.

2.3.   EHL and Film Thickness

For lubricated surfaces, the film thickness studies in EHL begin with Martin [7] in 1916. Martin assumed rigid surfaces with iso-viscous lubricant and calculated the minimum oil film thickness. Grubin [8] obtained an approximate solution to get a new elastohydrodynamic film thickness formula that depend on load, speed etc. This formula is used later by other researcher to get more exact elastohydrodynamic film thickness. The numerical calculations for oil film thickness obtained by Hamrock and Dowson [9] gives the film thickness expression which is convenient for isothermal and rolling contact conditions. However, this formula does not work at high rolling speeds. The other film thickness expression, given by Moes [10] groups the parameters that affect the film thickness in dimensionless forms. Moes [10] assumed that lubricant is incompressible and Barus type viscosity-pressure relation is applicable.

In 1979, Brewe, Hamrock, and Taylor [11] investigated the influence of geometry on the isothermal hydrodynamic film separating two rigid solids.

In 1983, Jacobson and Hamrock [12] obtained an ideal visco-plastic, non- Newtonian model for EHL lubrication regimes. In 1985, Tevaarwerk [13] developed a new lubricant friction model which includes sliding and rolling contacts or slide to roll ratio, and rheology and thermal behaviors.

In 1986, Houpert and Hamrock [14] developed a fast approach that allows lubricant compressibility, the use of Roelands's viscosity model, a general mesh (nonconstant step), and elastic deformations for calculating film thickness and pressure in elastohydrodynamic-lubricated contacts at high loads.

In 1989, Pan and Hamrock [15] numerically evaluated the film thickness and pressure in elastohydrodynamically lubrication conjunctions for the operating parameters given.

2.4. Rough EHL Contact

Patir and Cheng [16] obtained a new numerical solution for a rough surface in the partial lubrication regime. In the model, surface roughness parameter effects are taken into account. The solution is compared with smooth surface solutions.

In 1982, Majumdar and Hamrock [17] developed a numerical solution of an EHL line contact between two long cylinders with rough surfaces. The Reynolds equation and elastic deformation equations are used to express the film thickness and pressure. In the calculations, the surface roughness is taken into account. The solution also includes the frictional heating of asperities.

In 1985, Tripp and Hamrock [18] obtained a theoretical method using flow factors that results in the Reynolds equation and applicable for piezoviscous-elastic line contacts. In the method, the effects of surface roughness are studied.

Transient EHL models are also introduced. In 1997, Larsson [19] performed a transient elastohydrodynamic lubrication solution for spur gears. Along contact line, film thickness and load distribution is solved and calculated numerically includes with transient effects. In the model, isothermal lubrication and non-Newtonian fluid is applicable.

In 2006, Bair and Khonsari [20] showed the shear thinning behavior of the fluid and compared the analytical and experimental data. To account for shear thinning effect, Bair proposed a correction factor for predicting the film thickness in an EHL line contact.

2.5.   Mixed Lubrication

In 2002, Gelinck and Schipper [25] proposed a mixed elastohydrodynamic lubrication model by taking the Moes [10] central film thickness equation and Greenwood [2] asperity contact pressure expression, including Johnson [4] concept of applying a load share factor to the hydrodynamic component. This model is presented in order to predict the Stribeck curve for line contacts. With this model, it is possible to predict friction and determine the transitions between different lubrication regimes: elastohydrodynamic lubrication, mixed lubrication, and boundary lubrication.

In 2005, Faraon [26] investigated the influence of some parameters on the coefficient of friction and the Stribeck Curve. Faraon [26] studied Gelinck and Schipper [25] statistical and deterministic mixed lubrication model. These parameters are velocity, pressure, load, surface roughness etc. Moreover, Faraon [26] applied a starvation model to this mixed EHL model. And measured shear stress-pressure behavior and obtained the Stribeck curve.

In 2006, Xiaobin Lu, M. M. Khonsari, E. R. M. Gelinck [27], applied a mixed lubrication model for steady state and isothermal line contact conditions. The film thickness formula is determined with using Moes [10] thickness formulas and Roeland's viscosity-pressure-temperature model. Friction coefficient for bearing is

obtained by using numerical bisection iterative method. Also, change in friction coefficient with oil temperature and load is investigated and the Solutions are compared with experiments.

In 2008, S. Akbarzadeh M. M. Khonsari [21] applied the load-sharing concept of Johnson et al. [4] to predict the performance of a spur gear, the viscosity of lubricant changes with pressure. Akbarzadeh M. M. Khonsari [21] extended the model that includes smooth surface contacts with using surface roughness effects. In the model, the shear thinning effects are taken into account. The model calculates film thickness, fluid film load and friction coefficient of spur gears.

In 2009, R. Larsson [22] proposed a new numerical technique and calculated the flow factor with surface roughness effects. A two-level model considering lubrication in all regimes is presented. According to that study, the modeling takes place on two levels, global and cell levels. On the cell level, the surface roughness and the lubricant effects can be modeled. On the global level, the deformation effects of the contacting bodies can be modeled. It can be said that the deformation of the asperities are modeled in cell level. In the model, the average contact pressure and real contact area, friction coefficient at the boundary lubrication regime are calculated. The model optimizes friction with global and cell levels.

In 2010, J. Y. Jang M. M. Khonsari [23] applied the elastohydrodynamic line contact model for two rough surfaces. They used the Reynolds equation, the hydrodynamic pressure solution of Patir and Cheng [16] and asperity contact model. The non-Newtonian behavior and the shear thinning effect of the fluid are applicable in the model. In their study, it was proven that the film thickness for the rough surfaces is larger than that for the smooth surfaces. When surfaces are rough, the load is supported by the combination of the hydrodynamic pressure and the asperities.

In 2012, M. Masjedi M. M. Khonsari [24] developed the central and minimum film thickness formula in line contact EHL and derived the Reynolds equations written in dimensionless form including the surface roughness. The formulas are based on the simultaneous solution to the modified the Reynolds equation and surface

deformation equation with consideration of elastic, plastic and elasto-plastic deformation of the surface asperities. They run the governing equations that are discretized using the finite difference method and solved simultaneously for pressure and film profiles. Forward finite difference is used to solve the equations, and the Newton- Raphson algorithm is applied since the equations are nonlinear. Then**,** Masjedi M. M. Khonsari [24] investigated the effect of surface roughness on film thickness and pressure profiles. According to their study, the film thickness increases as the roughness increases. This can be attributed to contribution of the load carried by the asperities as well as by the flow factors in the Reynolds equation.

CHAPTER 3

MIXED EHL LUBRICATION MODEL

3.1. Introduction

A mixed lubrication presents between boundary and hydrodynamic lubrication .The fluid film thickness is slightly greater than the surface roughness; so that there is a little asperity contact, but the surfaces affect each other. Mixed lubrication model composes of rough surface EHL contact models that are asperity contact model with EHL film component and Hertz theory. EHL film is modeled using a variation of the Reynolds equation for fluid films, which is an integrated version of the Navier-Stokes equations across the film thickness. Rough surface contact is modeled using elastic deformable asperities.

In order to obtain mixed lubrication model, firstly, asperity contact model, load share model and EHL model should be studied. In this thesis, Greenwood and Williamson [2] elastic contact model, Johnson [4] load share concept and Gelinck and Schipper [25] mixed lubrication models are deeply studied.

3.2. Rough Surface Contact Models

3.2.1. Greenwood and Williamson Model

In the Greenwood and Williamson's [2] theory, elastic contact is applied for rough surface. In their model, the summits are considered as a parabolic, having the same radius. In their model, the contact occurs between an elastic deformable rough surface and a smooth flat surface in order to simulate two rough surfaces. It is known that if it is looked into, summits are seen on rough surface. If the mean line is placed

through the surface summit heights, asperity contact component can be calculated. Greenwood and Williamson [2] applied a Gauss distribution method for summit heights. In Figure 1, the contact between a smooth surface and a Rough surface with the corresponding Gaussian distribution of the summits is shown. If the mean line is placed through the surface heights, EHL component can be calculated.
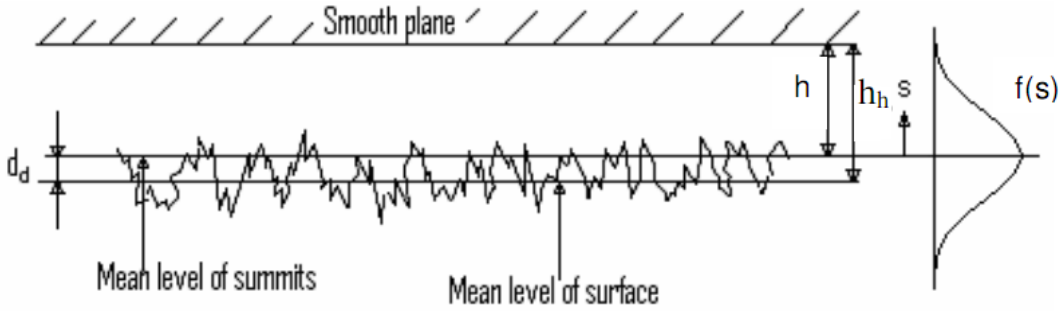
Figure 1 The Contact Between a Smooth Surface and a Rough Surface with the Corresponding Gaussian Distribution of the Summits [26]

The summits deform elastically according to the Hertzian theory. Greenwood and Williamson [2] derived expressions for the number of summits in contact is written:

$$N = nA_{nom}F_0(\frac{h}{\sigma_s}) \tag{3.1}$$

$$A_r = \pi n\beta\sigma_s A_{nom}F_1 \frac{h}{\sigma_s} \tag{3.2}$$

$$F_T = \frac{2}{3}n\beta\sigma_s \sqrt{\frac{\sigma_s}{\beta}} E A_{nom}F_{\frac{3}{2}} \frac{h}{\sigma_s} \tag{3.3}$$

where

β is an asperity radius, [m]

σ_s is the standard deviation of the summit heights.

E is the reduced elastic modulus, [Pa]

n is the density of asperities, $[m^{-2}]$

h is the film thickness, [m]

A_{nom} is the nominal contact area, $[m^2]$

A_r is the total real contact area, $[m^2]$

F_T is the applied normal load, [N]

In Eqn. (3.1), (3.2) and (3.3), integral identity is used. The general form of this identity is:

$$F_j = \int_h^\infty (s - h/\sigma_s)^j \emptyset(s)\, ds \tag{3.4}$$

where

$s = z/\sigma_s$, where z is argument of the height distribution $\emptyset(s)$, m

$f(s)$ is the normalized Gaussian distribution function.

$$\emptyset(s) = \frac{1}{\sqrt{2\pi}} \exp\left(\frac{-s^2}{2}\right) \tag{3.5}$$

Eqn. (3.4) gives the normal load carried by asperities. The division of total load to nominal area is written as:

$$p_{Contact} = \frac{F_T}{A_{nom}} \tag{3.6}$$

where

$p_{Contact}$ is the nominal contact pressure, [Pa]

3.2.2. Elastic-Plastic Contact Model

Many researchers studied on elastic-plastic contact models. Greenwood and Williamson [2] defines a critical indentation of an asperity for elastic deformations. This definition includes material hardness and asperity radius and defines elastic deformation criteria.

$$w_e = \left(0.94 \frac{H_m}{E}\right)^2 \beta \tag{3.7}$$

where

H_m is the hardness of the material, [GPa]

When the deformation of the asperity is larger than the critical indentation, elastic-plastic deformation occurs. When considering the contact between rough surfaces, the local pressure in an asperity pressure can be very high for heavy loads or high speeds. It causes the elasto-plastic or plastic deformation in an asperity contact. The contact plastic deformation affects the EHL load-carrying capacity.

Later, Johnson [4] obtained a new definition for the fully plastic deformations. If the deformation of asperity is 54 times of the critical indentation, plastic deformation occurs for metals.

Between these deformation regions elastic-plastic deformations occur. To investigate these regimes, Zhao [6] applied a new solution after Greenwood and Williamson [2] and Johnson [4].

According to solution, a contact area is determined for the elastic-plastic deformation regions and for spherical radius asperities.

$$A_{iep} = \pi\beta_i w_i \left[1 - 2\left(\frac{w_i - w_e}{w_p - w_e}\right)^3 + 3\left(\frac{w_i - w_e}{w_p - w_e}\right)^2 \right] \tag{3.8}$$

where

w_i is the indentation of an asperity for deformations, [m]

w_p is the critical indentation of an asperity for plastic deformations, [m]

According to Zhao [6], the deformation of asperity can be changed between elastic, elastic-plastic and plastic deformations. So, the asperity contact area is changes according to asperity indentation. In the Eqn. (3.9), the relation with asperity contact area and asperity indentation changes between deformation transitions.

$$A_i(w_i) = \begin{cases} A_{ie}(w_i) & if \quad w_i \leq w_e \\ A_{iep}(w_i) & if \quad w_e < w_i \leq w_p \\ A_{ip}(w_i) & if \quad w_i > w_p \end{cases} \tag{3.9}$$

where

$$A_{ie} = \pi\beta_i w_i \tag{3.10}$$

A_{ie} is the elastic contact area, $[m^2]$

$$A_{ip} = 2\pi\beta_i w_i \tag{3.11}$$

A_{ip} is the plastic contact area,$[m^2]$

Similarly, Zhao [6] determined the load carried by each asperity.

$$F_i\ w_i\ =\ \begin{matrix} F_{ie}\ w_i & if & w_i \le w_e \\ F_{iep}\ w_i & if & w_e < w_i \le w_p \\ F_{ip}\ w_i & if & w_i > w_p \end{matrix} \tag{3.12}$$

where

$$F_{ie} = \frac{4}{3}E'\beta_i^{0.5}w_i^{1.5} \tag{3.13}$$

F_{ie} is the load carried by an elastically deformed asperity, [N]

$$F_{iep} = \ H_m - 0.6H_m\frac{\ln\ w_p\ - \ln\ w_i}{\ln\ w_p\ - \ln\ w_e}\ A_{iep} \tag{3.14}$$

F_{iep} is the load carried by an elasto-plastically deformed asperity, [N]

$$F_{ie} = H_m A_{ip} \tag{3.15}$$

F_{ie} is the load carried by a plastic deformed asperity, [N]

Zhao [6] determined the total contact area and load according to Eqn. (3.9) and Eqn. (3.12).

$$A_r = \sum_1^n A_i(w_i) \tag{3.16}$$

$$F_T = \sum_1^n F_i(w_i) \tag{3.17}$$

In Figure 2, the relation between contact area and indentation is shown. This elastic-plastic contact model is applied to mixed lubrication model by Faraon [26]. To simulate and see the difference between elastic plastic transitions on the Stribeck curve, non-run-in and run-in surfaces are used for different load inputs.
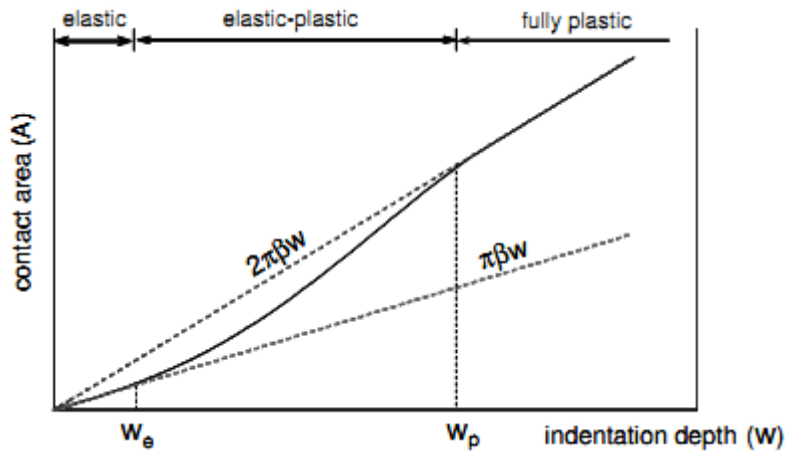
Figure 2 Contact Area as a Function of the Indentation Depth [26]

The following results occur for non-run-in surfaces according to Faraon [26]:

- At the elastic or the elastic-plastic contact conditions, the difference in the Stribeck curves is small. At this situation, the mean pressure is about 0.39 GPa. 64% of the deformed asperities are elastic-plastic deformed.
- When the mean contact pressure increases, 87% of the deformed asperities are elastic-plastic deformed.
- If plasticity is taken into account, mixed lubrication regime shifts to the left and the number of the elastic-plastic deformed asperities are increased.

There are some researchers in order to define a definition of plasticity. A plasticity index is defined by Kogut and Etsion [28]. This formula includes surface roughness parameters and surface indentation.

$$\psi = \frac{\overline{\sigma_s}}{\omega_c} \qquad (3.18)$$

Jackson and Green [29] defined a formula for spherical Hertz contacts. This formula includes an indentation for plastic deformation.

16

$$\omega_c = \left(\frac{\pi\ CS_y}{2E}\right)^2 R_{sa} \tag{3.19}$$

where

$CS_y = \min(\ C(\vartheta_1)S_{y1}\ , C\ \vartheta_2\ S_{y2})$

$C\ \vartheta\ = 1.295\exp\ 0.736\vartheta$

S_y is the yield strength, [Pa]

R_{sa} is the radius of hemispherical asperity, [m]

ϑ is Poisson's modulus, [-]

Using Eqn. (3.19), the plasticity index becomes:

$$\psi = \frac{2E}{\pi\ 1.295e^{0.736\vartheta}S_y}\ \sqrt{\frac{\sigma_s}{R_{sa}}} \tag{3.20}$$

It is appeared that the plasticity index is dependent to surface roughness. For more rough surfaces, asperities are tending to a plastic deformable state. Moreover, if plasticity index is high, asperities are tending to yield.

According to Greenwood and Williamson [2] for real surfaces the plasticity index value is changing between 0.1 and 100.

Wilson et al [30] obtained a new plasticity index formula with applying finite element method elastic plastic contact model. Wilson et al. [30] firstly derived a critical amplitude form von Mises yield criteria. If amplitude of the sinusoidal surface is smaller than critical amplitude, surfaces deform elastically.

$$\Delta_c = \frac{\sqrt{2}S_y e^{2/3\vartheta}}{3\pi E fr} \tag{3.21}$$

where

Δ_c is the amplitude of the sinusoidal surface, [m]

fr is the frequency, [Hz]

3.3.   Johnson Model

In the theory of Johnson et al. [4], the load is shared between asperity contact and hydrodynamic component. In this model Greenwood and Williamson [2] asperity contact model is used for asperity components.

According to Figure 3, the variation of pressure is Hertzian. So the fluid pressure is assumed to be semi-elliptical. The two surfaces are rough with a random distribution of asperity heights. The asperity pressure p_C , and the pressure in the lubricant film p_H, forms up the total pressure p_T. From figure, hydrodynamic pressure is larger than asperity pressure.
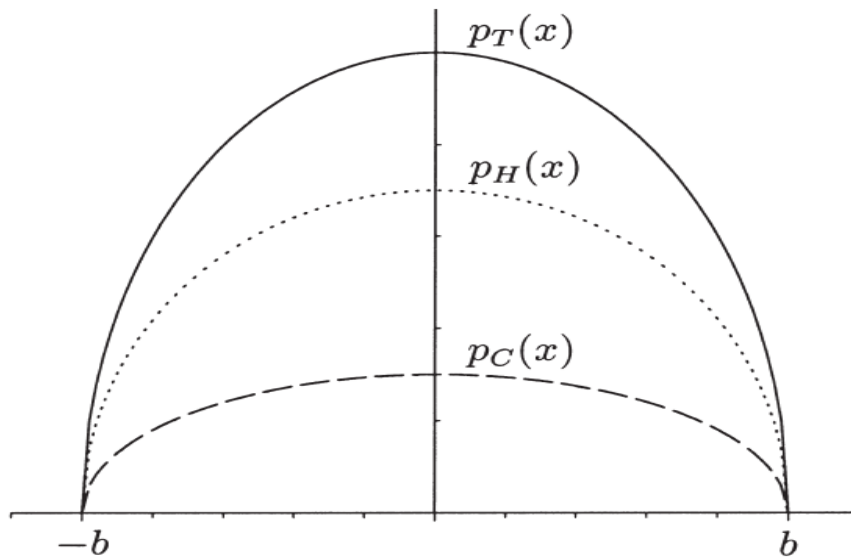
Figure 3 Variation of Pressure in Mixed Lubrication Contact according to

Johnson et al. [26]

According to Johnson et al. [4], the mixed lubrication regime is the transition regime between the boundary and the elastohydrodynamic lubrication regime. In the boundary lubrication regime, elastic asperity contact occurs and in the hydrodynamic or elastohydrodynamic regime fluid film carries the load mostly. Mixed lubrication regime carries two situations. The two load share factors γ_1 and γ_2 are generated to

simulate boundary lubrication and EHL load ratios. These factors are dependent to each other and give 1.

$$F_T = F_C + F_H \qquad (3.22)$$

where

F_C is the load carried by the interacting asperities, [N]

F_H is the load carried by the hydrodynamic component, [N]

The two factors are defined in Eqn. (3.23).

$$\gamma_1 = \frac{F_T}{F_H} , \gamma_2 = \frac{F_T}{F_C} \qquad (3.23)$$

where

γ_1 is the load share factor for hydrodynamic component in mixed lubrication according to Johnson [14] model, [-]

γ_2 is the load share factor for asperity component in mixed lubrication according to Johnson [14] model, [-]

3.4.   Gelinck et al. model

Gelinck and Schipper [25] defined a mixed lubrication model for rough surfaces. They combined the Greenwood and Williamson [2] contact model and Johnson et al. [4] load sharing model with EHL theory in a mixed lubrication model for line contacts. They predicted the Stribeck curve that shows the lubrication regimes varying with increasing velocity by using their model.

The total force is the sum of the forces of the interacting asperities and the shear force of the hydrodynamic component.

The load carried by the fluid is equal to:

$$F_H = B \int_{-\infty}^{\infty} p(x)\, dx \qquad (3.24)$$

According to Johnson [14], the normal load is written as:

$$F_T = \gamma_1 B \int_{-\infty}^{\infty} p_H \; x \; dx \qquad\qquad (3.25)$$

where

p_H is the hydrodynamic pressure, [Pa]

B is the length of cylinder or face width, [m]

Gelinck [25], in his approach assumed dimensionless pressure in the mixed lubrication regime as a Hertzian. The parameters are made dimensionless in terms of Hertzian parameters for simplicity. These parameters are

$$p = \frac{p}{p_{Hertz}} \;, \qquad X = \frac{x}{b}, \qquad W = \frac{F_T}{ER} \qquad\qquad (3.26)$$

where

b is the half width, [m],

R is the reduced radius of curvature, [m]

p is the dimensionless pressure, [-]

X is the dimensionless half width parameter, [-]

W is the dimensionless load number, [-]

p_{Hertz} is the Hertz pressure, [Pa]

For the velocity independent parameters like n and σ_s, similarity analysis is used.

$$\sigma_s' = \frac{\sigma_s}{R}, \qquad n' = nR \; \overline{\beta R} \qquad\qquad (3.27)$$

where

σ_s' is the dimensionless standard deviation of asperities, [-]

n' is the dimensionless density of asperities, [-]

For high loads the maximum pressure is equal to the maximum Hertzian pressure. The central pressure (at position X = 0) in the contact is equal to maximum pressure according to Figure 4. They obtained a curve fitting for line contact situations.
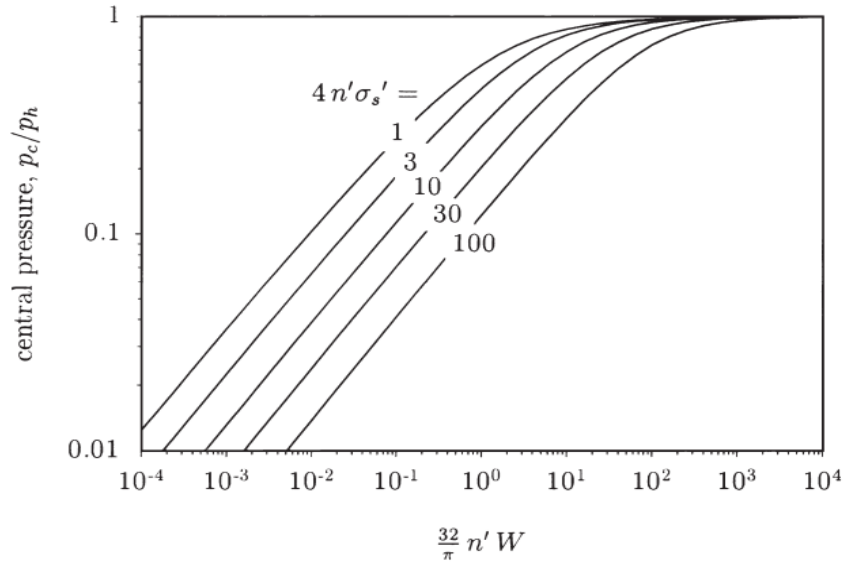
Figure 4 Central Pressure as a Function of $n'W$ for different Values of $n'\sigma_s'$ [25]

$$p_C = \left[1 + \left(a_1 n'^{a_2} \sigma_s'^{a_3} a_4 \right)^{\frac{1}{a_4}} \right] \tag{3.28}$$

where

$a_1 = 0.953, a_2 = 0.0337, a_3 = -0.442 \ and \ a_4 = -1.70.$

$$p_C = \frac{p_C}{p_{Hertz}}$$

p_C is the dimensionless central asperity pressure, [Pa]

$a_1, a_2, a_3 \ and \ a_4$ are the fitting parameters.

They also calculated the central pressure in an asperity contact. They used Greenwood & Williamson [2] model.

$$p_C = \frac{2}{3} n' \sigma_s'^{3/2} F_{\frac{3}{2}} \frac{H}{\sigma_s'} \tag{3.29}$$

The formula is adapted to Johnson model.

$$p_T = \gamma_2 p_C \tag{3.30}$$

where

p_T is the total pressure, [Pa]

21

Then, the dimensionless average central pressure become:

$$p_C = \frac{1}{\gamma_2}\left[1 + \left(a_1 n'^{a_2}\sigma_s'^{a_3}\gamma_2^{a_2}\right)^{a_4}\right]^{\frac{1}{a_4}} \tag{3.31}$$

In Gelinck and Schipper [25], the film thickness between the mean plane through the summits and the mean plane through the heights of the surface is applied using the distance d_d. The distance between these two mean lines is expressed by the standard deviation of surface heights.

The distance between these two mean lines is shown with a number that has a relation with standard deviation of surface heights.

$$d_d = 1.15\sigma_s \tag{3.32}$$

By Gelinck and Schipper [25], the central film thickness equation then is derived by curve fitting using the dimensionless numbers given by Moes [10]. Gelinck and Schipper [25] form the film thickness formula by using Moes Diagram according to Figure 5.

$$H_c = \left[\left(H_{RI}^{7/3} + H_{EI}^{7/3}\right)^{3s/7} + \left(H_{RP}^{-7/2} + H_{EP}^{-7/2}\right)^{-2s/7}\right]^{s^{-1}}$$

with

$$s = \frac{1}{5}\left(7 + 8e^{-2H_{EI}/H_{RI}}\right) \tag{3.33}$$

where;

$H_{RI} = 3M^{-1}$:Rigid-Isoviscous asymptote

$H_{RP} = 1.287L^{2/3}$:Rigid-Piezoviscous asymptote

$H_{EI} = 2.621M^{-1/5}$:Elastic-Isoviscous asymptote

$H_{EP} = 1.311M^{-1/8}L^{3/4}$:Elastic-Piezoviscous asymptote
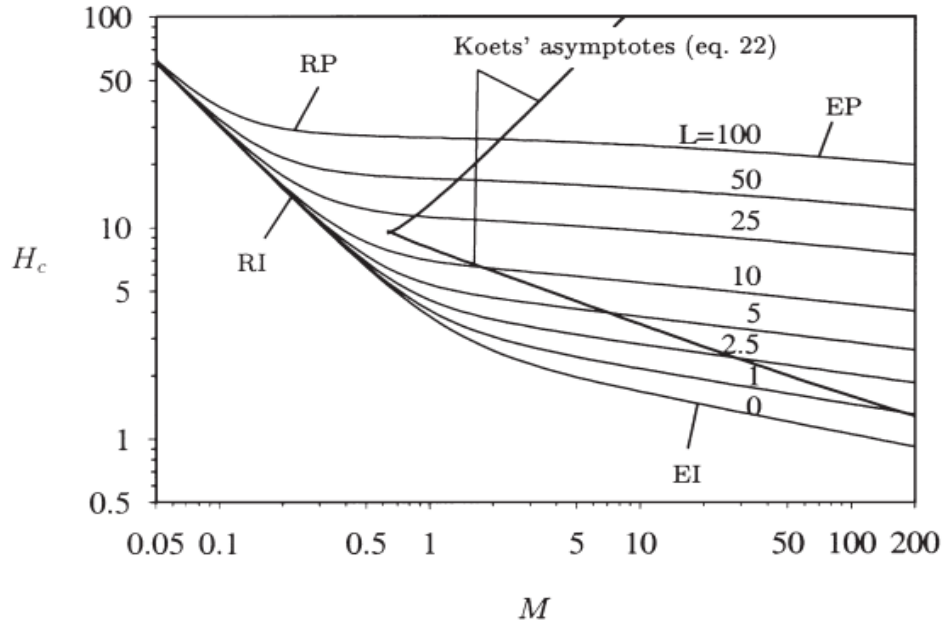
Figure 5 The Moes Diagram [25]

In the above calculations, the following dimensionless numbers are used. The first set contains four numbers. The second set consists of three numbers and follow the first set. These numbers are by Moes [10]:

$$H = \frac{h}{\overline{U_\Sigma}}; \quad M = \frac{W}{\overline{U_\Sigma}}; \quad L = G U_\Sigma^{1/4} \tag{3.34}$$

where

H is the film thickness, [-]

L is the lubricant number, [-]

M is the load number, [-]

$$G = \alpha E; \quad h = \frac{h}{R}; \quad U_\Sigma = \frac{\eta_0 u_s}{ER} \tag{3.35}$$

where

h is the dimensionless film thickness number, [-]

G is the dimensionless lubricant number, [-]

23

U_Σ is the dimensionless velocity number, [-]

α is the pressure viscosity index, $[Pa^{-1}]$

u_s is sum of the surface velocities, [m/s]

After obtaining the central film thickness and separation, the two dimensionless central pressures formula Gelinck and Schipper [25] model and Greenwood and Williamson [2] model including Johnson [4] model is equated.

$$p_C = \frac{1}{\gamma_2}\left[1 + \left(a_1 n'^{a_2}\sigma_s'^{a_3}\gamma_2^{a_2}\right)^{a_4}\right]^{\frac{1}{a_4}} = \frac{2}{3}n'\sigma_s'^{3/2}F_{\frac{3}{2}}\left(\frac{H}{\sigma_s}\right),$$ (3.36)

According to Gelinck and Schipper [25] model, the coefficient of friction in mixed lubrication for line contact conditions is obtained by solving the following parameters: F_H and F_C, film thickness and separation, asperity and hydrodynamic pressures and coefficient of friction.

Gelinck and Schcpper [25] plotted the Stribeck Curve by using the mixed EHL model. The Stribeck curve defined the transitions from boundary lubrication to mixed EHL and the transition from mixed EHL to elastohydrodynamic lubrication. In Figure 6, the variation of the friction coefficient with lubrication number as the Stribeck Curve is shown.
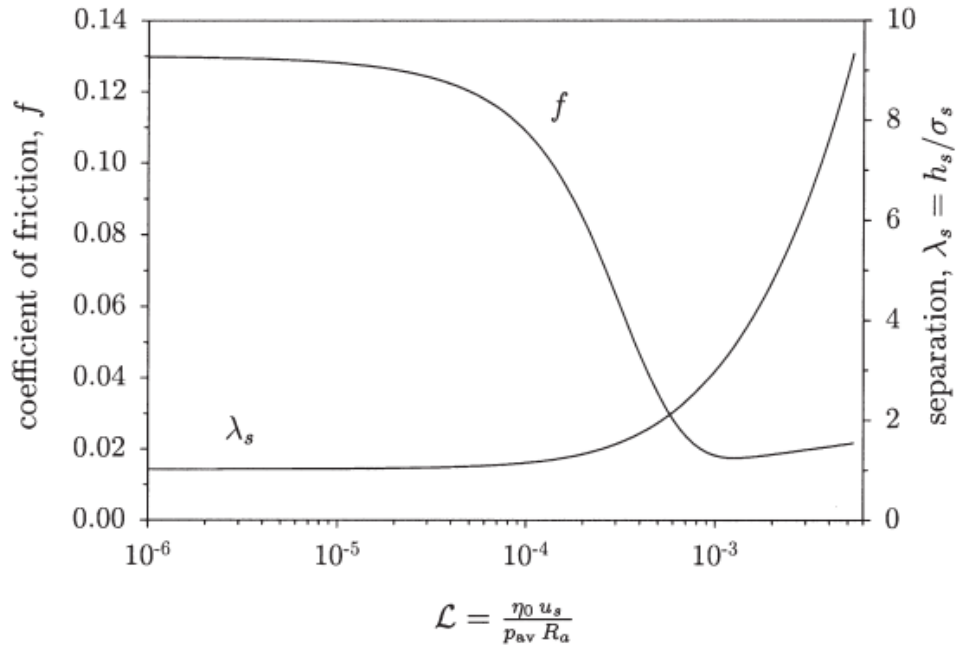
Figure 6 The Generalized Stribeck Curve and Separation of Gelinck and Schipper [25]

Lubrication number consists of ambient viscosity, average pressure in the contact, sum velocity and combined surface roughness values.

$$\int = \frac{\eta_0 u_s}{p_{av} R_a} \tag{3.37}$$

where

η_0 is the ambient viscosity, [Pa.s]

p_{av} is the average pressure in the contact, [Pa]

R_a is the combined surface roughness values, [m]

3.5.   Flow Rheology

In order to determine the friction in EHL contact, the rheological behavior of the lubricant is very important.

25

In Figure 7, elastic, viscous, non-linear viscous and linear viscous behaviors of the fluid are described with hydrodynamic shear stress shear strain relation. This figure shows a study of Evans [31] in 1983.

In the curve I, low hydrodynamic shear stress changes linearly with increasing shear rate. This situation says that the lubricant has a Newtonian fluid behavior.
In the curve II, hydrodynamic shear stress changes linearly with increasing shear strain again in the first part of the curve. At higher shear stress, it increases less and non-linearly. This situation says that the lubricant has a non-Newtonian fluid behavior. Eventually at even higher shear rates, thermal effects cause a reduction in viscosity, and thus also in the friction.
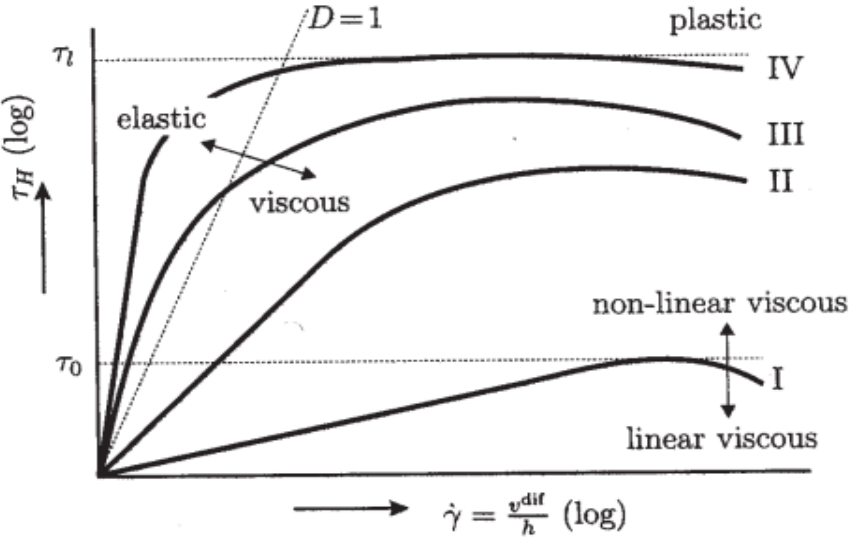
Figure 7 Types of Friction Curves [31]

However, at higher pressures, the lubricant behaves as visco-elastic material. For define the transition behavior that is changing to viscous to elastic, Deborah number is generated. Deborah number is the ratio of the time for deformation to the passing time of fluid into the contact region. So, if fluid remains in the contact region at a long time, velocity is decreased and deformation time is larger. If Deborah number is

smaller than 1, fluid behaves viscous, if this number is larger than 1, fluid behaves elastic.

According to figure, it can be said that the slope of the linear part of all curves shows that the lubricant behavior is viscous Newtonian. This situation can be written as the relation between shear stress and shear strain.

$$\tau = \eta\gamma \qquad\qquad 3.38$$

where

τ is the shear stress, [Pa]

γ is the shear rate, $[s^{-1}]$

At higher slip and non-linear increase, fluid behaves non-Newtonian. According to Eyring, the relation between shear stress and shear strain is described in this time with Eyring shear stress to define non-Newtonian behavior. Shear rate is written as:

$$\gamma = \frac{\tau_0}{\eta}\sinh\ \frac{\tau}{\tau_0} \qquad\qquad (3.39)$$

where

τ_0 is the Eyring shear stress, [Pa]

Eyring shear stress defines the non-linear parts. If $\tau \ll \tau_0$, at this time fluid has Newtonian behaves.

In the curve IV, at an increased shear strain when shear stress is constant, the fluid has a plastic behavior. However, when shear stress is increasing at non-linearly, fluid behaves elastically. In plastic behavior, the shear stress of the fluid has limited.

Bair &Winer [32] in their model developed a relation between shear stress and shear strain for limiting case of the shear stress.

$$\gamma = \frac{1}{G_l}\frac{d\tau}{dt} - \frac{\tau_1}{\eta}\ln\ \ 1 - \frac{\tau}{\tau_1} \qquad\qquad (3.40)$$

In the Figure 8, the relation between viscosity and shear rate is described.
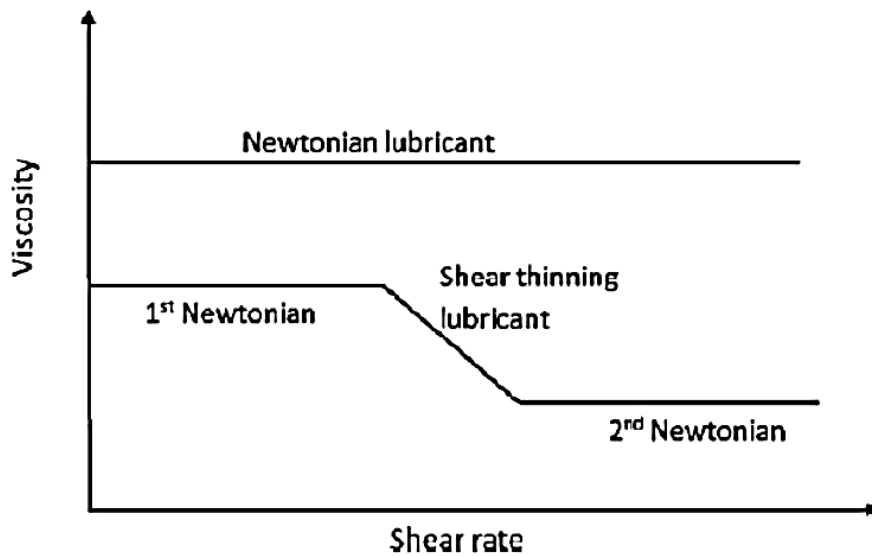
Figure 8 Characteristics of Shear Thinning Lubricant [21]

According to S. Akbarzadeh M. M. Khonsari [21], at very low and very high shear rates, the fluid has a Newtonian behavior and in the intermediate region it drops linearly. In this region, the fluid is shear thinning fluid. It represents a non-Newtonian fluid behavior.

In their model, a lubrication model is applied for Newtonian fluids. Then, the model is checked whether is applicable for non-Newtonian fluids. In the model, a correction factor that was proposed by Bair is applied. The correction factor is the ratio of the Newtonian film thickness to the shear thinning film thickness. According to film thickness calculations, film thickness and friction coefficient are smaller when shear thinning lubricant is used.

3.6.   Mixed EHL Mathematical Model

In the calculations, at first, the Reynolds equation is obtained. Then other formulations are used respectively in order to obtain coefficient of friction in the model. For all elastohydrodynamic lubrication (EHL) calculations, there are three

basic equations: the Reynolds lubrication equation, the film thickness equation and the force balance equation. The equation for thin film lubricant flow between two parallel surfaces is the generalized the Reynolds equation which is obtained with combination of equation of motion for a fluid and linear momentum equations known as Navier Stokes equation for fluid films. In Figure 9, two contacting surfaces with velocities according to their coordinates are drawn as a sample.
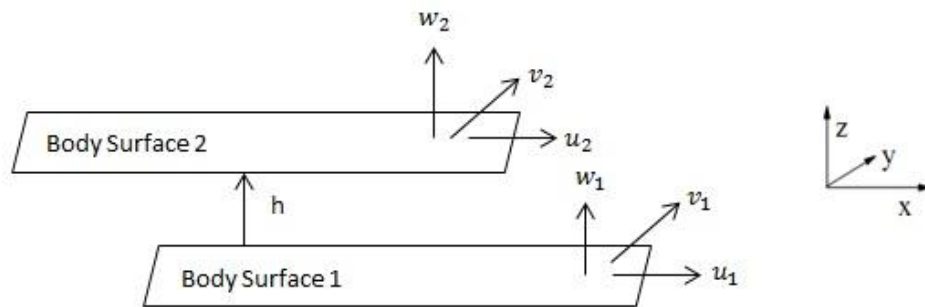
Figure 9 Two Contact Surfaces

According to Figure 9;

x is the direction of the fluid, [m]

y is the direction axis perpendicular to x direction, [m]

z is the direction of the height, [m]

u is the velocity component in x direction, [m/s]

v is the velocity component in y direction,[m/s]

w is the velocity component in z direction,[m/s]

Assuming no motion along the y-direction and also no time dependence that is considered a steady-state condition, the steady-state Reynolds equation in x dimension for a line contact is written as [25]:

$$\frac{\partial}{\partial \mathrm{x}}\left(\frac{\rho \mathrm{h}^3}{\eta}\frac{\partial p}{\partial \mathrm{x}}\right) = 6u_s\frac{\partial (\rho \mathrm{h})}{\partial \mathrm{x}} \qquad (3.41)$$

The sum velocity is constant in the direction of motion and defined as summing of two surface velocity; $u_s = u_1 + u_2$. The rolling velocity defined as the mean surface velocity of the two contacting surfaces; $u_R = (u_1 + u_2)/2$. The sliding velocity is defined as the difference between two surface velocities; $u_{dif} = u_1 - u_2$.

where

u_R is the rolling velocity, [m/s]

u_{dif} is the sliding velocity, [m/s]

ρ is the density of the oil, $kg\ m^3$

Load Distribution:

Load distribution is obtained including surface roughness effects. In a rough EHL contact, the load is shared between the fluid and the asperities. Johnson's model is used for load balance problem. According to Johnson, the total normal load (pressure) in mixed lubrication regime is sheared between the load carried by the contacting asperities and the load carried by the EHL fluid film. The mixed lubrication regime is the transition regime between the boundary and the elastohydrodynamic lubrication regime, having the characteristics of both regimes. The two coefficients γ_1 and γ_2 are dependent and refer to the Boundary Lubrication component and the EHL component respectively.

The external load applied to the contact is totally supported by the lubricant film. Therefore, the equilibrium of forces requires that the total pressure generated in the contact domain balances the external applied load F:

$$\int_{\Omega_c} p(x,y)\ d\Omega = F \qquad (3.42)$$

30

$$F = \int_{\Omega_a} p_{asperity}\, d\Omega \;+\; \int_{\Omega_H} p_{hydrodynamic}\, d\Omega \tag{3.43}$$

The total normal load F_T acting on a contact is shared between the hydrodynamic action and the interacting asperities of the surfaces.

The Asperity Contact or Boundary Lubrication Component of The Mixed Lubrication:

In the mixed lubrication regime, to calculate the pressure carried by the asperities, Greenwood and Williamson [2] model is used. Greenwood and Williamson [2] assume a normal distribution of the summits in which the probability that a random summit is in contact with the opposite surface is:

$$P(s > h) = \int_h^{\infty} \emptyset(s)\, ds \tag{3.44}$$

The hydrodynamic component of the mixed lubrication:

The EHL component in mixed lubrication regime is:

$$p_T = \gamma_1 \cdot p_H \tag{3.45}$$

So, the Reynolds equation can be reduced in the below form for the line contact as and is used in elastic deformation formula:

$$\frac{\partial}{\partial x}\left(\frac{\rho h^3}{\eta}\frac{\partial p_H}{\partial x}\right) = 6u_s \frac{\partial(\rho h)}{\partial x} \tag{3.46}$$

in which the pressure is replaced by the hydrodynamic component p_H.

Elastic Deformation of Surfaces: Oil Film Thickness:

The film thickness equation presents the elastic deformation of the surfaces caused by the pressure in the film. Moreover, the film thickness equation results from the superposition of a constant known as the rigid body displacement h_0, the initial undeformed geometry and the elastic deformation of the contacting surfaces induced by the pressure generation within the lubricant film in x direction:

$$h\ x\ = h_0 + \frac{x^2}{2R} + D\ x \qquad (3.47)$$

where

$D\ x$ is the elastic deformation, [m]

h_0 is the initial film thickness, [m]

The reduced radius of curvature is written as:

$$\frac{1}{R} = \frac{1}{R_1} + \frac{1}{R_2} \qquad (3.48)$$

where

1 and 2 represents two contacting surfaces.

The contact between two non-conforming bodies, with deformations small enough to justify the use of the linear small strain theory of elasticity, is very small compared with the radii of curvature of the undeformed surfaces. The contact stresses are concentrated close to the region of contact, consequently, the region of interest lies close to the actual contact interface. These stresses can be accurately approximated considering each body as a semi-infinite elastic solid. The linear elastic deformation, as a result of a distributed load, is obtained by integrating this equation over the pressure distribution by Timoschenko & Goodier [33]:

$$D\ x\ = \frac{2}{\pi E} \int_{-\infty}^{\infty} ln\ \frac{x - x'}{x_0}\ p\ x'\ dx' \qquad (3.49)$$

changing x' to s;

$$D(x) = -\frac{4}{\pi E} \int_{-\infty}^{\infty} p(s) \ln|x-s| \, ds \tag{3.50}$$

where

p is the distributed pressure, [Pa]

In the film shape equation the pressure p which gives the deformation is replaced by $\gamma_1 \cdot p_H$ [25]:

$$h(x) = h_\infty + \frac{x^2}{2R} - \frac{4\gamma_1}{\pi E} \int_{-\infty}^{\infty} p_H(s) \ln|x-s| \, ds \tag{3.51}$$

Then the force balance equation in which the pressure p is again replaced by the product $\gamma_1 \cdot p_H$:

$$F_N = B\gamma_1 \int_{-\infty}^{\infty} p_H(x) \, dx \tag{3.52}$$

For the EHL calculations in the mixed lubrication regime the following substitutions can be used:

$$F_N \to \frac{F_N}{\gamma_1} \, , \qquad E \to \frac{E}{\gamma_1}$$

Then, the film thickness relation mentioned in Gelinck et al [25] model (Eqn. 3.34) is used.

In the calculations, Moes [10] central film thickness equation is used.

The central film thickness formula is adapted to Johnson [4] load sharing factors. So that, EHL central film thickness formula is changed to an equation for central film thickness in mixed lubrication model.

$$H_c = \left[\left(\gamma_1^{s/2} \left(H_{RI}^{7/3} + H_{EI}^{7/3} \right)^{3s/7} + \gamma_1^{-s/2} \left(H_{RP}^{-7/2} + H_{EP}^{-7/2} \right)^{-2s/7} \right)^{s^{-1}} \right] \cdot \gamma_1^{1/2} \tag{3.53}$$

where

33

$$s = \frac{1}{5}\left(7 + 8e^{-2H_{EI}/H_{RI}}\right)$$

Combining EHL and rough line contact models:

The average central pressure generated by the asperities according to Greenwood and Williamson [2] asperity contact model is written as:

$$p_c(x) = \frac{2}{3}n\beta\sigma_s\left(\frac{\overline{\sigma_s}}{\beta}\right)E\int_h^\infty (s-h)^{3/2}\emptyset(s)\,ds \tag{3.54}$$

The dimensionless form of the asperity pressure is written as:

$$p_C = \frac{2}{3}n'\sigma_s'^{3/2}F_{\frac{3}{2}}\left(\frac{H_s}{\sigma_s'}\right) \tag{3.55}$$

According to Gelinck and Schipper [25]; the relation between central (max) pressure and Hertz pressure is obtained by curve fitting method.

$$p_C = \left[1 + \left(a_1 n'^{a_2}\sigma_s'^{a_3}\right)^{a_4}\right]^{\frac{1}{a_4}} \tag{3.56}$$

Then, Johnson et al. [4] load sharing model is applied to Eqn. (3.57), the equation becomes:

$$p_C = \left[1 + \left(a_1 n'^{a_2}\sigma_s'^{a_3}\right)^{a_4}\right]^{\frac{1}{a_4}}\frac{1}{\gamma_2} \tag{3.57}$$

Constitutive Relations:

It is necessary to use the constitutive relations as supporter formulations. In the case of viscous fluids under isothermal conditions, the following set of constitutive relations can be used.

Dependence of density on pressure:

One of the relationships used in the EHL for mineral oil is given by Dowson and Higginson [34]:

$$\rho\ p\ = \rho_0 \frac{0.59 + 1.34p}{0.59 + p} \tag{3.58}$$

where

ρ_0 is the density at ambient pressure, $[kg/m^3]$

Dependence of viscosity on pressure and temperature:

Roelands [35] pressure dependent viscosity formula is:

$$\eta\ p\ = \eta_\infty \left(\frac{\eta_0}{\eta_\infty}\right)^{1+p\ p_r\ \alpha} \tag{3.59}$$

where

$\eta_\infty\ and\ p_r$ are constants.

The temperature expanded form of Roeland [35] formula is written as:

$$\eta\ p,T\ = \eta_\infty \left(\frac{\eta_\infty}{\eta_\infty}\right)^{1+p\ p_r\ \alpha} \left(T_0 + 135\ \ T + 135\right)^{s_0} \tag{3.60}$$

where;

T_0 is the ambient temperature, $[°C]$

T is the temperature of lubricant, $[°C]$

s_0 is a constant, [-]

Eyring Shear stress - Shear rate relation:

According to Eyring model, the relation between shear rate and shear stress can be described as:

$$\gamma = \frac{\tau_0}{\eta} \sinh\ \frac{\tau_H}{\tau_0} \tag{3.61}$$

So, in case of Newtonian behavior of the lubricant the shear is given by:

$$\tau_H = \mu \gamma \tag{3.62}$$

The shear rate for a fluid flow between two contact surfaces is:

$$\gamma = \frac{u_{dif}}{h} \tag{3.63}$$

So, for the hydrodynamic condition, the shear stress can be written as:

$$\tau_H = \tau_0 \ \sinh^{-1} \ \frac{\eta u_{dif}}{h \eta_0} \tag{3.64}$$

Coefficient of Friction calculation:

The ratio of friction force to total normal force gives friction coefficient. It can be written as simply:

$$f = \frac{F_f}{F_T} \tag{3.65}$$

$$F_f = F_{f_C} \ + \ F_{f_H} \tag{3.66}$$

where

F_{f_C} is the asperity friction force, [N]

F_{f_H} is the hydrodynamic friction force, [N]

$$F_{f_C} = \ f_C . F_C \tag{3.67}$$

$$F_{f_H} = \ \tau_H \ . A_H \tag{3.68}$$

The coefficient of friction f_C of an asperity can be written as:

$$\sum_{i=1}^{N} \int_{A_{ci}} f_C \, p_{C_i} dA_{C_i} = f_C F_C \tag{3.69}$$

where

A_{C_i} is the area of contact of a single asperity, $[m^2]$

τ_{C_i} is the shear stress at the asperity contact. [Pa]

The total friction force according to Johnson model is:

$$F_f = \sum_{i=1}^{N} \int_{A_{ci}} \tau_{C_i} \, dA_{C_i} + \int_{A_H} \tau_H \, dA_H \tag{3.70}$$

where

A_H is the contact area of the hydrodynamic component, $[m^2]$

τ_H is the shear stress of the hydro-dynamic component, [Pa]

The formula of the friction coefficient becomes:

$$f = \frac{F_f}{F_T} = \frac{f_C.F_C + \tau_0 \; \sinh^{-1}\left(\frac{\eta u_{dif}}{h\eta_0}\right) A_H}{F_T} \tag{3.71}$$

Hydrodynamic shear stress can be determined by applying Eyring shear stress and shear rate. The hydrodynamic area is written for line contact conditions:

$$A_H = 2bB \tag{3.72}$$

Finally, the coefficient of friction is written for line contact conditions:

$$f = \frac{f_C.F_C + 2bB \, \tau_0 \; \sinh^{-1}\left(\frac{\eta u_{dif}}{h\eta_0}\right)}{F_T} \tag{3.73}$$

3.7. Solution Scheme of the Mixed EHL Model

The simple form of solution scheme of the steady state, Newtonian, isothermal mixed EHL model is shown in Table-1.

Table 1 Solution Scheme of the Model

Eqn. No	Formulation	Remarks
(3.22)	$F_T = F_C + F_H$	Total load equation according to force balance.
(3.23)	$\gamma_1 = \dfrac{F_T}{F_H}, \gamma_2 = \dfrac{F_T}{F_C}$	Load share factors according to Johnson et al. [4]
(3.53)	$H_c = \left(\left(\gamma_1^{s/2} \left(H_{RI}^{7/3} + H_{EI}^{7/3} \right)^{3s/7} \right) + \left(\gamma_1^{-s/2} \left(H_{RP}^{-7/2} + H_{EP}^{-7/2} \right)^{-2s/7} \right)^{s} \right)^{-1} \cdot \gamma_1^{1/2}$ where; $s = \dfrac{1}{5} \left(7 + 8e^{-2H_{EI}/H_{RI}} \right)$	Dimensionless central film thickness equation according to Moes [10] number, and Gelinck and Schipper [25] EHL line contact model.
(3.55)	$p_C = \dfrac{2}{3} n' \sigma_s'^{3/2} F_{\frac{3}{2}} \left(\dfrac{h(x)}{\sigma_s} \right)$	The central pressure generated by the asperities according to Greenwood Williamson [2] model.
(3.57)	$p_C = \left(1 + \left(a_1 n'^{a_2} \sigma_s'^{a_3} \right)^{a_4} \right)^{\frac{1}{a_4}} \dfrac{1}{\gamma_2}$	According to Gelinck and Schipper [25] curve fitting model, the relation between central (max.) pressure and Hertz pressure.

Table 1 (Continued)

Eqn. No	Formulation	Remarks
(3.64)	$$\tau_H = \tau_0 arcsinh\ \frac{\eta\gamma}{\eta_0}$$	Eyring shear stress equation in case of Newtonian behavior of the lubricant.
(3.65)	$$f = \frac{F_f}{F_T} = \frac{f_C.F_C + \tau_H A_H}{F_T}$$	Coefficient of friction formula for the Stribeck curves according to Gelinck and Schipper [25] model.
(3.73)	$$f = \frac{f_C.F_C + 2bB\ \tau_0\ \sinh^{-1}\ \frac{\eta u_{dif}}{h\eta_0}}{F_T}$$	

Assuming load carried by asperities and taking into account the input parameters (lubricant behaviors like viscosity, gear geometries, total load, speed etc.), central film thickness and central pressure generated by the asperities according to asperity contact model is calculated. On the other hand, with using the calculated load share factor, the central pressure that related with the Hertz pressure is determined. Later, the central pressure generated by the asperities will be checked with the equivalence of central pressure that related with the Hertz pressure by Gelinck and Schipper [25]. If they are equal with each other, assuming values are true and thus the coefficient of friction can be determined during an increasing velocity. This equivalence is in an iterative algorithm in order to find the right ratio between the load carried by the asperities and the load carried by the fluid.
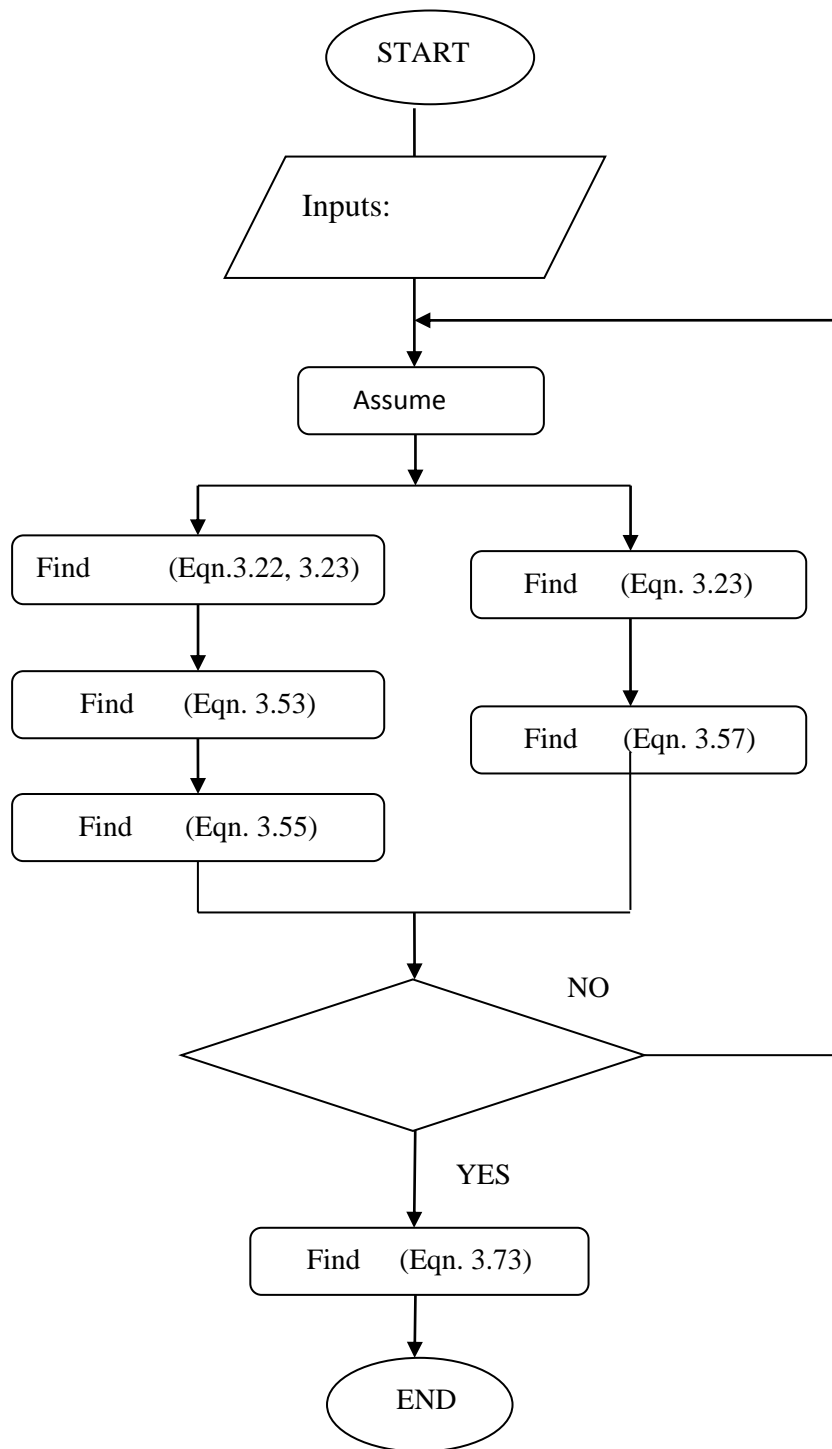
Figure 10 Flowchart of the Algorithm

3.8. Calculations and Results

The model is obtained and mathematical program is developed via Matlab program. The input parameters are shown in Figure 11.

Total Force, [N]

Combined Elasticity Modulus, [Pa]

Face Width, [m]

Reduced Radii of Curvature, [m]

Density of Asperities, [m-2]

Radius of Asperities, [m]

Standard Deviation of Asperity Height Dist., [m]

Viscosity at Ambient Pressure, [Pa.s]

Viscosity Pressure Index, [-]

Eyring shear stress, [Pa]
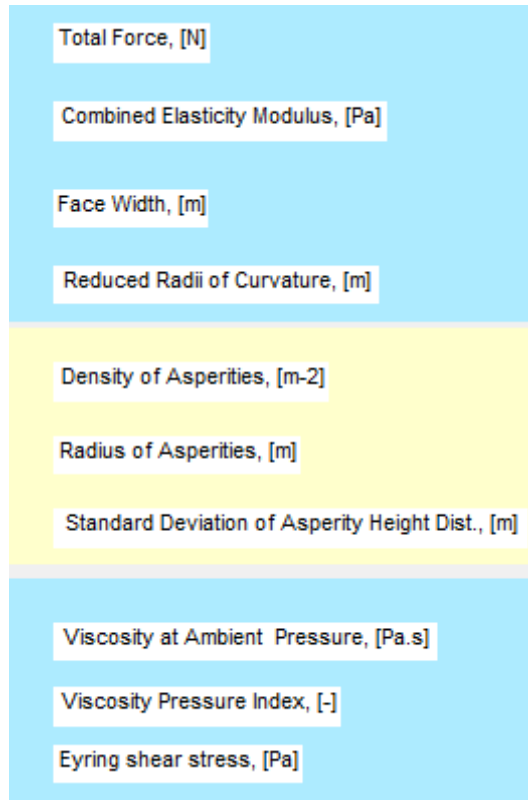
Figure 11 Input Parameters

According to solution scheme, with given input parameters the variation of the Stribeck curve, friction coefficient, film thickness, separation and pressure can be calculated. Then the operating parameters are changed and the effect on the Stribeck curve and friction coefficient is analyzed. Calculations are done for line and point contact conditions. For film thickness calculations, isothermal conditions are taken into account. Thermal conditions are also calculated without solving energy equations. Film thicknesses and friction coefficients are analyzed into two groups: fully flooded and starved conditions. Finally, the Stribeck curve is plotted using lubrication number.

The calculations are shown in Figure 12.
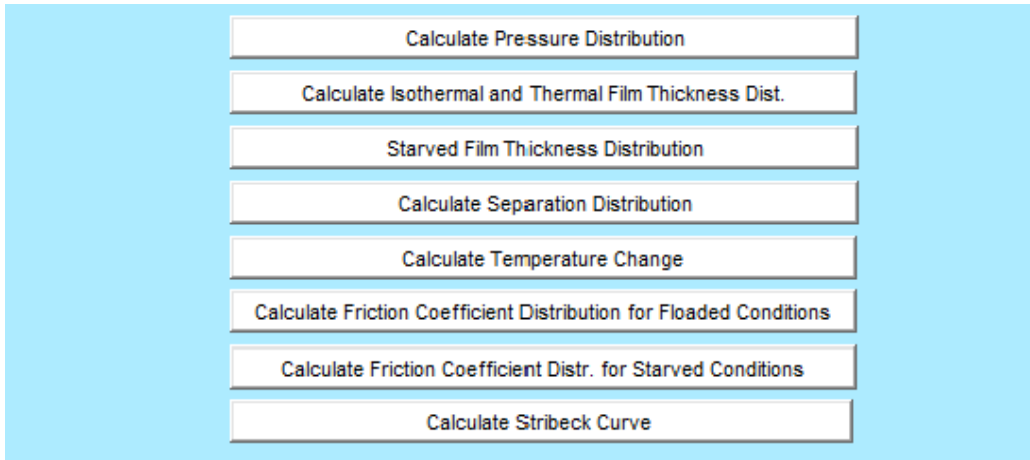
Figure 12 Calculations

3.8.1. Mixed EHL Model Calculations for Line Contacts

In the calculations, Gelinck and Schipper [25] mixed EHL model and the input parameters passed in their study is used. These parameters are shown in Table - 2.

Table 2 Input Parameters of Spur Gear Transmission [25]

Property	Value
n	$1.0 \; x \; 10^{11} m^{-2}$
β	$10.0 \; \mu m$
σ_s	$0.05 \; \mu m$
F_T	$500 \; N$
B	$10 \; mm$
E	$231 \; GPa$
R	$20 \; mm$
η_o	$20 \; mPa.s$
α	$2.0 \; x \; 10^{-8} \; Pa^{-1}$
τ_0	$2.5 \; MPa$
f_C	0.13

The main assumptions of the model are:

1. Isothermal Conditions.
2. Spur gear mesh is considered.
3. Line Contact Conditions.
4. Steady State Problem.
5. Load Sharing Concept.
6. Elastic Rough Surface Contact.
7. Flow is Laminar.

3.8.1.1. Calculation of the Pressure

In the calculations, Gelinck [25] approach is used. The asperity pressure component and the film pressure component are proportional to the Hertzian pressure. The summation of the two components gives the total pressure. Gelinck calculated the pressure for rough line contacts based on the Greenwood & Williamson model [2]. The program is run in order to obtain dimensionless pressure that is shown in Figure 13. According to Figure 13, P_H is hydrodynamic pressure, P_C is asperity pressure and P_T is total pressure.
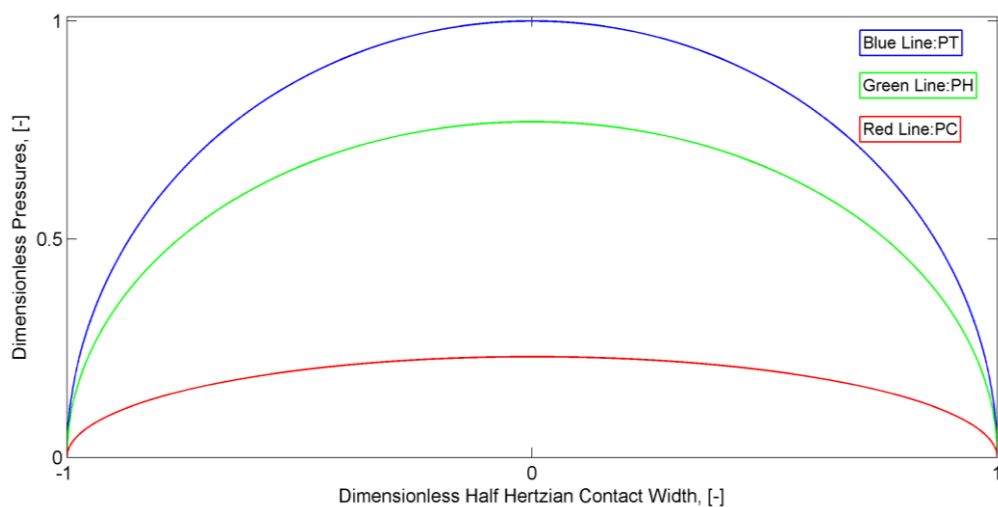
Figure 13 Dimensionless Pressure Distributions

43

3.8.1.2. Isothermal Central Film Thickness Calculations for Fully Flooded Conditions

The presence of a lubricant between two rolling sliding solids introduces a fluid body that transmits the load between these two elements ensuring that metallic contact does not occur. The generated film thickness in elastohydrodynamic contact depends mainly on the surface velocity, lubricant properties and lubricant rheological behavior at the temperatures occurring inside the contact. The lubricant film avoids metal to metal contact, reducing friction between surfaces in relative movement.

In the calculations, Gelinck and Schipper [25] mixed EHL model and the input parameters (Table -2) in their study is used as a reference. Film thickness is determined with below instructions:

1. General form of film thickness forms on elastic deformed surfaces (Eqn. 3.52).

2. This formula changes to below form with obtaining Moes [10] dimensionless formula (Eqn. 3.33).

3. Johnson's load sharing concept is applied to dimensionless film thickness formula (Eqn. 3.53).

4. Dimensionless formula is converted to central film thickness:

$$h_c = \frac{H_c\,R}{\overline{U_\Sigma}} \tag{3.74}$$

5. Then the main algorithm is applied described in Section 3.7. At this time, the final calculation of the flowchart is changed with oil film thickness formula. It means that if the mentioned pressures are equal to each other, it can be said that the assumed load and the calculated oil film thickness are true.

6. The film thickness formula can be extended including the distance between the mean plane through the summits and the mean plane through the heights of the surface.

$$h_s = h_c - d_d \tag{3.75}$$

where

h_s is the film thickness between the mean plane through the summits and the mean plane through the heights of the surface, [m]

The variation of the central oil film thickness for all lubrication regimes and also for mixed lubrication regimes with a separate capture is shown in Figure 14.
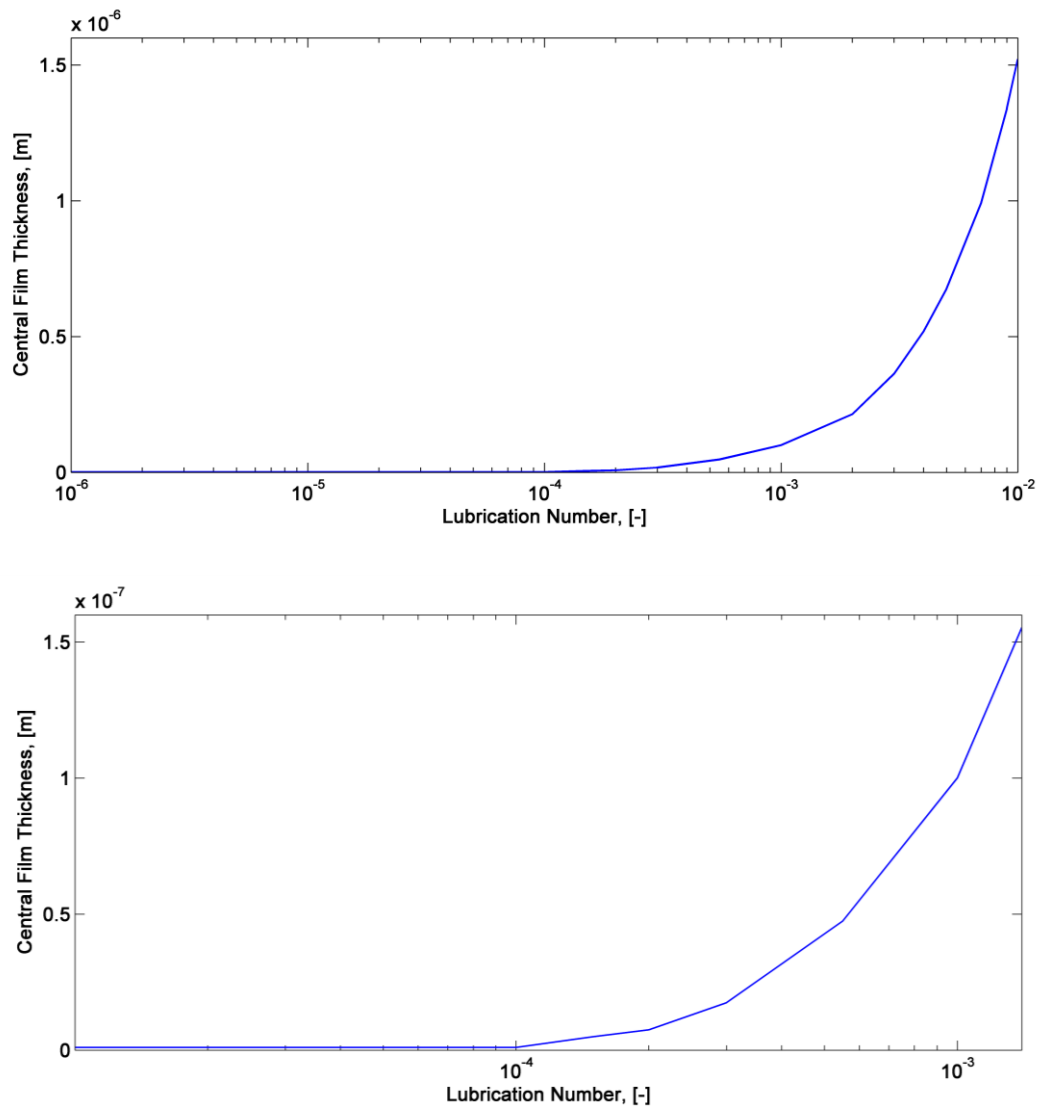
Figure 14 Variation of Isothermal Central Oil Film Thickness

3.8.1.3. Thermal Central Oil Film Thickness Calculations for Fully Flooded Conditions

In order to determine thermal oil film thickness, a formula of the Wilson and Sheu [36] available in the literature is applied in the study. The formula is a correction factor that defines a relation between isothermal oil film thickness and thermal oil film thickness.

In order to obtain it, firstly, isothermal oil film thickness is obtained using the instructions described in Section 3.8.1.2. Then a correction factor is applied gives thermal oil film thickness empirically without obtaining energy equations.

a.   The formula of Wilson and Sheu [36]

Wilson and Sheu [36] obtained a semi-empirical equation for EHL line contact defined as:

$$C_T = \frac{h_{thermal}}{h_{isothermal}} = [\,1 + 0.241\ \ 1 + 14.8\ 2SR^{\ 0.83}\ Q^{0.64}\ ]^{-1} \tag{3.76}$$

where

C_T is a constant for EHL line contact, [-]
Q is the thermal loading parameter, [-]

Thermal loading parameter is written as:
$$Q =\ \mu_0 \gamma\ u_R^2\ k \tag{3.77}$$
where
η_0 is the viscosity at ambient pressure, [Pas]
γ is the temperature coefficient of viscosity, $[K^{-1}]$
k is the thermal conductivity, $[W\ \ m.K]$

The thermal is taken as the central film thickness:
$$h_{thermal} =\ h_c[\,1 + 0.241\ \ 1 + 14.8\ 2SR^{\ 0.83}\ Q^{0.64}\ ]^{-1} \tag{3.78}$$

The calculated thermal oil film thicknesses are compared with the isothermal oil film thickness in Figure 15.
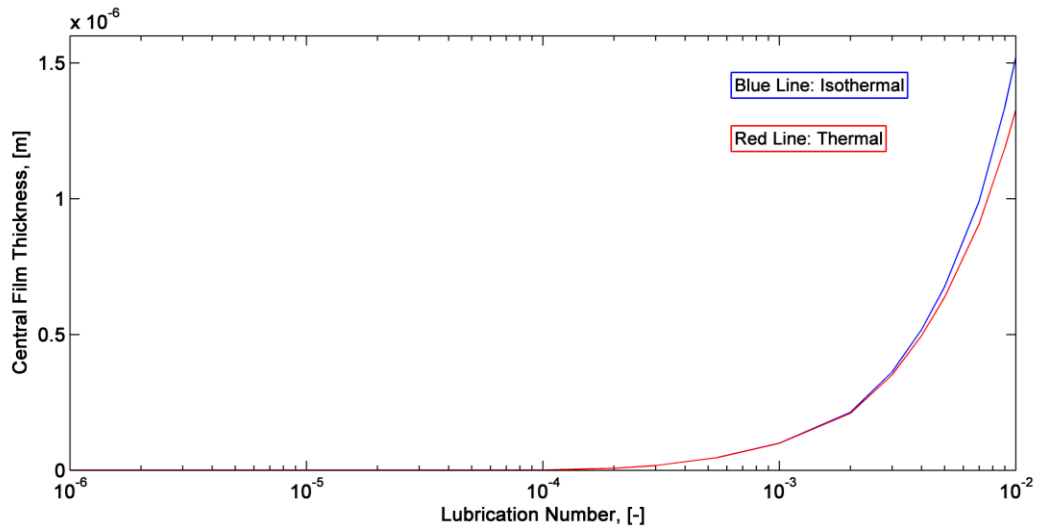
Figure 15 Comparison of Thermal and Isothermal Oil Film Thicknesses

In the below figure, thermal oil film thickness change with oil temperature is shown.
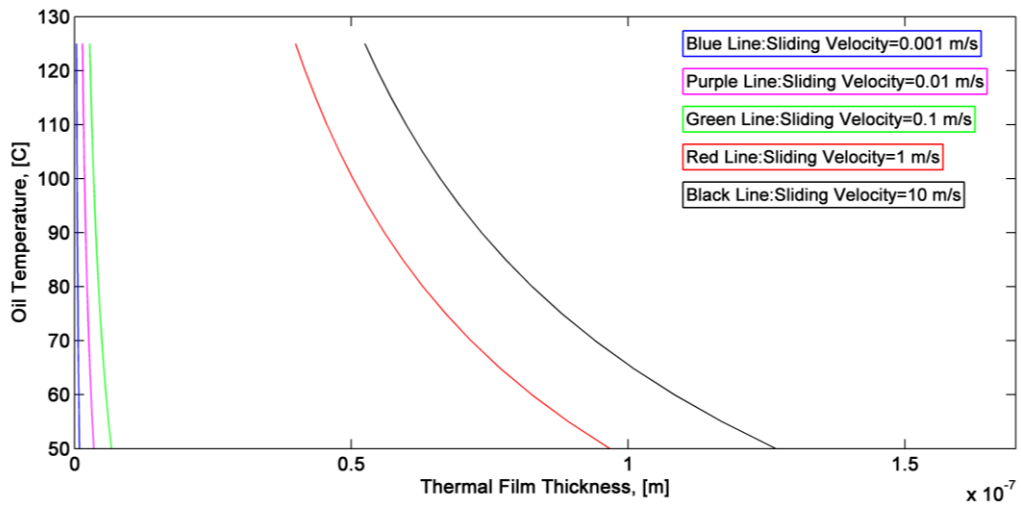
Figure 16 Variation of Film Thickness with Oil Temperature

47

3.8.1.4.   Separation Calculation for Fully Flooded Conditions

Separation can be calculated that oil film thickness is divided to the standard deviation of the height distribution of the summits.

$$\lambda_s = \frac{h_s}{\sigma_s}$$

(3.79)

This number is plotted for all lubrication regimes and also for mixed lubrication regimes with a separate capture in Figure 17.
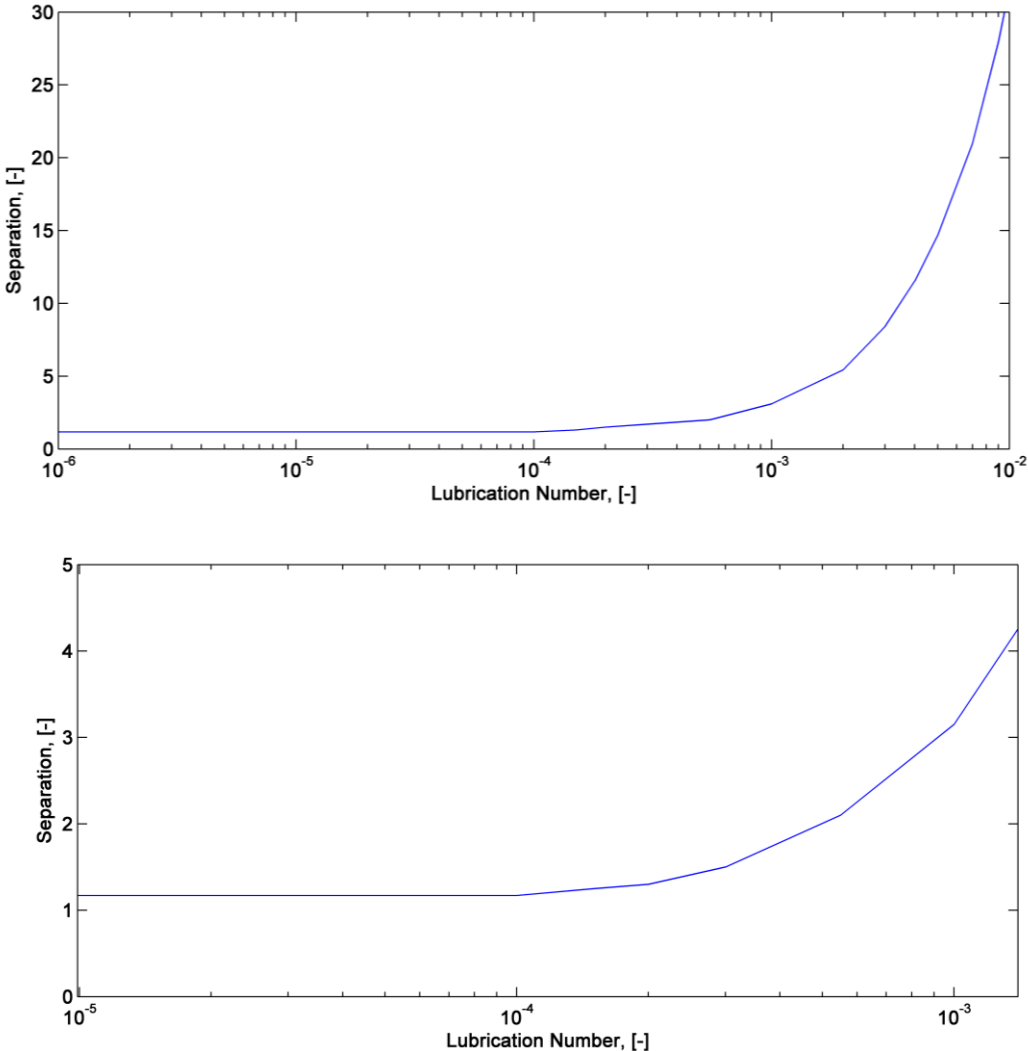
Figure 17 Variation of Separation

3.8.1.5. Starved Film Thickness Calculation for Starvation Conditions

Oil starvation is an important issue for gear box health. Starved oil film thickness is calculated, and then oil starvation estimation is applied using Schipper and Faraon [37] correction factor.

The calculations are performed with the instructions given below:

1. Gelinck and Schipper [25] mixed EHL model is applied.
2. Isothermal and thermal oil film thickness is calculated pass in Equations (3.74) and (3.78).
3. Then the main algorithm is applied described in Section 3.7. At this time, final calculation of the flowchart is changed with oil film thickness formula. In means that if the mentioned pressures are equal to each other, it can be said that assumed load is true and calculated oil film thickness is true.
4. Starved Oil Film thickness is obtained by using Schipper and Faraon's [37] formula.

This formula consists of Schipper and Faraon's [37] modified correction factor of numerical solution of Wolveridge [38].

The ratio β_W between the film thickness for the starved and oil film thickness is derived by Wolveridge et al. [38].

$$\beta_W = \frac{h_{starved}}{h_{thermal}} = f(\psi_i) \tag{3.80}$$

$$\psi_i = \frac{b^{1/3} x_i}{2R {h_{thermal}}^{2/3}} \tag{3.81}$$

In order to implement the numerical solution of Wolveridge et al. [38], a fitting equation is obtained. This fitting equation that is shown in Figure 18 is defined as:

$$\beta_W = \frac{2}{\pi} \arctan 2.7 \psi_i \tag{3.82}$$

where

β_W is the correction factor of numerical solution of Wolveridge, [-]

ψ_i is the dimensionless lubricant inlet length, [-]
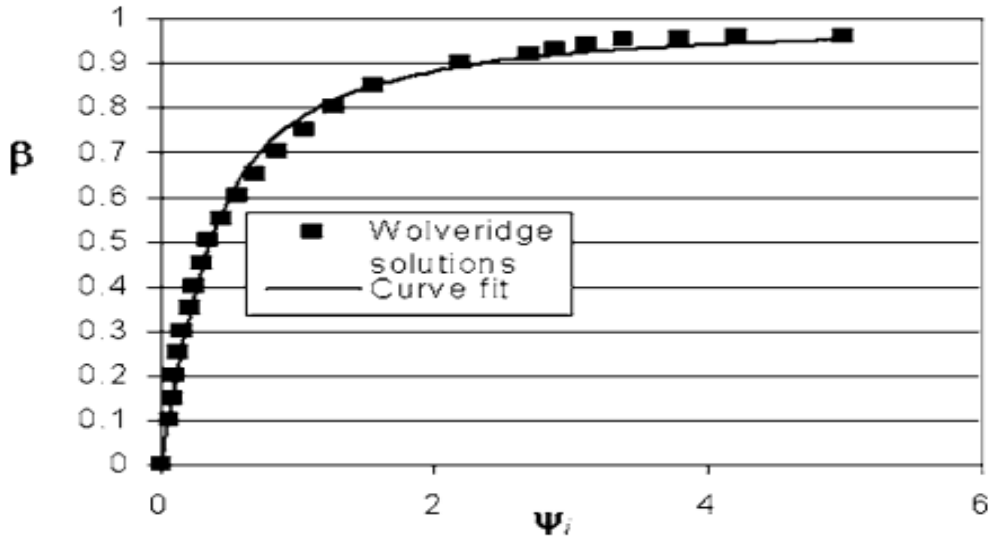
Figure 18 The Approximation of Schipper and Faraon of Numerical Solution of Wolveridge [38]

5.   Starved oil film thickness is determined by multiplying correction factor of Schipper and Faraon [37] and thermal oil thickness.

$$h_{starved} = \beta_W h_{thermal} \qquad (3.83)$$

The starved oil film thickness is calculated and shown in Figure 19. It can be said that oil film thickness decreases in starvation conditions. In Figure 19, inlet lubricant length is equalizing to half contact width.
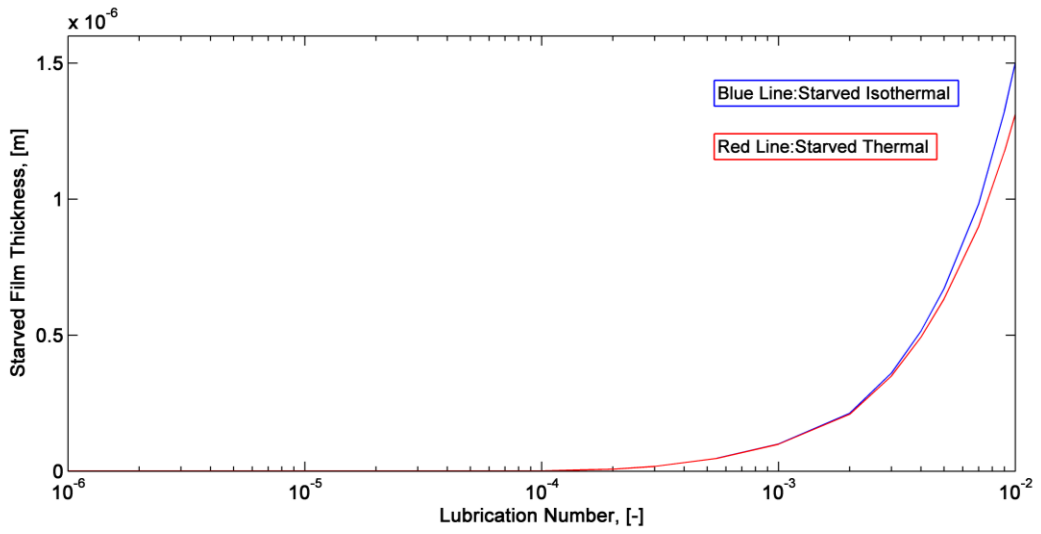
Figure 19 Variation of Starved Oil Film Thickness

When inlet length is smaller than half Hertzian contact width, starved oil film thickness is much smaller. In the calculations, correction factor is taken as $\beta_W = 0.99$ and $\beta_W = 0.10$.

$$b = \sqrt{\frac{8F_T R}{\pi B E}} \tag{3.84}$$
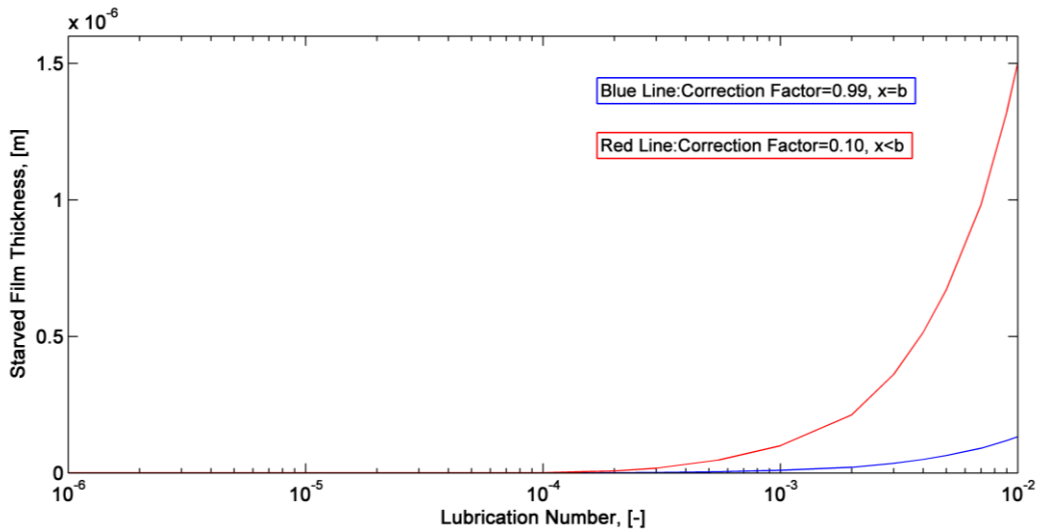
Figure 20 Variation of Starved Isothermal Film Thickness with x_i and β.

According to all film thickness graphics, film thicknesses are changed between 10^{-9} and $10^{-6} \, m$ range. It can be seen that, at the regime where the velocity between 0.001 and $0.1 \, m \; s$, film thickness is much smaller with comparing to higher velocities which are large than $0.1 \, m \; s$. In right side of the figure, film thickness is much higher. These show that film thickness is different for each lubrication regime or region.

3.8.1.6. Oil Starvation Estimation

Oil starvation estimation is obtained by determining the starved film thickness firstly.

$$\lambda_{starved} = h_{starved} \; \sigma_s \qquad\qquad (3.85)$$

According to Schipper and Faraon [37], if the calculated starved separation is between 6 and 0.7, it can be said that the gear pair is under oil starvation conditions, if this ratio is larger than 6, it is said that the condition is fully flooded.

3.8.1.7. Coefficient of Friction Calculation for Fully Flooded Conditions

The main purpose of this thesis is to calculate the friction coefficient and investigate the effects of parameters on the friction coefficient formula. The ratio of friction force to total normal force gives friction coefficient. Friction is sum of hydrodynamic friction force and asperity friction force.

In order to calculate friction coefficient the flowchart of the algorithm (Figure 10) is applied with input parameters. In the calculations, Gelinck and Schipper [25] mixed EHL model and the input parameters (Table -2) passed in their study is used as a reference.

The variation of friction coefficient is plotted in Figure 21. In the boundary lubrication regime, it can be seen the coefficient is larger; however in the mixed lubrication regime, the coefficient is decreased.
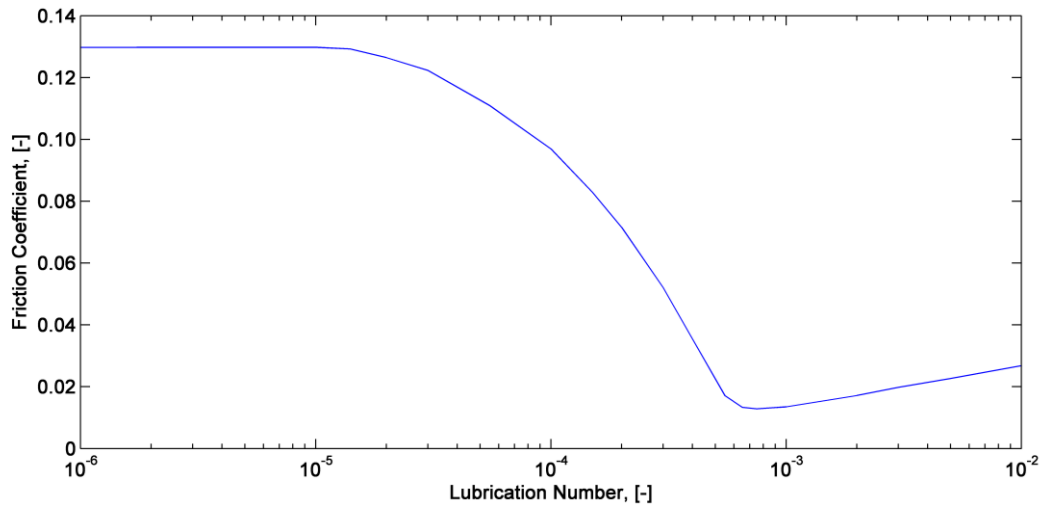
Figure 21Variation of Friction Coefficient

According to Figure 21, friction coefficient shows a decreased tendency. Film thickness is firstly high when the velocity is much smaller. This region known as boundary lubrication regime when the running in starts. At the middle region, the coefficient is decreased. In this region total load is carried by thin film thickness and elastically deformed asperity surface heights. Mixed lubrication regime mostly occurs when the velocity is between 0.01 and 1 m/s. The middle region is naming as mixed lubrication regime. At the right side of the figure, friction coefficient is increased slightly because of viscosity and shear effects but film thickness is much higher where the hydrodynamic lubrication is occurred.

3.8.1.8. Coefficient of Friction Calculation for Starved Conditions

The same procedure given in '3.8.1.7 Coefficient of Friction Calculation for Fully Flooded Conditions' is applied. However, the oil film thickness is changed with starved oil film thickness.

3.8.2. Mixed EHL Model Calculations for Point Contacts

Up to now, all the modeling and calculations are performed for line contact conditions. However, it doesn't mean that every gear pair operates in line contact conditions. It can be said that spur gears, planet gears operates in line contact conditions; unlike spiral bevel gears, hypoid gears operates in point contact conditions.

In the study, isothermal point contact mixed EHL model of Liu [39] is applied. This model is very similar to Gelinck and Schipper [25] mixed EHL line contact model. Only dimensionless oil film thickness and nominal hydrodynamic areas are changed according to point contact conditions. Gelinck and Schipper [25] curve fitting formula for central asperity pressure is not applicable for point contacts.

The calculations are performed with below instructions:

1.   The simplified Reynolds equation is generated (Eqn. 3.41).
2.   Force balance rule is applied (Eqn. 3.43).
3.   Johnson's load sharing concept is applied.
4.   Film thickness equation according to two surfaces elastic deformation is defined (Eqn. 3.51).
5.   Dimensionless film thickness formula for point contact according to Moes is applied.

$$H_c = \left[\left(H_{RI}^{3/2} + \left(H_{EI}^{-4} + H_{00}^{-4} \right)^{-3/8} \right)^{2s/3} + \left(H_{RP}^{-8} + H_{EP}^{-8} \right)^{-s/8} \right]^{1/s}$$

with

$$s = 1.5 \left[1 + exp \left(-1.2 \frac{H_{EI}}{H_{RI}} \gamma_1^{-7/5} \right) \right] \tag{3.86}$$

6.   Johnson [14] load share factors are taken into account.

$$H_c = \gamma_1^{1/2} \left[\left(\gamma_1^{9/4} H_{RI}^{3/2} + \left(\gamma_1^{-2/5} H_{EI}^{-4} + H_{00}^{-4} \right)^{-3/8} \right)^{2s/3} + \left(\gamma_1^4 H_{RP}^{-8} + \gamma_1^4 H_{EP}^{-8} \right)^{-s/8} \right]^{1/s}$$

with

$$s = 1.5 \left[1 + exp \left(-1.2 \frac{H_{EI}}{H_{RI}} \right) \gamma_1^{-7/5} \right] \tag{3.87}$$

7. The central pressure generated by the asperities according to Greenwood Williamson [2] asperity contact model (Eqn. 3.55) and dimensionless form of the central asperity pressure is calculated (Eqn. 3.56).

8. Dimensionless asperity pressure is equalized to hydrodynamic pressure components [41]:

$$p_h = \frac{F_T}{A_{nom} \gamma_2 p_{Hertz}} \tag{3.88}$$

$$A_{nom} = \left[A_H \left(\frac{F_T}{F_H} \right)^{2/3} \right] \tag{3.89}$$

9. With assuming load carried by asperities and taking into account the input parameters (lubricant behaviors like viscosity, gear geometries, total load, speed etc.), central pressure generated by the asperities will be checked with the equivalence of central pressure that related with the Hertz pressure by Gelinck and Schipper [25]. If they are equal with each other, assuming values are true and thus the coefficient of friction will be determined during an increasing velocity. This equivalence is in an iterative algorithm in order to find the right ratio between the load carried by the asperities and the load carried by the fluid.

10. If the equivalence does not implement, new asperity load is assumed and procedure is applied again.

For point contact conditions, the Stribeck curve shows the same shape likely line contact solutions. Friction coefficient variation with different sliding velocity indicates similar decreasing line. The main difference in the calculations, also it can be seen from solution procedure, is that film thickness formulation is changed. Moreover, in the pressure equivalence part, Gelinck and Schipper [25] fitting method for asperity pressures don't be applied. In this part, nominal contact area is used to obtain pressures.

In Figure 22, the film thicknesses are shown comparatively for the same input parameters and operating conditions.
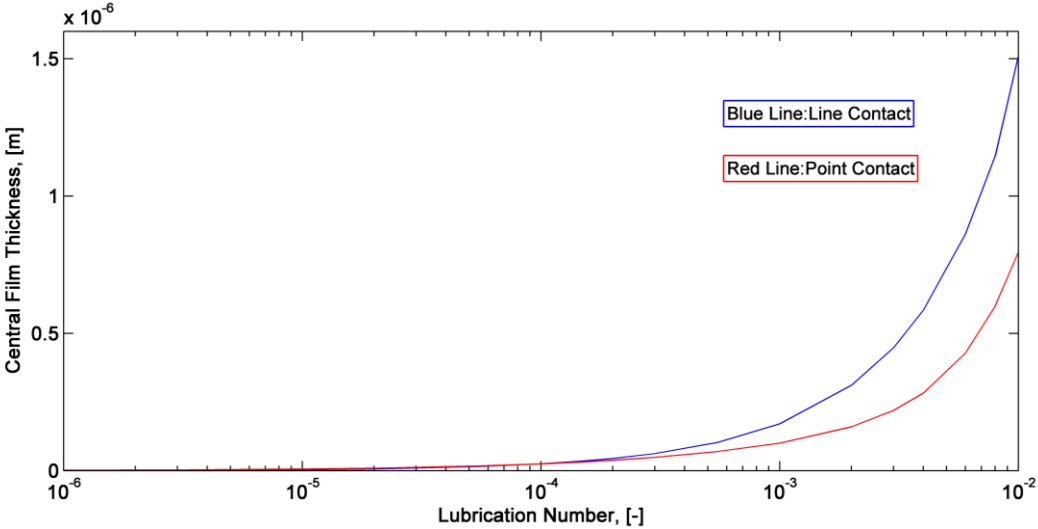
Figure 22 The Comparison of Oil Film Thicknesses of Line and Point Contacts for the Same Operating Conditions

CHAPTER 4

PARAMETERS THAT EFFECT THE STRIBECK CURVE AND OPTIMISATION

4.1.   Introduction

In the generalized Stribeck curve, the coefficient of friction is plotted as a function of a lubrication number or velocity. This curve is an important tool to estimate lubrication regimes. Three lubrication regimes can be distinguished in this curve, i.e. the boundary lubrication, the mixed lubrication and the elastohydrodynamic lubrication regimes. At higher velocities, elastohydrodynamic or hydrodynamic lubrication regimes occur. At lower velocities, boundary lubrication regime occurs. In boundary lubrication regime, film thickness is thinner, asperity contacts occurs and load is carried by asperities mostly. In mixed lubrication regime, the load is partly carried by the asperities and partly by fluid film. In hydrodynamic lubrication regime, film thickness is thicker – larger than surface roughness- and load is mostly carried by fluid film hydro dynamically.

4.2.   The Stribeck Curve

In Figure 23, the generalized Stribeck curve is shown.
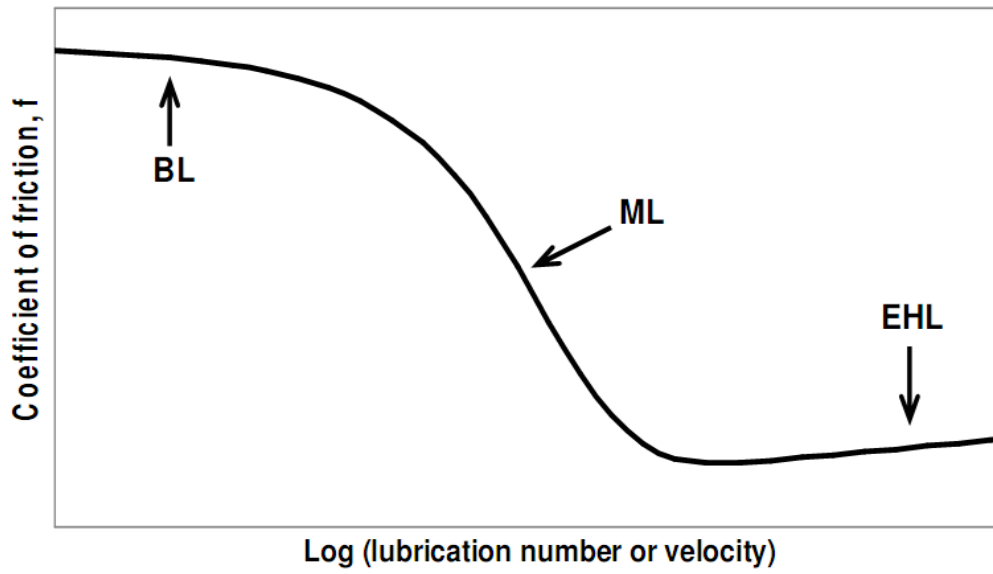
Figure 23 The Generalized Stribeck Curve

The plotted the Stribeck Curve using developed program is shown in Figure 24.
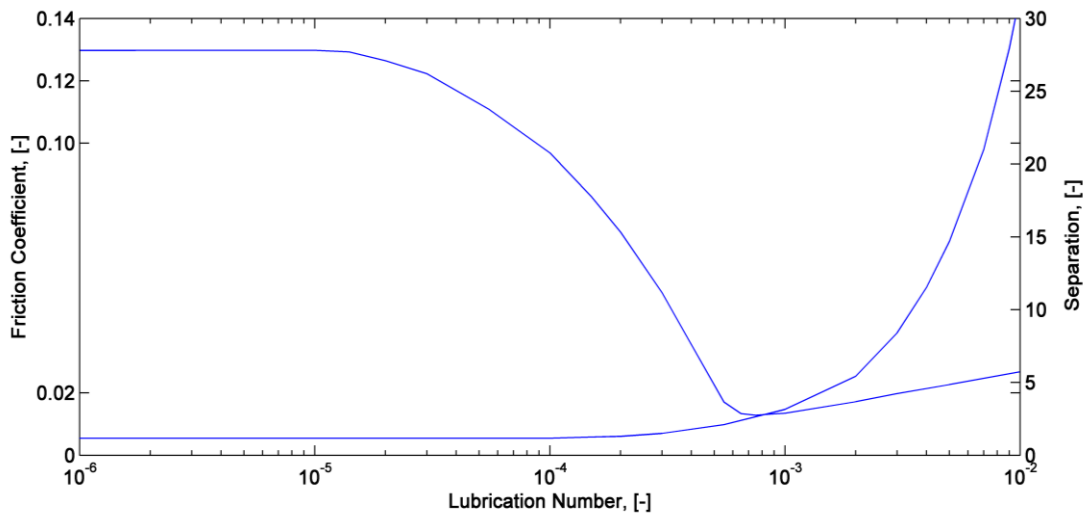
Figure 24 The Stribeck Curve with Separation

The Stribeck curve is plotted as a function of lubrication number or velocity. Lubrication number includes sum velocity, ambient viscosity, average pressure and surface roughness parameters. Ambient viscosity and sliding velocity parameters are directly proportion to Lubrication number however average pressure and combined surface roughness values are inversely proportion to Lubrication number. If the ambient viscosity, average pressure and surface roughness parameters kept constant, friction coefficient is decreased with increasing velocity in mixed and boundary lubrication regimes.

4.3. Load Effects on the Stribeck Curve

The Stribeck curve is created with three different loads; 20N, 500 N and 16000 N.

It is observed from the Figure 25, that coefficient of friction is increased with increasing load values in mixed lubrication regime.

The asperity pressure is load independent. With the increasing load, the contact area increases and consequently the number of asperity contacts increases. The transition from mixed lubrication to EHL is more influenced by the load. Higher load has higher friction coefficient. Moreover, the transition from boundary lubrication to mixed lubrication shifts to the left with increasing normal load.
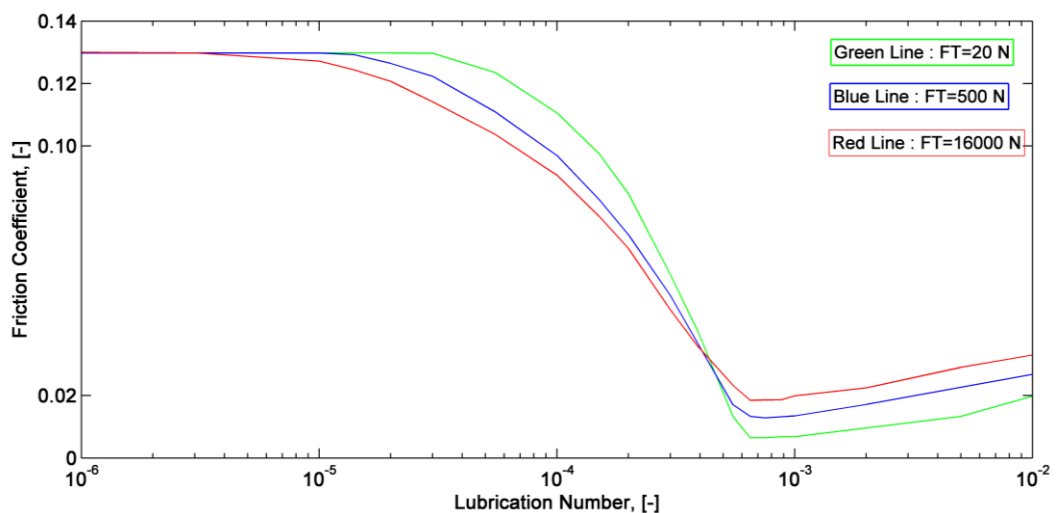
Figure 25 The Stribeck Curve for 20N, 500 N and 16000 N Load Values

In Figure 26, for different load values, change of load share factors can be seen. It can be seen from Figure 27, high load is adverse effect on central film thickness.
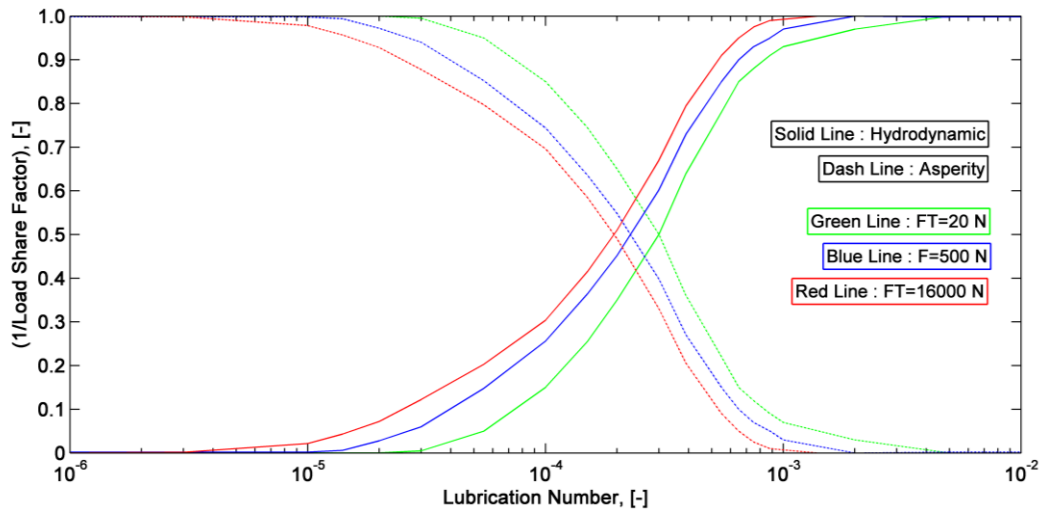
Figure 26 Variation of 1 / Load Share Factor on the Stribeck Curve for 20N, 500 N and 16000 N Load Values

According to Figure 26, hydrodynamic load share factors are decreased and asperity load share factors are decreased with increased lubrication number. If load is increased, 1 γ_2 decreased at boundary and mixed lubrication regimes and is increased at hydrodynamic lubrication regime. Contrarily, 1 γ_1 is decreased at hydrodynamic regime and increased at boundary and mixed lubrication regime with increasing load.
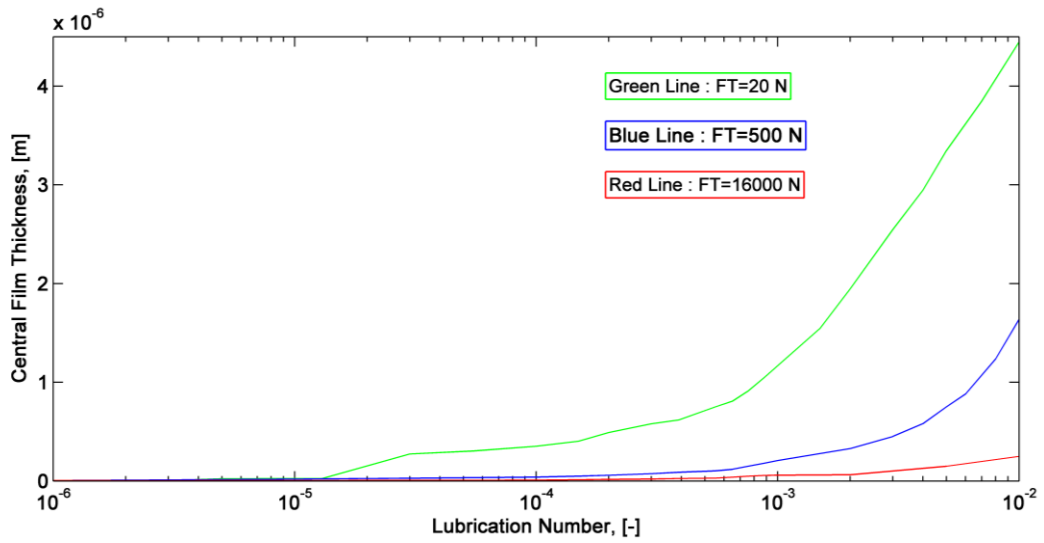
Figure 27 Variation of Central Film Thicknesses on Stribeck Curve for 20N, 500 N and 16000 N Load Values

4.4. Surface Roughness Effects on the Stribeck Curve when $n\beta\sigma_s$ is Kept Constant

The Stribeck Curve is created for different surface roughness values. $n\beta\sigma_s$ is kept constant having the value of 0.05 and surface roughness is increased and mixed EHL model is applied. In Figure 28, the Stribeck curve is plotted for standard deviation of asperities: $0.025x\ 10^{-6}$ and $0.5x\ 10^{-6}$ [m].
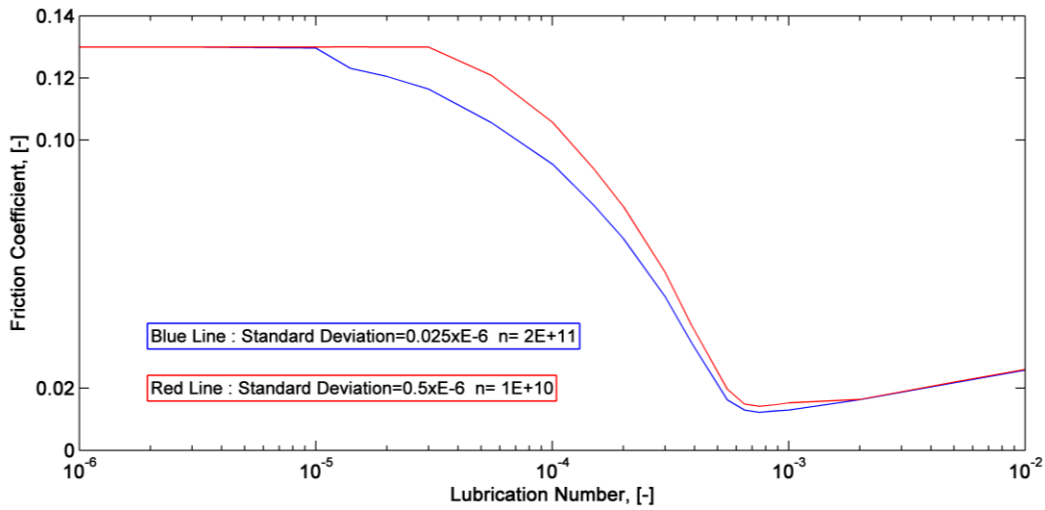
Figure 28 The Stribeck Curve for Different Surface Roughness Parameters σ_s

It is observed that the surface roughness is an important effect on the Stribeck curve and friction coefficient. In the mixed lubrication regime, the coefficient of friction is lower for smoother surfaces. It can be said that the surface roughness is inverse effect on friction coefficient. For hydrodynamic lubrication regime, the surface roughness effect on friction coefficient is insignificant. In boundary lubrication regime where sliding velocity is much lower, there is no significant effect on friction coefficient.

It can be noticed, that by increasing the value of σ_s, the Stribeck curve shifts to the right. In this case the shift of the Stribeck curve is caused by a higher separation between the surfaces which increases with σ_s .
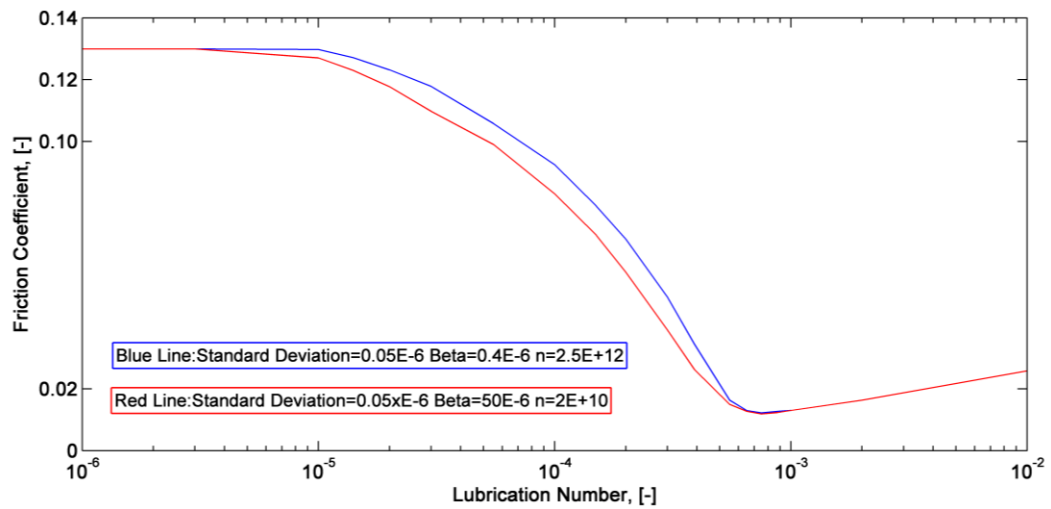
Figure 29 The Stribeck Curve for Different Surface Roughness Parameters β and n

In figure 29, $n\beta\sigma_s$ is again kept constant having the value of 0.05 and β is increased while n is decreased. The standard deviation of the surface roughness is constant at this time. In this situation, the curve shifts to left that means for the same lubrication number the coefficient of friction decreases in the mixed lubrication region. Since there is no mixed condition in the boundary and hydrodynamic lubrication regimes, no variations are observed in those regimes.

Also, it can be said that, the separation in the mixed lubrication regime decreases with increasing β and decreasing n. Due to the decrease in separation the surface becomes less stiff.

With increasing β, the surfaces in contact deform more in order to carry the load. So, it can be said that the load carried by asperities is proportional to β.

4.5. Slip Ratio Effects on the Stribeck Curve

In the calculations, slip ratio effects are also investigated. Slip ratio is the ratio of sliding velocity to rolling velocity. According to Figure 30, if the ratio is higher, friction coefficient is smaller in mixed lubrication regime.
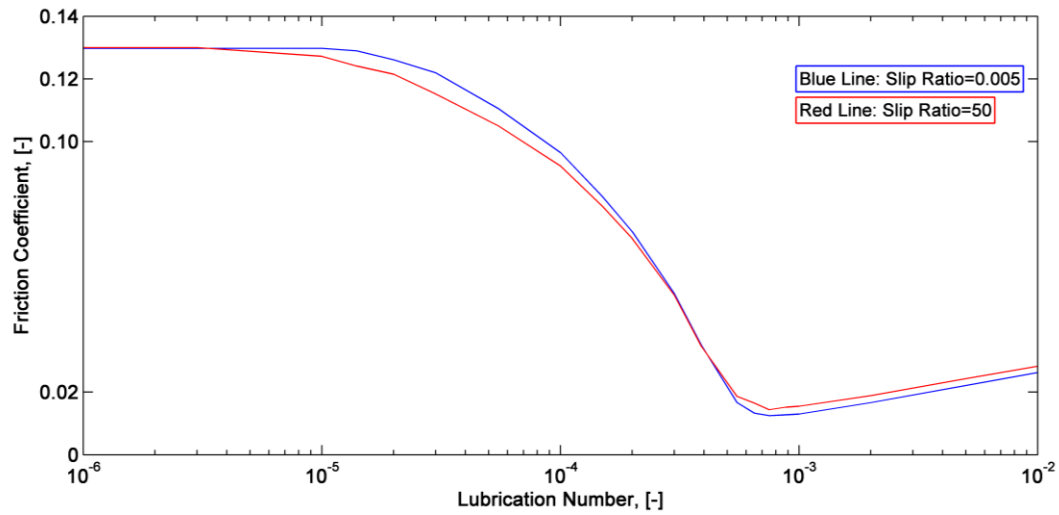
Figure 30 The Effect of Slip-Ratio on the Stribeck Curve

CHAPTER 5

MIXED EHL LUBRICATION MODEL WITH NON-GAUSSIAN DISTRIBUTION

5.1.   Introduction

In the Greenwood and Williamson [2] contact model is used for asperity contact regime for mixed lubrication regimes. In their model, it is mentioned in Section 3 that asperities have the same asperity radius and asperity height distribution is Gaussian distribution. In real, asperities have spheres or ellipsoids radius type. And this is more important that asperity heights do not behave in Gaussian distribution. Greenwood and Williamson [2] model has accurate results for assumed values. So, it can be said that if surface roughness deviates from Gaussian distribution, the mixed EHL model is applicable. But the main disadvantage of this model is the assumed Gaussian distribution of summits.

After Greenwood and Williamson [2], many three dimensional surface topography measurements are developed. Then, the new contact models including non-Gaussian distributions are obtained in order to modify Greenwood and Williamson [2] model.

To simulate contact between real rough surfaces, it is to be assumed that the asperities have different radii and ellipsoids type and the surface heights have non-Gaussian distribution.

In Figure 31, contact between a smooth surface and a rough surface is shown. In this figure, all the asperities have different radii. For a given distance, the real contact area and the total force carried by the contact are calculated taken into the number of asperities and each height between surface heights is accounted locally. New model

calculates each asperity deformation independently. Deformations are determined with summing up local deformations.
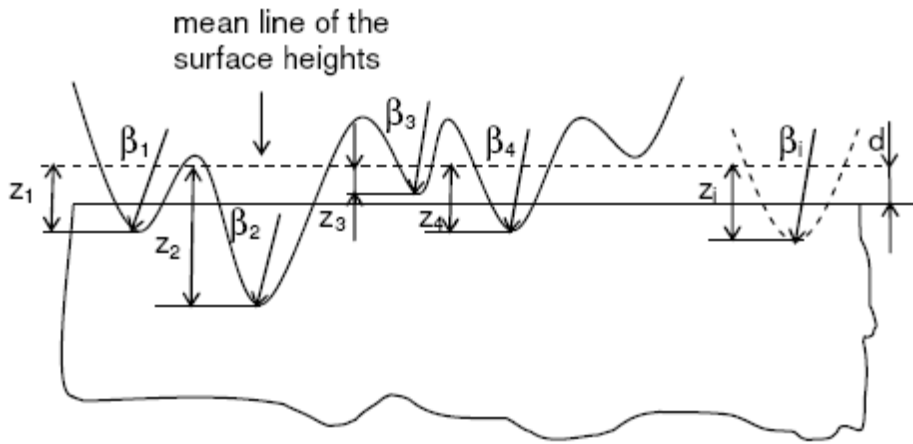
Figure 31 The Contact between a Rough Surface and a Smooth Surface [26]

The compliance of one asperity is calculated as:

$$w_i = z_i - h_s \tag{5.1}$$

where

z_i is the individual summit height, [m]

By knowing w_i of each deformed asperity, the total real contact area and total normal force on the surface is calculated by adding each asperity components.

The Stribeck curve is determined by applying the new model to mixed EHL model. It is said that when the measured surface height distribution is Gaussian, the difference between on the Stribeck curve is insignificant. However, when the distribution of the surface heights deviates from the Gaussian, the Stribeck curve is also affected due to change in asperity contact.

5.2. The Weibull Distribution

The Weibull distribution is used for non-Gaussian surface height distributions in the literature. The Weibull distribution is used as non-Gaussian asperity heights distributions by some scientists [40]. For the Gaussian height distribution, the standardized height distribution of the summits is given as:

$$\emptyset(z) = \frac{1}{\sigma_s\sqrt{2\pi}}exp\left(\frac{-z^2}{2\sigma_s^2}\right) \tag{5.2}$$

For the Weibull distribution, this function is given as:

$$\emptyset(z) = \frac{\beta_{Weibull}z^{\beta_{Weibull}-1}}{\eta_{Weibull}^{\beta_{Weibull}}}\exp\left(-\left(z/\eta_{Weibull}\right)^{\beta_{Weibull}}\right),$$

$$z > 0, \quad \beta_{Weibull} > 0, \quad \eta_{Weibull} > 0 \tag{5.3}$$

where

$\beta_{Weibull}$ is the shape parameter, [-]

$\eta_{Weibull}$ is the scale parameter, [-]

The n-th moment of the Weibull distribution is written as:

$$M_n = E(z^n) = \int_0^\infty z^n\emptyset(z)\,dz = \eta_{Weibull}^n B_n \tag{5.4}$$

where

B_n is the Gamma function, [-]

$$B_n = \Gamma\left(1 + n/\beta_{Weibull}\right) \tag{5.5}$$

The mean expectation of the distribution is given as:

$$E(z) = \eta_{Weibull}B_1 = M_1 \tag{5.6}$$

The variance is

$$\sigma_s^2 = M_2 - M_1^2 \tag{5.7}$$

The Skewness and Kurtosis of Weibull functions are given as:

$$Sk = \frac{B_3 - 3B_2B_1 + 2B_1^3}{\left(B_2 - B_1^2\right)^{3/2}} \quad , \quad Ku = \frac{B_4 - 4B_3B_1 + 6B_2B_1^2 - 3B_1^4}{\left(B_2 - B_1^2\right)^2} \tag{5.8}$$

The Skewness and Kurtosis parameters are dependent on the shape parameter.

To calculate the parameters, one of the parameter: Skewness or Kurtosis can be assumed zero. The Skewness formula is solved for a corresponding value and the shape parameter is determined. By using the shape function parameter, the scale parameter is calculated by Eqn. (5.7).

The standardized height distribution of the summits of Weibull distribution depends on the shape and scale parameters. This function is converted to the non-dimensional form to get the Weibull distribution plots.

$$s = \frac{z - \eta_{Weibull}B_1}{\eta_{Weibull}\sqrt{B_2 - B_1^2}} \tag{5.9}$$

$$\emptyset(s) = \beta_{Weibull}\left(B_1 + s\sqrt{B_2 - B_1^2}\right)^{\beta_{Weibull}-1} exp\left(-\left(B_1 + s\sqrt{B_2 - B_1^2}\right)^{\beta_{Weibull}}\right) \tag{5.10}$$

The variance, Skewness and Kurtosis values are extracted and measured from the surface roughness profile. In the present work, those parameters are taken from the literature. The Skewness parameter is sensitive to oscillations on deep valleys or high peaks and the kurtosis parameter is defined as the probability density sharpness of the profile.

In Figure 32, the Skewness parameter (Sk) is taken as following values: -1, 0.5, 0, 0.5 and 1. For the values larger than 1, the Weibull distribution shapes are like one sided distribution of the rough surface. Moreover, the values larger than -1, the Weibull distribution is impractical. So in the calculations, the Skewness values are chosen between -1 and 1. When the Skewness parameter value is zero, the distribution becomes symmetric as Gaussian distribution.

For the values -1, 0.5, 0, 0.5 and 1, Eqn (5.8) is solved, and then the shape parameter is determined between 40.7 and 1.6. For Sk=0, the scale parameter is determined as 3.6. With using shape values, the scale parameter can be determined by Eqn (5.7). The standard deviation is taken as $0.05 \, \mu m$.

In the Table-3, the calculated parameters for the selected range of the Skewness parameters are listed.

Table -3 Calculated Parameters for different Skewness Parameters and $\sigma_s = 0.05 \, \mu m$

Skewness Parameter	Shape Parameter	Scale Parameter $(\sigma_s = 0.05 \, \mu m)$	Kurtosis Parameter
-1	40.7	1.6	4.8
-0.5	7.5	0.3	3.3
0	3.6	0.2	2.72
0.5	2.2	0.1	3.0
1	1.6	0.1	4.2

In Figure 32, the dimensionless Weibull distribution is plotted for changing dimensionless asperity height by using Eqn (5.10). It can be seen that, for Sk=0, the Weibull distribution is symmetrical. For negative Sk values, the curves shows a trend to the right side and for positive Sk values, the curves goes to negative side of the mean line.

At Sk=0, it is obtained that the shape parameter is 3.6. If Eqn (5.8) is solved by taking the shape parameter as 3.6, the Kurtosis parameter is obtained as 2.72.
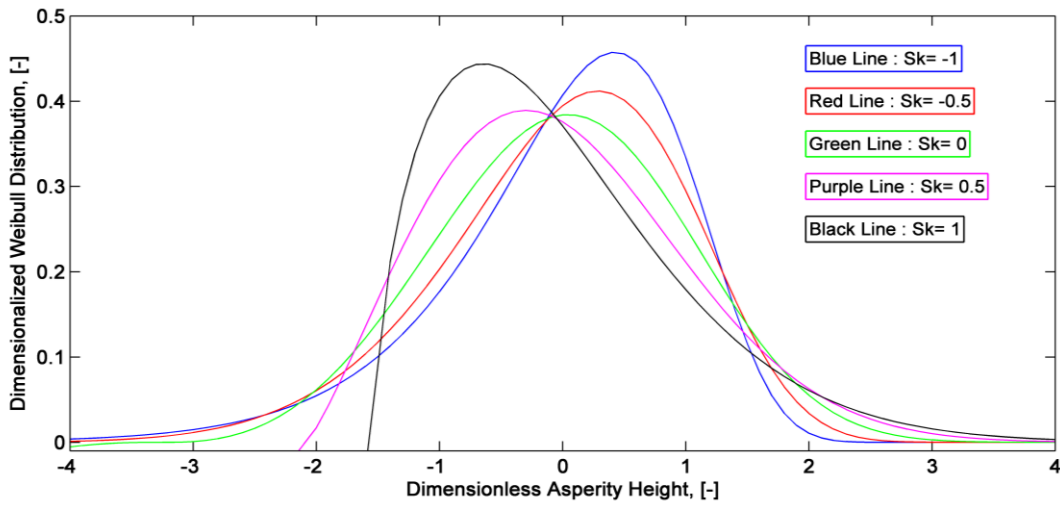
Figure 32 Dimensionless Weibull Distributions for different Skewness Parameters

Another way to find the Weibull distribution is solving for Kurtosis parameter. At this time, Eqn (5.8) is solved for assumed Kurtosis parameter which is changed between 2.72 and 6. For Ku=2.72, the Weibull distribution becomes symmetric as Gaussian distribution. For the values larger than 2.72, the Weibull distribution can be plotted and shows non- symmetric distributions.

In the Table-4, the calculated parameters for selected range of the Kurtosis parameters are listed.

Table-4 Calculated Parameters for different Kurtosis Parameters and $\sigma_s = 0.05 \ \mu m$

Kurtosis Parameter	Shape Parameter	Scale Parameter $(\sigma_s = 0.05 \ \mu m)$	Skewness Parameter
2.72	3.6	0.2	0
3	2.3	0.1	0.5
4	1.6	0.1	0.9
5	1.5	0.1	1.2
6	1.3	0.1	1.4

In Figure 33, the dimensionless Weibull distribution using Eqn (5.10) is given for Ku = 2.72, 3, 4, 5 and 6. For the larger values of Ku, the Weibull distribution is very large and impractical.
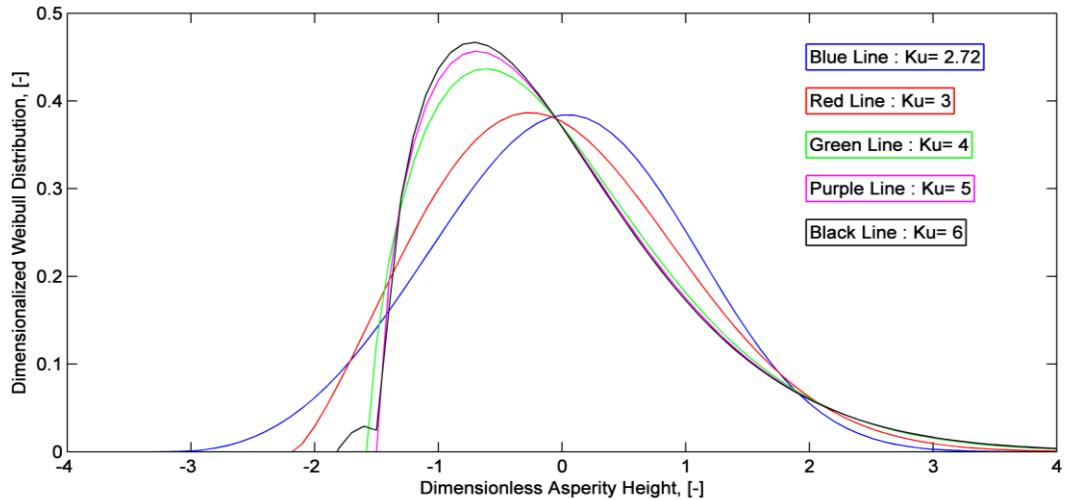
Figure 33 Dimensionless Weibull Distributions for different Kurtosis Parameters

At the following subject, the calculated Weibull distribution is applied to mixed EHL model successfully.

5.3. The Mixed EHL Model with non-Gaussian Distribution

In order to determine friction coefficient by the mixed EHL model for non-Gaussian surface height distributions, the Weibull distribution is applied.

The solution procedure can be given as;

1. The variance, Skewness and Kurtosis parameters are measured from surface roughness profile. In this study, these parameters are taken according to the data given in literature and convenient for non-Gaussian distribution.

2. Sk is taken as -1, 0, 1.

3. Eqn (5.8) is solved for different Sk values and shape parameters are determined.

4. Eqn (5.7) is solved by using calculated shape parameters, scale parameters are determined.

5. Weibull distribution is obtained in Eqn (5.3).

6. Developed mixed EHL algorithm is applied according the solution procedure of Table 1.

7. Weibull distribution formula is substituted instead of Gaussian distribution formula in Table 1.

$$\emptyset(s) = \frac{1}{\sqrt{2\pi}}\exp\left(\frac{-s^2}{2}\right) \rightarrow \emptyset(s) = \beta_{Weibull}\left(B_1 + s\sqrt{B_2 - B_1^2}\right)^{\beta_{Weibull}-1}$$

$$\sqrt{B_2 - B_1^2}\exp\left(-\left(B_1 + s\sqrt{B_2 - B_1^2}\right)^{\beta_{Weibull}}\right) \qquad (5.11)$$

8. Friction coefficient is determined and the Stribeck curve is plotted.

In Figure 34, the model is applied for Sk=-1, 0, 1 and variation of film thickness is plotted in mixed lubrication regime for Gaussian and non-Gaussian surface height distributions for the same operating conditions. In Figure 35, the model is applied for Ku=2.72, 4, 6 and variation of film thickness is plotted in Mixed lubrication regime for Gaussian and non-Gaussian surface height distributions for the same operating conditions.
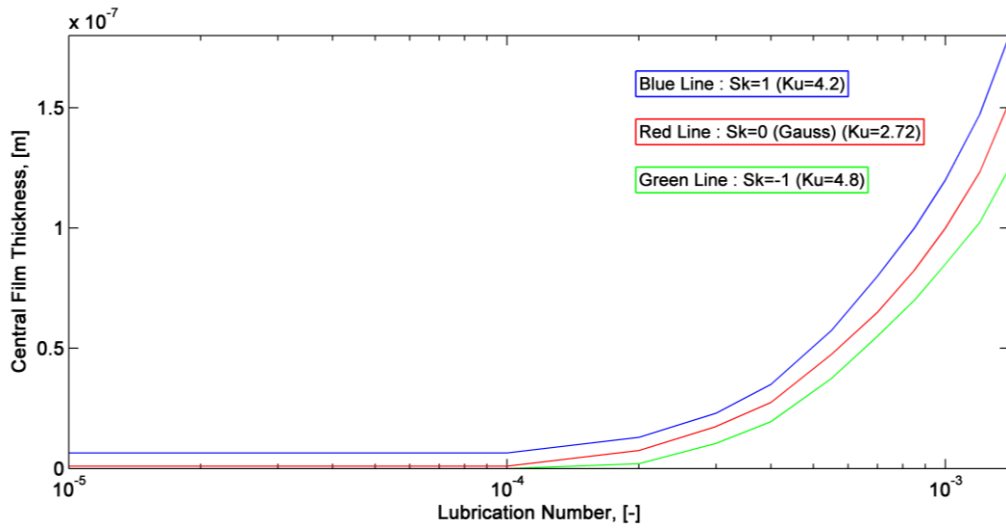
Figure 34 Variation of Film Thickness in Mixed Lubrication Regime for Sk=-1, 0, 1
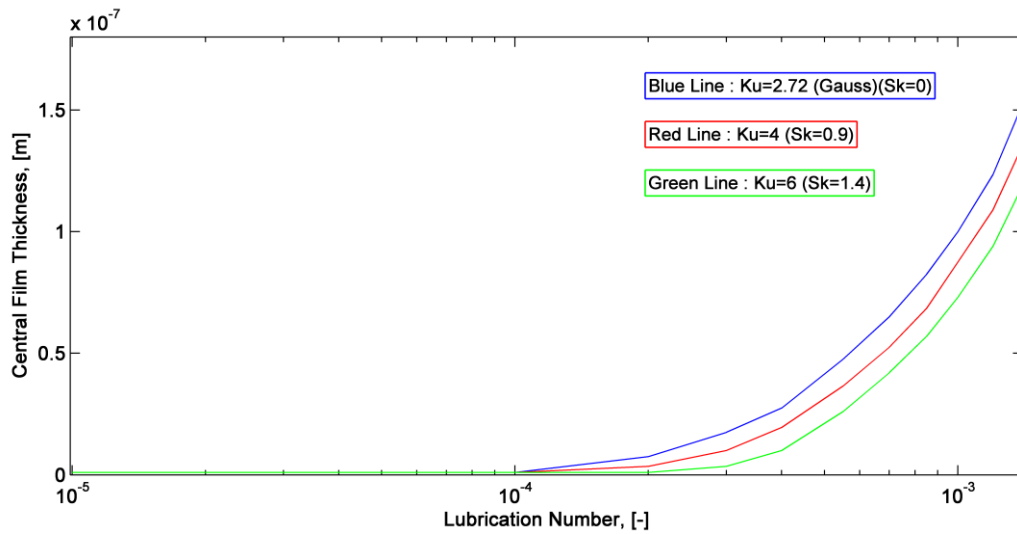
Figure 35 Variation of Film Thickness in Mixed Lubrication Regime for

Ku=2.72, 4, 6

In Figure 36 and 37, the variation of separation in mixed lubrication regime is plotted for Sk=-1, 0, 1 and Ku=2.72, 4, 6.

73
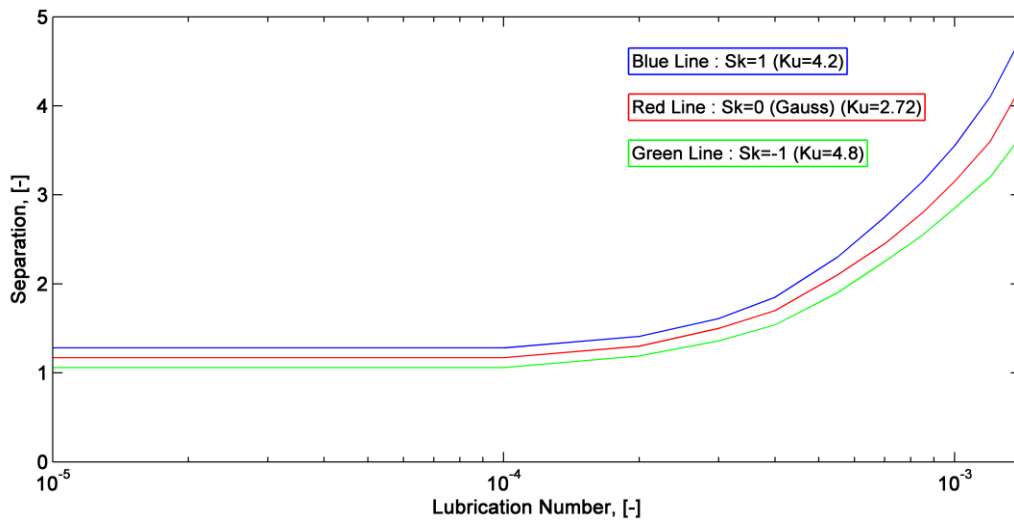
Figure 36 Variation of Separation in Mixed Lubrication Regime for Sk =-1, 0, 1
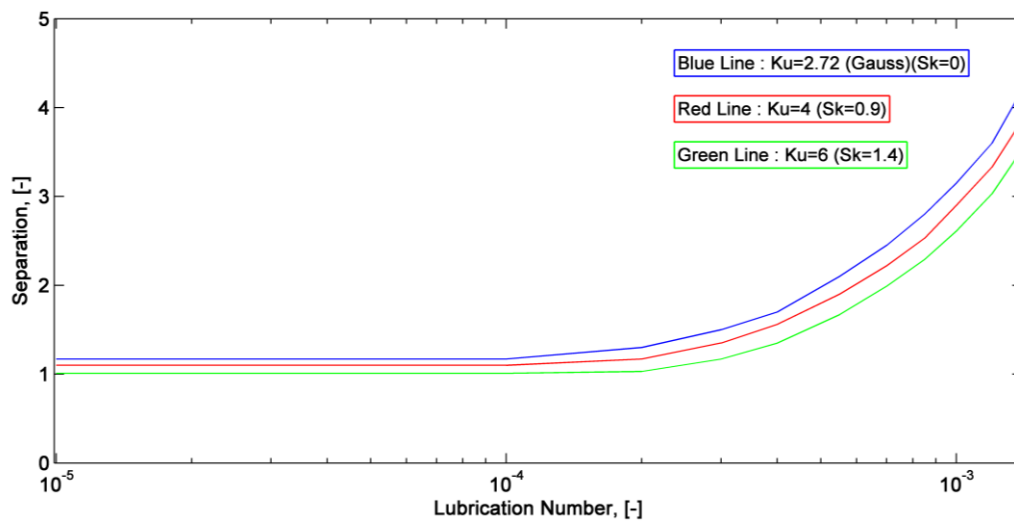
Figure 37 Variation of Separation in Mixed Lubrication Regime for Ku=2.72, 4, 6

In Figure 38 and 39, the 1/load share factor for hydrodynamic load and asperity load variations are for Sk=-1, 0, 1 and Ku=2.72, 4, 6.
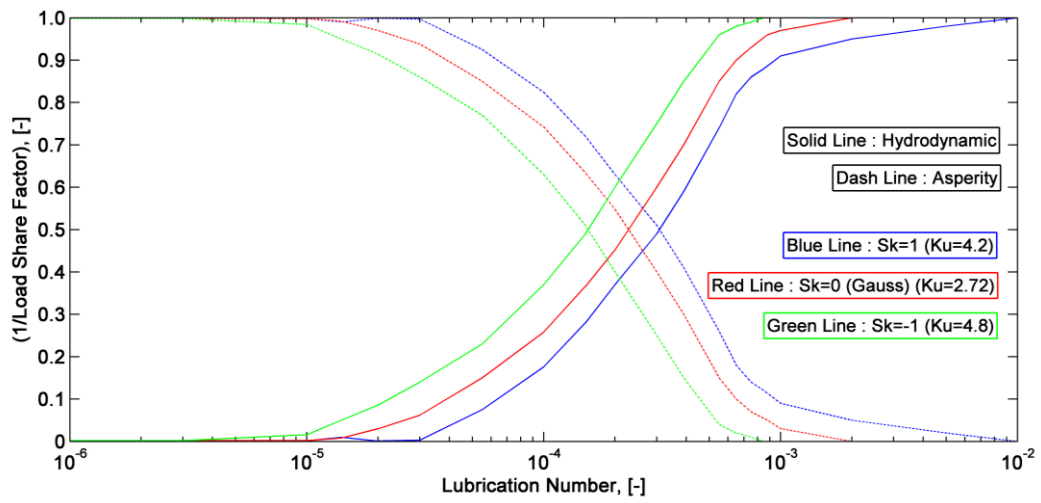
Figure 38 Variation of 1 / Load Share Factor for Sk =-1, 0, 1
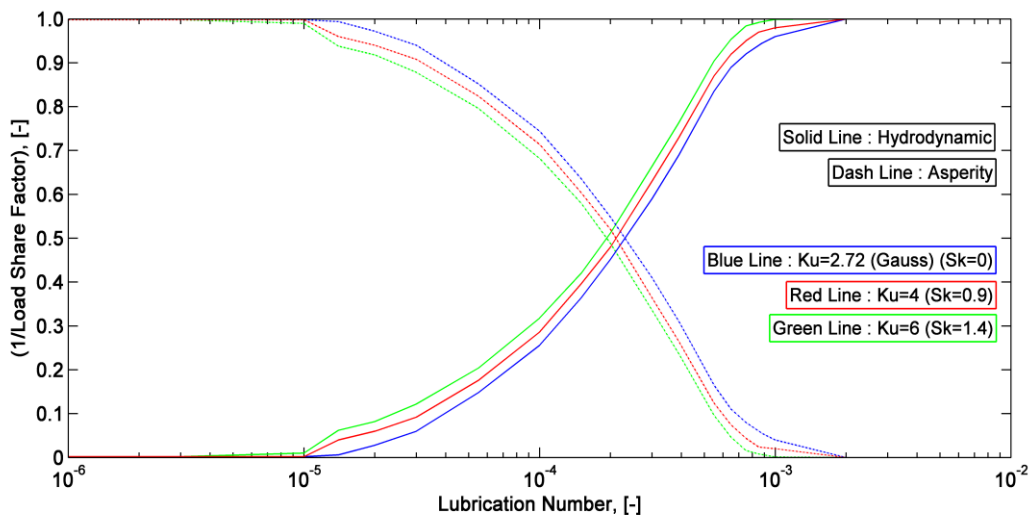
Figure 39 Variation of 1 / Load Share Factor for Ku=2.72, 4, 6

In Figure 40, the Stribeck curve is plotted for Sk =-1, 0, 1. In Figure 41, the Skewness parameter is changed for Ku=2.72, 4, 6.
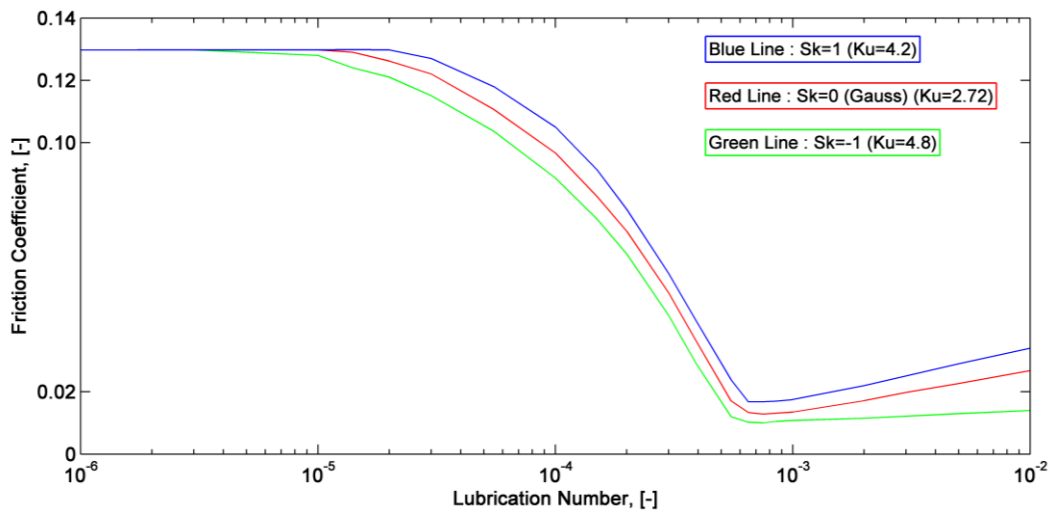
Figure 40 The Stribeck Curve for Sk =-1, 0, 1
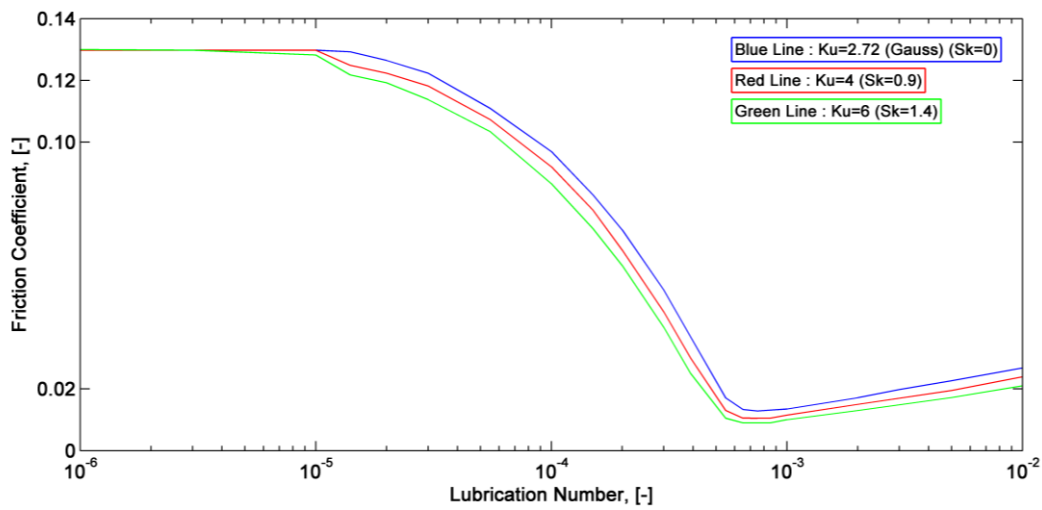
Figure 41 The Stribeck Curve for Ku=2.72, 4, 6

It can be said that the film thickness, separation, load share factors and coefficient of friction is same with Gaussian distributions when Sk=0 and Ku=2.72. For Sk=-1 and Ku=4, 6; the Stribeck curve shifts to the left and the film thickness, separation and friction coefficient values are lower.

CHAPTER 6

POWER LOSS CALCULATIONS WITH SAMPLE GEAR PAIR

6.1. Introduction

There are many benefits to improving gear efficiency as well by getting low power losses. Since the power losses amount to additional heat generation within the gearbox, several gear failure modes including scoring and contact fatigue failures are directly impacted by the efficiency of the gear pair. A more efficient gear pair generates less heat, and therefore, it is likely to perform better in terms of such failures. In the process, demands on the capacity and the size of the lubrication system and the amount and quality of the gearbox lubricant are also eased with improved efficiency. This also reduces the overall weight of the unit contributing to further efficiency improvements [41].

The total power loss of the gear system is includes sliding and rolling friction losses between the gear teeth, windage or churning losses and oil splashing, oil pocketing losses, frictional and churning losses occurring in bearing and seals. Both sliding and rolling actions at the gear contact contribute to gear mesh friction. Windage and churning losses contribute to gear load independent losses. Sliding friction is a direct product of the relative sliding between the two contacting surfaces while rolling friction originates from the resistance to the rolling motion. Sliding friction losses occur when two surfaces slide against each other. When these two surfaces are rough (in reality) a frictional heat is generated. In order to avoid frictional heat, oil that has high viscosity is used. But, this causes larger rolling losses sometimes. Rolling loss is

generated when two surfaces roll against each other from the pressure build up in the lubricant as it is squeezed in between the surfaces.

6.2. Power Loss Calculations

Gear pair total power loss depends on load dependent and load independent power losses. The Load independent power losses include gear pair churning (or windage) power losses, bearing power losses and sealing power losses. The load dependent power loss of the system is the sum of the gear sliding losses, gear rolling losses and bearing friction losses.

In this chapter, the load dependent power losses are explained and sliding power loss is calculated. By using the mixed EHL model, the power loss for a gear pair can be calculated simply.

Sliding friction power loss is determined.

$$P_{Sliding} = f F_T u_{dif} \qquad (6.1)$$

where

$P_{Sliding}$ is the sliding power loss, [W]

6.3. Frictional Power Loss on Sample Spur Gear

The Mixed EHL model explained in the chapters is applied to a given sample spur gear pair. The variation of sliding and rolling velocity, friction coefficient and total power loss is determined for gear contact line. The sample pinion and gear geometry properties are listed in Table-5.

Table -5 Input Values for Sample Gear Pair [42]

Property	Value	
	Pinion	**Gear**
Speed, [rpm]	5000	1600
Number of Teeth	32	100
Outside Radius, r_o [mm]	71.96	215.90
Root Radius, [mm]	62.46	206.38
Module, [mm/tooth]	4.23	
Face Width, [mm]	63.50	
Pressure Angle, [deg]	25	
Power Transmitted [kW]	51.25	
Normal Load [N]	1593.61	

Sliding and rolling velocities are used in friction coefficient calculation. However, to find the velocities, firstly, the line of action, contact length and contact ratio are to be determined.
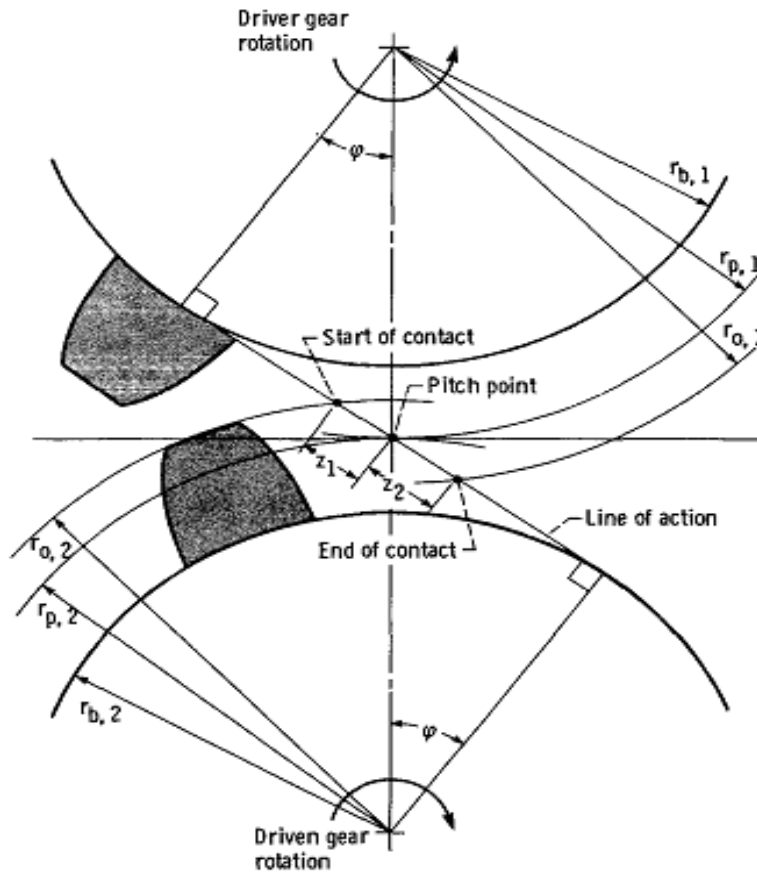
Figure 42 Gear Pair Geometry [42]

Line of action is calculated as:

$$Line\ of\ Action = r_{p,1} \sin \varphi \ + r_{p,2} \sin \varphi \qquad (6.2)$$

where

$r_{p,1} = \frac{1}{2} N_1 m$ is the pitch radius for pinion, [mm]

$r_{p,2} = \frac{1}{2} N_2 m$ is the pitch radius for gear, [mm]

φ is the pressure angle, [degree]

The distance between the start of contact and the end of contact is calculated as:

$$Z = z_1 + \ z_2 \qquad (6.3)$$

where

$$z_1 = \sqrt{r_{o,2}^2 - r_{b,2}^2} - r_{p,2} \sin \varphi \quad , \quad z_2 = \sqrt{r_{o,1}^2 - r_{b,1}^2} - r_{p,1} \sin \varphi$$

where

$r_{b,1}$ is the base radius for pinion, [mm]

$r_{b,2}$ is the base radius for gear, [mm]

$r_{o,1}$ is the outer radius for pinion, [mm]

$r_{o,2}$ is the outer radius for gear, [mm]

N_1 is the number of teeth, pinion, [teeth]

N_2 is the number of teeth, gear, [teeth]

m is the module, [mm/tooth]

Base pitch and contact ratio is calculated as:

$$p_b = \frac{2\pi r_{b,1}}{N_1} \tag{6.4}$$

$$CR = \frac{Z}{p_b} \tag{6.5}$$

Reduced radius of curvature is calculated as:

1. At the ith contact position the radius of curvature of the pinion and gear are:

$$R_{1,i} = r_{p,1} \sin \emptyset + x_i \quad , \quad R_{2,i} = r_{p,2} \sin \emptyset - x_i \tag{6.6}$$

    where

$$x_i = -z_1 + i - 1 \, \Delta x \quad for = i \, to \, j + 1$$

$\Delta x = \frac{Z}{j}$; where j is the total number of intervals.

2. Reduced radius of curvature is determined according to Eqn. (3.48).
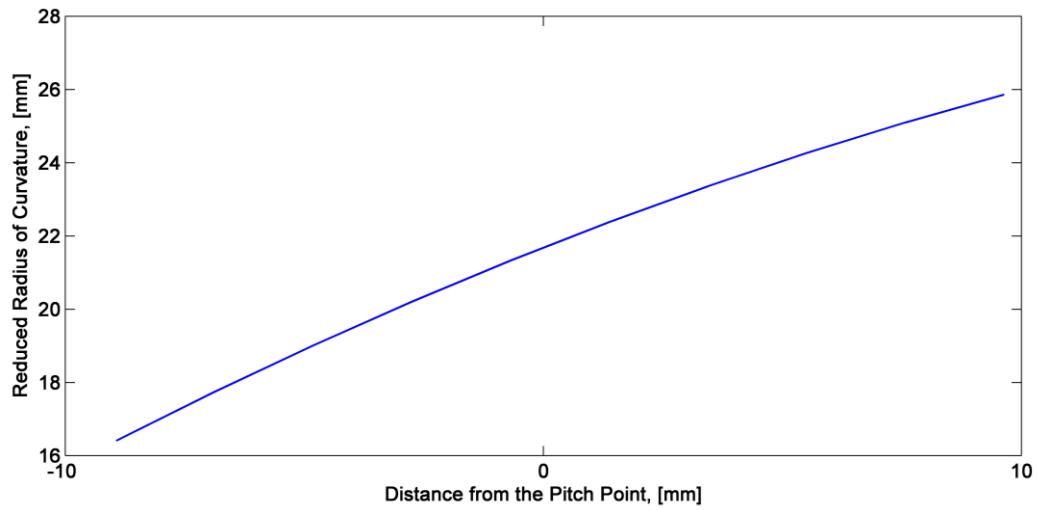
Figure 43 Variation of Reduced Radius of Curvature

The calculated pitch radius, base radius, line of action, contact length and contact ratio are given in Table-6.

Table- 6 Calculated Gear Geometry Parameters

$r_{p,1}$	$67.77\ mm$
$r_{p,2}$	$211.65\ mm$
$r_{b,1}$	$61.38\ mm$
$r_{b,2}$	$191.82\ mm$
$Line\ of\ Action$	$118.09\ mm$
Z	$18.58\ mm$
p_b	$12.05\ mm$
CR	1.54

In Figure 44, gear contact normal load variation is shown along path of contact.
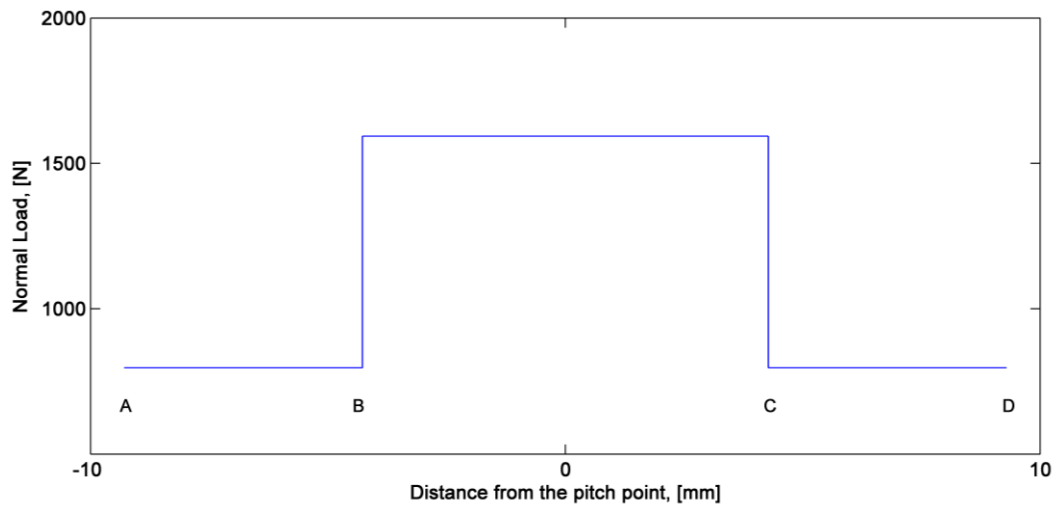
Figure 44 Variation of Gear Contact Normal Load

Double-tooth contact occurs between the distances A and B and C and D along the path of contact. Gear load is shared by two teeth and half of the load is transferred per contact. Between the distances B and C, single-tooth contact occurs and normal load is carried by one tooth.

The contact ratio is 1.54. It can be said that, the gear pair has low contact ratio (it is between 1 and 2). The contact ratio of 1.54 means that two pairs of teeth are in contact 54 percent of the time and one pair is in contact 46 percent of the time [42].

Sliding and Rolling Velocity

Simple procedure for calculating sliding and rolling velocities for spur gear pair is given as [43]:

1. Tangential velocities are calculated at a given point on the profile. (Point A is arbitrarily chosen and shown in Figure 45).
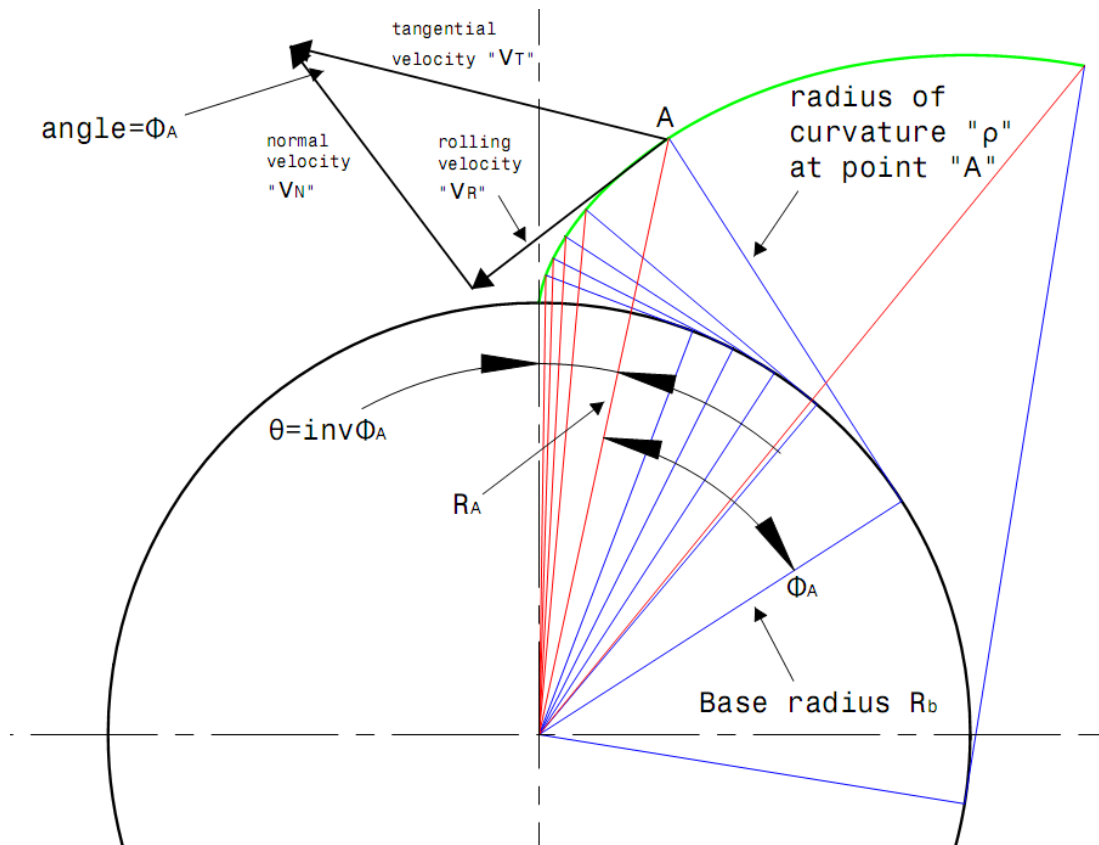
Figure 45 Velocities at any Contact Point A [43]

$$v_{TA1} = \frac{2\pi R_{A1}}{60} n_1, \quad v_{TA2} = \frac{2\pi R_{A2}}{60} n_2 \qquad\qquad (6.7)$$

where

v_{TA1} is the tangential velocity at point A, pinion, [m/s]

v_{TA2} is the tangential velocity at point A, gear, [m/s]

n_1 is the pinion speed, [rpm]

n_2 is the gear speed, [rpm]

R_{A1} is the radius to point A, pinion, [mm]

R_{A2} is the radius to point A, gear, [mm]

2. Rolling velocities of the gear and point at point A is calculated.

$$v_{RA1} = v_{TA1} sin(\phi_A) , \qquad v_{RA2} = v_{TA2} \sin \phi_A \qquad\qquad (6.8)$$

where

ϕ_A is the pressure angle at point A, [degree]

3. Sliding velocity is calculated as the difference between rolling velocities of a gear and a pinion:

$$u_{dif} = v_{RA1} - v_{RA2} \qquad\qquad (6.9)$$

where

v_{RA1} is the rolling velocity at point A, pinion, [m/s]

v_{RA2} is the rolling velocity at point A, gear, [m/s]

4. Sliding velocity can be expressed in terms of pinion and gear speed and the distance along the line of action.

$$u_{dif} = s_p(\omega_1 - \omega_2) \qquad\qquad (6.10)$$

where

ω_1 is the angular velocity of pinion, [rad/sec]

ω_2 is the angular velocity of gear, [rad/sec]

s_p is the distance along the line of action to the arbitrary point chosen from the pitch point, [m]

The calculated sliding and rolling velocities are used as input parameters in the developed mixed EHL model.

In figure 46, the sliding velocity shows absolute values. The sliding velocities are negative at negative side of the contact line. At the center of contact line, the sliding velocity changes its direction. Similarly, the rolling velocity reaches its maximum value at the pitch point.
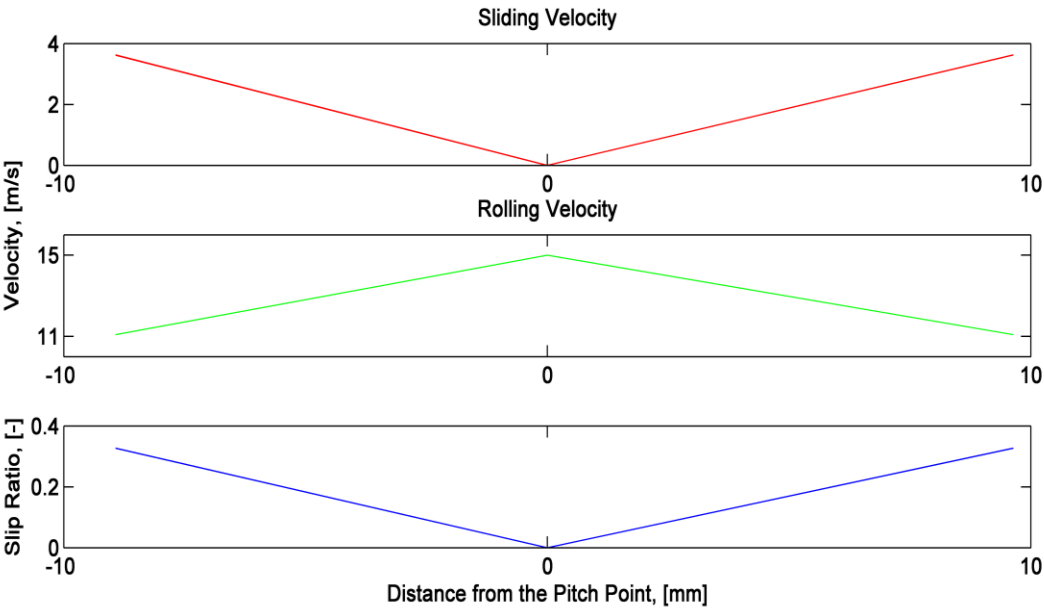
Figure 46 Sliding Velocity, Rolling Velocity and Slip Ratio along Distance from the Pitch Point

The Coefficient of friction is determined according to the procedure given in section '3.8.1.7 Coefficient of Friction Calculation for Fully Flooded Conditions' for line contacts. In order to calculate the friction coefficient, surface roughness, material and oil properties should be given as input values.

In Table 7, the gear tooth surface roughness, material and oil properties are listed.

Table -7 Sample Gear Surface Roughness, Material and Oil Properties

Surface Roughness Input Parameters	
n	$1.0 \; x \; 10^{11} m^{-2}$
β	$10.0 \; \mu m$
σ_s	$0.05 \; \mu m$
Material Input Parameters	
E	$231 \; GPa$
Oil Property Input Parameters	
η_o	$20 \; mPa.s$
α	$2.0 \; x \; 10^{-8} \; Pa^{-1}$
τ_0	$2.5 \; MPa$

In Figure 47, lubrication number is plotted.
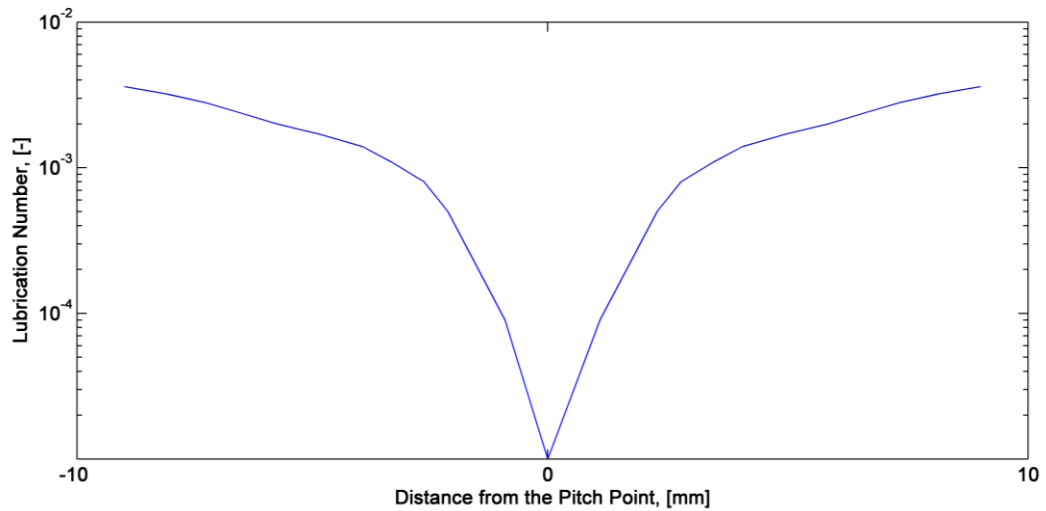
Figure 47 Variation of Lubrication Number along Distance from the Pitch Point

In Figure 48, the calculated friction coefficient and separation variation with contact line is shown.
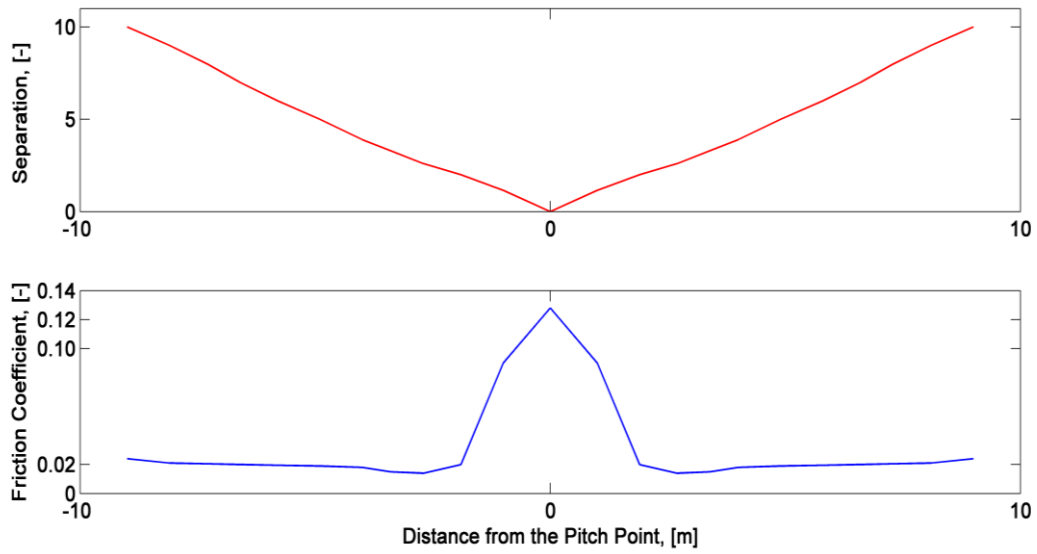
Figure 48 Variations of Friction Coefficient and Separation along Distance from the Pitch Point

In Figure 49, the frictional power loss is obtained according to solution procedure in Section 6.2.
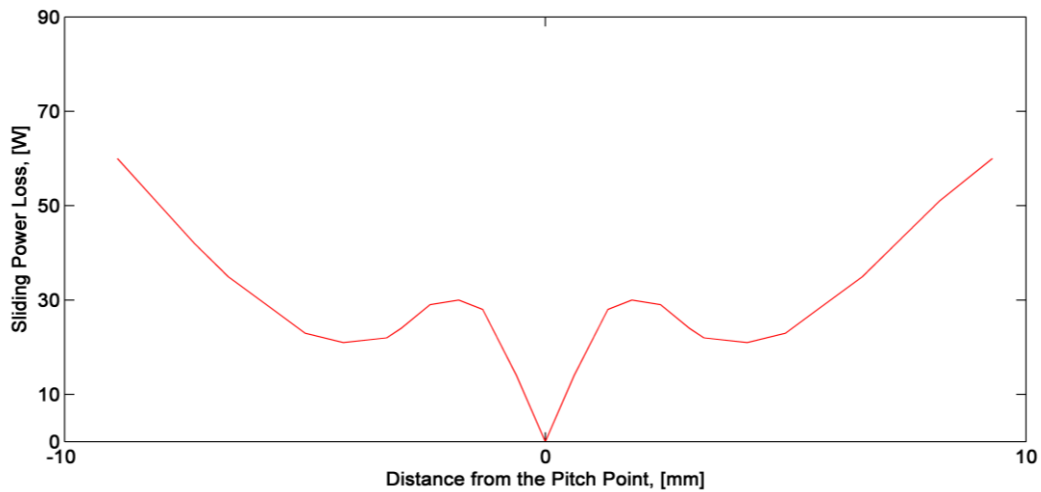
Figure 49 Variation of Sliding Power Loss along Distance from the Pitch Point

In Figure 50, friction coefficient and sliding power loss variation is plotted for different standard deviation parameters.
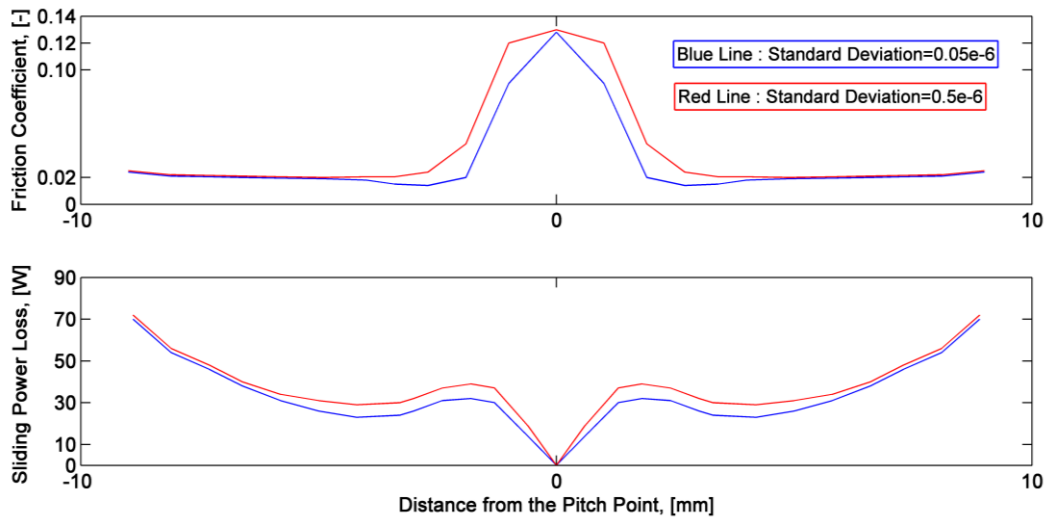
Figure 50 Variations of Friction Coefficient and Sliding Power Loss along Distance from the Pitch Point for Different Standard Deviation Parameters

$$\sigma_s = 0.05x10^{-6}, 0.5x10^{-6}\ m$$

In Figure 51 and 52, sliding power loss is plotted along the line of action of the gear pair for Sk=-1, 0, 1 and Ku=2.72, 4, 6.
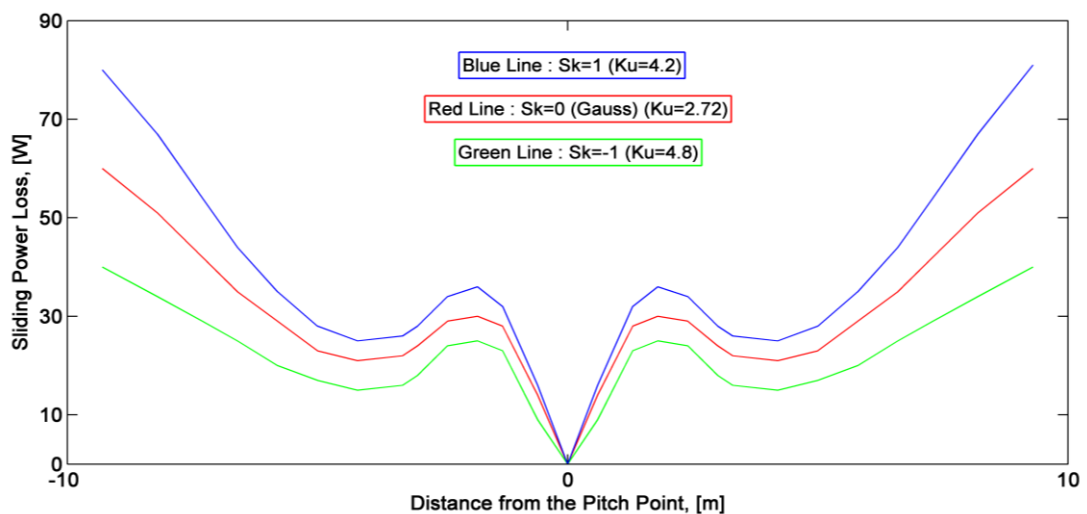
Figure 51 Variation of Sliding Power Loss for Sk =-1, 0, 1
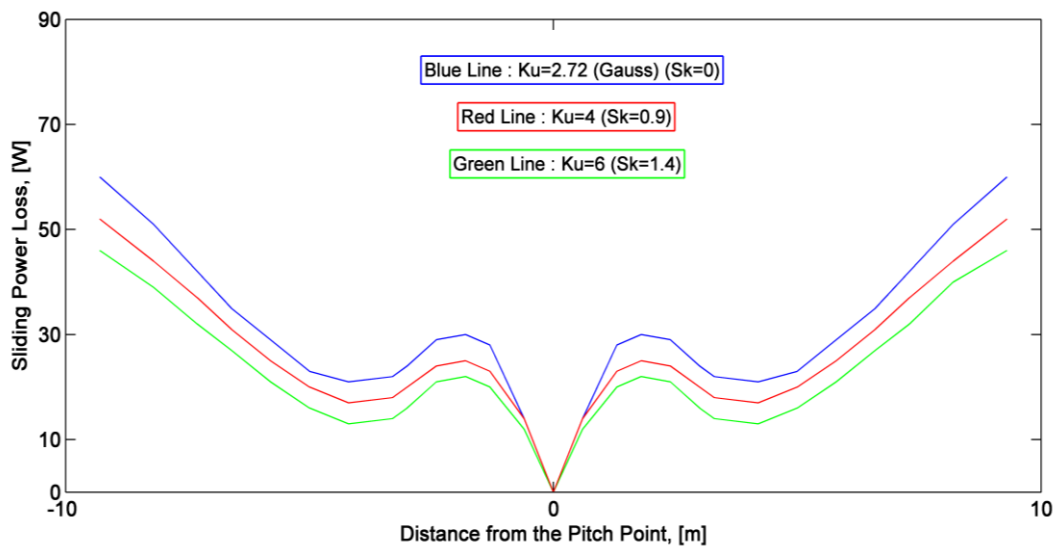
Figure 52 Variation of Sliding Power Loss for Ku=2.72, 4, 6

It is determined that for Sk values lower than the Gaussian value of 0 and for Ku values higher than the Gaussian value of 2.72, the friction coefficient values are lower than the Gaussian asperity summit distribution and giving lower power loss. Depending on the values of Sk and Ku, the decrease in the sliding power loss is observed at the start end of the contact length.

For a given gear pair, frictional rolling power loss, bearing power losses, sealing power losses and load independent power losses (churning, windage etc) can be calculated and with the known transmitted power, the overall system efficiency can also be determined.

CHAPTER 7

CONCLUSIONS

This thesis presents calculation method for friction coefficient and development of mixed EHL lubrication mathematical model for steady state and isothermal conditions for any gear pair contacts. The lessons learned are discussed in this chapter.

In the present study, mixed EHL mathematical model is obtained for line and point contact conditions. Load, surface roughness, oil viscosity, oil temperature, surface velocities and any other inputs contributes to friction coefficient calculations. The algorithm is developed in Matlab program.

Mixed EHL model based on combination of asperity rough surface contact, EHL line contact, EHL central film thickness and load shape concept. Hydrodynamic pressures and central film thickness are obtained for a given total normal load. Asperity pressure is obtained including Greenwood and Williamson [2] contact model to a Gaussian distribution of the summits heights. For a Gaussian distribution, it is assumed that asperities have the same parabolic radius. The main disadvantage of this model is that the assumed Gaussian distribution of equal summits. With this model, mixed EHL is applied statistically.

Gelinck and Schipper's [25] asperity pressure formula is determined and equalized with Greenwood and Williamson's asperity pressure formula. Gelinck and Schipper [25] curve fitted a formula that assumes central asperity pressure in the contact is equal to maximum pressure (Hertz pressure) for line contact conditions.

After an initial assumption of asperity load, load share ratio between hydrodynamic and asperity components is found with an iterative process and friction coefficient is obtained.

Friction coefficient is the ratio between the friction force that is sum of the friction force between the interacting asperities and the shear force of the hydrodynamic component and the total normal force for two contacting surfaces. Hydrodynamic friction force is ratio of shear stress that can be determined by applying Eyring shear stress and shear rate to hydrodynamic area. In the present study, Roeland's viscosity pressure formula is applicable.

In the calculations part, variation of pressure, isothermal film thickness, thermal film thickness, separation, friction coefficient and the Stribeck curve can be plotted for line contact conditions.

The program can also calculate starved oil film thickness. In the starved film thickness calculations, Schipper and Faraon's [38] modified correction factor of numerical solution of Wolveridge [39] is multiplied with film thickness.

Moreover, the program can capable of calculating of isothermal film thickness, separation and friction coefficient for point contact conditions. The calculations are mostly similar. Film thickness formula is changed. The variation of friction coefficient has similar decreasing tendency.

Besides, load, surface roughness parameters and slip ratio effects on the Stribeck curve is analyzed. The Stribeck curve represents three lubrication regimes: boundary lubrication regime at lower velocities, mixed EHL regime and hydrodynamic lubrication regimes at higher velocities. It is shown that the friction of the lubricated rough contact is strongly dependent on the operating factors: load, velocity, surface roughness etc. The friction of the contacting surfaces can increase or decrease with the sliding velocity depending on the type of lubricant. Mixed lubrication region highly effected with load and surface roughness. With more rough surface roughness, the Stribeck curve in mixed lubrication region shifts to the right. If $n\beta\sigma_s$ is kept

constant having the value of 0.05 and n is decreased and β is increased, mixed lubrication region shifts to left. It is seen that at the hydrodynamic region, surface roughness parameters are insignificant effects. Contrarily, load is adverse effect on hydrodynamic regime. At boundary lubrication regime, the increased load increases the contact area and consequently the number of asperity contacts, but friction coefficient changes insignificant. Nevertheless, mixed lubrication region is highly changed with load and the Stribeck curve shifts to left for higher loads giving low friction coefficient for the same conditions.

For rough surfaces that do not show a Gaussian distribution of asperity summit height, new contact model is applied. Mixed EHL model is adopted to simulate non-Gaussian surface heights. Greenwood and Williamson [2] assumed that surface asperities have the same radius and deviates from each other as Gaussian. This method is more simply but in real, surface asperities are not in the same radius and types. After many three dimensional surface topography measurements are developed, new contact model is obtained in order to Greenwood and Williamson [2] model. In this approach, non-Gaussian distribution of asperity summit height is considered. Weibull distribution method is a way to apply non-Gaussian surface heights distribution. In practice, the surface roughness parameters (Skewness, Kurtosis and variance) that represent surface roughness profile are measured. However, in the present work, those parameters are taken from the literature. Skewness and Kurtosis parameters are equalized to zero respectively. However, two parameters are assumed and solved separately. Then, shape and scale parameters can be obtained. Weibull distribution is shape and scale parameters dependent. If the Skewness parameter is assumed as zero and the Kurtosis parameter is assumed as 2.72, the Weibull distribution shape is symmetric and shows Gaussian distribution. Weibull distribution can be applied to mixed EHL model instead of Gaussian distribution included in asperity pressure formula. Then, two dimensionless asperity pressure formulas are equalized and the same procedure is applied. Variation of film thickness, separation, load share and the Stribeck curve is plotted for Gaussian and non-Gaussian distributions for different Skewness and Kurtosis parameters.

In last chapter, sliding and rolling velocities are calculated for a sample spur gear pair. Then, sliding frictional power loss is determined for Gaussian and non-Gaussian asperity summit distributions. For Sk values smaller than zero and for Ku values higher than the Gaussian values, frictional sliding power loss is lower than the Gaussian sliding power loss.

In future work, the mixed lubrication model can be extended for transient and thermal conditions during meshing of the gear set. In the mixed lubrication, the asperity contact model can be improved by considering elastic, elastic-plastic and fully plastic deformation of asperities. The effect of asperity deformation on the asymmetric asperity height distribution can be studied and the effect can be included in the contact model and in the EHL model.

REFERENCES

1. http://en.wikipedia.org/wiki/Frictional_contact_mechanics (Accessed:01.03.2014)

2. Greenwood, J. A., and Williamson, J. B. P., *Contact of Nominally Flat Surfaces,* Proc. R. Soc. London, 1966, Ser. A, 295, pp. 300–319.

3. Greenwood, J.A. and Tripp, J.H., *The contact of two nominal flat rough surfaces*, Proc. Inst. Mech. Engrs., 1970, Vol. 185, pp. 625-633.

4. Johnson, K. L., Greenwood, J. A., and Poon, S. Y., *A Simple Theory of Asperity Contact In Elastohydrodynamic Lubrication*, Wear, 1972, Vol. 19, pp. 91–108.

5. E.R.M. Gelinck, D.J. Schipper, *Deformation of rough line contacts,* ASME Journal of Tribology, 1999, Vol. 121, pp. 449-454.

6. Zhao YW, Maietta DM, Chang L. *An asperity microcontact model incorporating the transition from elastic deformation to fully plastic flow*, Journal of Tribology Transactions of the ASME, 2000, Vol. 122, pp. 86-93.

7. Martin HM. *The lubrication of gear teeth*, Engineering, London, 1916, Vol. 119.

8. Grubin, A.N. and Vinogradova, I.E., *Central Scientific Research Institute for Technology and Mechanical Engineering Book 30,* Moscow, 1949, D.S.I. R. Trans. No. 337.

9. Hamrock BJ, Dowson D. *Isothermal elastohydrodynamic lubrication of point contacts, Part II Ellipticity parameter results,* 1976, Trans ASME, J Lubrication Tech, Vol. 98, pp. 375–83.

10. Moes, H., *Optimum similarity analysis with applications to elastohydrodynamic lubrication*, Wear, 1992, Vol. 159, pp. 57-66.

11. D.E.Brewe, B.J. Hamrock, C.M. Taylor, *Effect of geometry on hydrodynamic film thickness*, Trans. ASME, J. Basic Eng, 1979, Vol. 101, pp. 231-237.

12. B.J. Hamrock, B.O. Jacobson, *Elastohydrodynamic lubrication of rectangular contacts*, NASA Technical Paper, 1983, vol.2111.

13. J.L. Tevaarwerk, *Constitutive modeling of lubricants in concentrated contacts at high slide-to-roll ratio,* NASA CR-175029 , 1985.

14. L.G. Houpert, B.J. Hamrock, *Fast approach for calculating film thickness and pressure in elastohydrodynamic lubricated contacts at high loads,* ASME Journal of Tribology, 1986, Vol.108, pp. 411-420.

15. P. Pan, B. J. Hamrock, *Simple formulas for performance parameters used in elastohydrodynamically lubricated line contacts,* ASME Journal of Tribology, 1989, Vol. 111, pp. 246-251.

16. Patir N., Cheng H.S., *An average flow model for determining effects of three-dimensional roughness on partial hydrodynamic lubrication,* ASME, Journal of Lubrication Technology, 1978, Vol. 100, pp. 12-17.

17. B.C. Majumdar, B.J. Hamrock, *Frictional heating due to asperity interaction of elastohydrodynamic line contact surfaces,* NASA Technical Paper., 1982.

18. J.H. Tripp, B.J. Hamrock, *Surface roughness effects in elastohydrodynamic contacts,* NASA Technical Paper 2488, 1985.

19. R. Larsson, *Transient non-Newtonian elastohydrodynamic lubrication analysis of an involute spur gear,* Wear, 1997, Vol. 207, pp. 67-73.

20. Bair S., Khonsari M. M., *Reynolds Equations for Common Generalized Newtonian Models and an Approximate Reynolds-Carreau Equation*, Proc. Inst. Mech. Eng., Part J: J. Eng. Tribol., 2006, Vol. 220, pp. 365–374.

21. Akbarzadeh S., Khonsari M. M., *Performance of Spur Gears Considering Surface Roughness and Shear Thinning Lubricant,* ASME Journal of Tribology, 2008, Vol. 130, pp. 021503-1- 8.

22. Larsson R., *Modeling the effect of surface roughness on lubrication in all regimes*, Tribology International, 2009, Vol. 42, pp. 512–516.

23. Jang J. Y., Khonsari M. M., *Elastohydrodynamic Line-Contact of Compressible Shear Thinning Fluids With Consideration of the Surface Roughness,* ASME Journal of Tribology, 2010, Vol. 132, pp. 034501-1- 6.

24. M. Masjedi, M. M. Khonsari, *Asperity micro-contact models as applied to the deformation of rough line contact,* Tribology International, 2012, Vol. 52, pp. 61-74.

25. Gelinck, E. R. M., and Schipper, D. J., *Calculation of Stribeck Curves for Line Contacts, Tribol. International*, 2000, Vol. 33, pp. 175–181.

26. Faraon I. C. *Mixed Lubricated Line Contacts,* Ph.D. Thesis, 2005, University of Twente, Enschede, the Netherlands.

27. Xiaobin Lu, M. M. Khonsari, E. R. M. Gelinck, *TheStribeck Curve: Experimental Results and Theoretical Prediction,* Journal of Tribology, 2006, Vol. 128, pp. 789-794.

28. Kogut L, Etsion I., *Elastic–plastic contact analysis of a sphere and a rigid flat,* Journal of Applied Mechanics Transactions of the ASME, 2002, Vol. 69, pp. 657–662.

29. Jackson RL, Green I., *A finite element study of elasto-plastic hemispherical contact against a rigid flat,* Journal of Tribology Transactions of the ASME, 2005, Vol 127, pp. 343-354.

30. Wilson, W. E., Angadi, S. V., and Jackson, R. L., *Surface Separation and Contact Resistance Considering Sinusoidal Elastic Plastic Multi-Scale Rough Surface Contact,* Wear, 2010, Vol. 268(1-2), pp 190-201.

31. Evans, C.R. *Measurements and mapping of the rheological properties of elasto hydrodynamic lubricants,* PhD thesis, 1983, University of Cambridge, UK.

32. Bair, S. and Winer, W.O., A rheological model for elastohydrodynamic contacts based on primary laboratory data, ASME, Journal of Lubrication Technology,vol. 101, pp 251-257.

33. Timoschenko, S.P. and Goodier, J.N, *Theory of Elasticity,* 3 edn MCGraw-Hill, 1982, New York.

34. Dowson D, Higginson GR. *A numerical solution to the elastohydrodynamic Problem,* J MechEngSc, 1959, Vol.1, pp. 1–6.

35. Roelands, C.J.A., *Correlation Aspects of the Viscosity temperature Pressure relationship of lubricating Oils,* PhD Thesis, 1966, University of Delft, The Netherlands.

36. Wilson, W. R. D. and Sheu, S. *Effect of inlet shear heating due to sliding on elastohydrodynamic film thickness,* ASME J. Tribol., 1983, Vol. 105, pp. 187–188.

37. Schipper D. J., Faraon I. C., *Stribeck Curve for Starved Line Contacts,* Journal of Tribology, 2007, Vol. 129, pp. 181-187.

38. Wolveridge P.E., Baglin K.P. Archard J.F. *The Starved Lubrication of Cylinders in Line Contact*, Proc. Inst. Mech. Eng., 1971, Vol. 181, pp. 1159-1169.

39. Quiang Liu, *Friction in Mixed and Elastohydrodynamic Lubricated Contacts Including Thermal Effects,* Ph.D. Thesis, 2002, University of Twente, Enschede, The Netherlands.

40. PrasantaSahoo, S Mohamed Ali, *Elastic–plastic adhesive contact of non-Gaussian rough surfaces,* Sadhana, India, 2008, Vol.33, pp.367–384.

41. Hai Xu, *Development of A Generalized Mechanical Efficiency Prediction Methodology For Gear Pairs,* PhD Thesis, 2005, The Ohio State University.

42. David G. Lewicki, *Predicted Effect of Dynamic Load on Pitting Fatigue Life for Low Contact Ratio Spur Gears*, NASA Technical Paper 2610, 1986, NASA.

43. http://www.geardesign.pro/pliki/sliding%20velocity.pdf (Accessed: 01.05.2014)